Microbially Induced Inflammation Results in Host and Microbial Changes in Contralateral Healthy Tissues within the Oral Cavity and is Correlated with Clinical Responder Phenotypes

Kristopher A. Kerns

A dissertation
submitted in partial fulfillment of the
requirements for the degree of

Doctor of Philosophy

University of Washington
2021

Reading Committee:

Jeffrey S. McLean, Chair
Richard P. Darveau
Diane Daubert

Program Authorized to Offer Degree:
Oral Health Sciences
School of Dentistry

University of Washington

Abstract

Microbially Induced Inflammation Results in Host and Microbial Changes in Contralateral Healthy Tissues within the Oral Cavity and is Correlated with Clinical Responder Phenotypes

Kristopher A. Kerns

Chair of the Supervisory Committee
Professor Jeffrey S. McLean
Department of Periodontics

Gingival inflammation as the result of microbial plaque accumulation during cessation of oral hygiene within humans has been investigated for over 50 years; however, it was not until recently in which variation in clinical response had been temporally characterized through the simultaneous application of high resolution clinical, host, and microbiome analysis in parallel – resulting in characterization of key host and microbial factors distinguishing High and Low clinical responders as well as a discovery of a novel third responder phenotype (Slow). Additionally, only a limited number of studies within the literature have aimed to temporally characterize the molecular and subclinical changes within distant otherwise generally healthy tissues in the oral cavity with the same resolution. In the present study, using the plaque-induced experimental gingivitis model with a split mouth design, in which each individual provides their own intra-oral control, we were able to robustly characterize the temporal dynamics of a panel of 41 host mediators (chemokines, cytokines) as well as the subgingival microbiome within healthy control sites among these different Clinical Responder Phenotypes (CRPs) (High, Low, Slow) while plaque-induced inflammation was being induced in a controlled way within test sites located contralaterally in the mouth. Our results highlight a temporal shift in host mediators, including pro-inflammatory markers IL-8, IL-6, and TNF-a, within healthy contralateral control sites across CRPs, similarly to

respective test sites, despite maintained normal oral hygiene, no significant visible plaque accumulation (VPI or PI), or clinical gingival inflammation (GI, BOP) among control sites. Additionally, through the application of the inverse Firmicutes/Bacteroidetes Ratio (*i*FBR), our results highlight a significant dysbiotic shift within healthy control sites that is also similarly observed within the respective contralateral test sites among the different CRPs. Together these results provide new comprehensive evidence of an oral contralateral effect within the human oral cavity in which healthy homeostasis within control sites is altered due to microbially-induced inflammation occurring in distant test sites within the mouth – with the variation in this contralateral effect being directly related to an individual's CRP. These results ultimately led to the development of multiple predictive models using the Random Forest Machine Learning algorithm in order to identify an individual's Clinical Responder Phenotype from their natural oral health state. In conclusion, results from this study as part of this dissertation research project have great implications for future clinical gingivitis research with the major findings being that distant otherwise generally healthy sites are affected by microbially-induced inflammation occurring elsewhere in the mouth with the severity being related to an individual's Clinical Responder Phenotype. While clinical implications of these results highlight our ability to now predict an individual's likelihood to be one of the three Clinical Responder Phenotype which may be related to their risk and severity of inflammation that results in progression to a more devastating gingival disease state (periodontitis) and may even be used to dictate patient surveillance and treatment planning – together representing a major advance.

Acknowledgements

I would like to first acknowledge the amazing mentorship from Professor Jeffrey S. McLean. Without his amazing support, guidance, and dedication to my success, none of this would have ever been possible. Thank you for everything!

I would like to express my gratitude to my dissertation committee members Dr. Richard Darveau, Dr. Diane Daubert, Dr. Travis Nelson, and Dr. Daniel Enquobahrie for their mentorship, guidance, and constant support throughout my training and research.

I would like to thank all the people I have been fortunate enough to work with in the McLean lab as they have help mold me into the research and colleague I am today. Thank you, Dr. Jenny (Thao) To, Dr. Erik Hendrickson, Elleanor Lamont, and Archita Gadkari. You are all truly brilliant.

A special thanks to Dr. Shatha Bamashmous for allowing me to be a part of her amazing study and setting the stage for my future dissertation research project.

I would like to thank all my professors, peers, and department administrators in Periodontics and Oral Health Sciences for all the friendships, insightful conversations, and help throughout the years. Specifically, Margaret Collins in Periodontics and Kathy Hobson in Oral Health Sciences for all their additional help and guidance and going above and beyond to help me stay afloat.

I would like to thank all my family and friends for all your support on my academic journey over the years. Without your support and friendship, I don't know if this would have ever been possible.

Dedication

Dedicated to my loving wife, my three beautiful children, and my parents for their unwavering love, support, and dedication.

Table of Contents

Table of Figures 9

Table of Tables 10

Chapter 1. Background and Literature Review 11

1.1 The Microbiome in Oral Health and Disease 11
1.1.1 ***The Oral Microbiome*** 11
1.1.2 ***Next Generation Sequencing and the Oral Microbiome*** 12
1.1.3 ***The Anatomy of the Periodontium in Relationship to the Oral Microbiome*** 16
1.1.4 ***Periodontitis and Gingivitis*** 17
1.1.5 ***Experimental Gingivitis Model*** 19

1.2 Human Variation in Clinical Inflammation 20
1.2.1 ***Clinical Responder Phenotypes (CRPs) associated with plaque-induced gingivitis*** 20
1.2.2 ***Key Host Pro-Inflammatory Mediators during Gingival Inflammation*** 22
1.2.3 ***Machine Learning and the Oral Microbiome*** 24

Chapter 2. The Oral Contralateral Effect within the Human Oral Cavity During Experimental Gingivitis 26

2.1 Introduction 26

2.2 Study Design and Methods 28
2.2.1 ***Human Induced Gingivitis Experiment*** 28
2.2.2 ***Characterization of In Vivo Chemokine Responses during Experimental Gingivitis*** 28
2.2.3 ***Characterization of Microbial Changes in Response to Plaque Accumulation*** 29
2.2.4 ***Variation in Clinical Gingival Inflammatory Responses*** 30
2.2.5 ***Statistical Analysis*** 30

2.3 Results 31
2.3.1 ***Despite regular oral hygiene Control Sites Among Clinical Responder Phenotypes are not Static*** 31
2.3.2 ***Changes in Subgingival Plaque Diversity is Observed in Healthy Control Sites and Varies by Clinical Responder Phenotype*** 33
2.3.3 ***A Unique Responder Dependent Microbiome Composition Shift is Evident within Healthy Control Sites*** 35
2.3.4 ***Amplicon Sequence Variants are Detected Contralaterally between Test and Control Sites among Study Subjects*** 40
2.3.5 ***Amplicon Sequence Variants by Subjects among Clinical Responder Phenotypes during Experimental Gingivitis*** 42
2.3.6 ***Induced Inflammation in Test Sites Results in Changes in Chemokine Profiles in Control Sites across Clinical Responder Phenotypes*** 44
2.3.7 ***Temporal Resolution of Subgingival Microbiome and Host Mediator Shifts by Clinical Responder Phenotype*** 47

2.4 Discussion 50

Chapter 3. Using Machine Learning to Predict Risk and Severity of Microbially-Induced Inflammation 62

3.1 Introduction 62

3.2 Study Design and Methods 67

3.2.1 ***Human Induced Gingivitis Experiment - EG-1*** 67
3.2.2 ***Variation in Clinical Gingival Inflammatory Responses - EG-1*** 69
3.2.3 ***Human Induced Gingivitis Experiment - EG-2*** 69
3.2.4 ***Variation in Clinical Gingival Inflammatory Responses -EG-2*** 70
3.2.5 ***Developing a Predictive Model to Identify Clinical Responder Phenotypes using Relative Abundance Microbiome Data from EG-1*** 70
3.2.6 ***Developing a Predictive Model to Identify Clinical Responder Phenotypes using Host Mediators Data from EG-1*** 71
3.2.7 ***Developing a Comprehensive Predictive Model to Identify Clinical Responder Phenotypes Incorporating Microbiome and Host Mediator Data*** 72
3.2.8 ***Validating the Predictive Model to Identify Clinical Responder Phenotypes.*** 73

3.3 Results **74**
3.3.1 ***Identifying Clinical Responder Phenotypes within a Second Experimental Gingivitis Study*** 74
3.3.2 ***Developing a Predictive Model to Identify Clinical Responder Phenotypes using Relative Abundance Microbiome Data from EG-1*** 76
3.3.3 ***Developing a Predictive Model to Identify Clinical Responder Phenotypes using Host Mediator Data from EG-1*** 81
3.3.4 ***Developing a Comprehensive Random Forest Model to Predict Clinical Responder Phenotypes Incorporating Microbiome and Host Mediator Data*** 85
3.3.5 ***Validating the Random Forest Model for Predicting Clinical Responder Phenotypes*** 89

3.4 Discussion **91**

Chapter 4. Summary and Future Directions ***98***

Table of Figures

Figure 1. Clinical Measures for Gingivitis by Clinical Responder Phenotype……**21**
Figure 2. Microbiome Alpha and Beta Diversity by Clinical Responder Phenotype……..…**21**
Figure 3. Clinical Parameters for Test and Control Sites During Experimental Gingivitis by Clinical Responder Phenotype……...**32**
Figure 4. Microbiome Diversity Shifts in Healthy Controls. A) Alpha diversity measured by Observed Amplicon Sequence Variants (ASVs) and Shannon Indices…….**34**
Figure 5. Relative abundance by Phylum Over the Induction Phase (Day 0-21) by Clinical Responder Phenotype with Respective Controls……...……**37**
Figure 6. Phylum and Genus Level Relative Abundance by Clinical Responder Phenotype…..**38**
Figure 7. The Inverse Firmicutes/Bacteroidetes Ratio (iFBR) by Clinical Responder Phenotype……..**39**
Figure 8. Contralaterally Detected Amplicon Sequence Variants (ASVs) within Subgingival Plaque during Induced Inflammation…….**41**
Figure 9. Amplicon Sequence Variant Trajectories for Test and Control Sites by Clinical Responder Phenotypes……...**43**
Figure 10. Host Mediators Dynamics Among Clinical Responder Phenotypes..……**46**
Figure 11. Temporal Resolution of the Oral Contralateral Effect…...…….**49**
Figure 12. Overview of Experimental Gingivitis Studies EG-1 and EG-2……...……**67**
Figure 13. Identifying Clinical Responder Phenotypes within EG-2……..…….**74**
Figure 14. Multi-way Importance Plot of Variables of Importance Identified within Subgingival Plaque at Time of Inclusion for EG-1……..……**76**
Figure 15. Evaluation of the Predictive Model to Identify Clinical Responder Phenotypes using Species Level Microbiome Data from EG-1……...……..**79**
Figure 16. Multi-way Importance Plot of Variables of Importance Identified within Gingival Crevicular Fluid at Time of Inclusion for EG-1……...….**81**
Figure 17. Evaluation of the Predictive Model to Identify Clinical Responder Phenotypes using Host Mediator Data from EG-1……...……..**83**
Figure 18. Top 5 Variables of Importance for Species and Chemokines Identified by the Random Forest Model for Predicting Clinical Responder Phenotypes…….**86**
Figure 19. Evaluation of the Comprehensive Predictive Model to Identify Clinical Responder Phenotypes using Species Level Microbiome and Host Mediator Data from EG-1…….....**87**
Figure 20. Validating of the Comprehensive Predictive Model to Identify Clinical Responder Phenotypes using Species Level Microbiome and Host Mediator Baseline Data from EG-1..…**89**

Table of Tables

Table 1. Research Articles on PubMed.gov using various Next Generation Sequencing (NGS) Techniques to investigate the Oral Microbiome, Gingivitis, and Periodontitis. **14**
Table 2. Performance of Variables of Importance Identified from Subgingival Plaque Isolated at Time of Inclusion for EG-1 ..... **78**
Table 3. Performance of Variables of Importance Identified from Gingival Crevicular Fluid Isolated at Time of Inclusion for EG-1 ..... **83**
Table 4. Performance of Variables of Importance Identified from Subgingival Plaque and Gingival Crevicular Fluid Isolated at Time of Inclusion for EG-1 ..... **86**

Chapter 1. Background and Literature Review

1.1 The Microbiome in Oral Health and Disease

1.1.1 *The Oral Microbiome*

The oral microbiome is an ecological community composed of symbiotic, commensal, and pathogenic microorganisms and contains all forms of life including Bacteria, Archaea, Eukarya (Fungi), and even members of the proposed Candidate Phyla Radiation (CPR)(1,2). The oral cavity is a unique habitat made up of many diverse microenvironments, from the hard tooth surfaces and mucin lined gingiva to the crevassed regions of the posterior tongue. Although there are currently between 800-1000 bacterial species that have been identified within the human oral microbiome(3), an individual only has about 100-200 species on average – with the community being rather stable over time(4).

These microbial hitchhikers begin their colonization within the oral cavity as early as six months post-partum and can even be detected days after birth(5,6). This is known as plaque, a biofilm rich in microbial diversity resulting from a class system (initiators, colonizers, and secondary colonizers) with its own developmental stages (attachment, adhesion, proliferation, assembly and maturation, and dispersion)(6). The accumulation and maturation of plaque over time is associated with multiple oral diseases including the two most common being dental caries and periodontal disease(4,7–10). Recent studies have focused on identifying differences within plaque derived from both healthy and diseased states in order to better understand and identify key etiological agents and etiological processes for each respective microbially associated oral disease(4,8,11–15). Some recent studies have even suggested that strain level variations in some species are responsible for differences in disease severity(16). Thus, studies that aim to investigate the oral microbiome must consider niche specific microenvironments as

well as other host and environmental factors when trying to identify associations between different etiological agents and etiological processes as the oral microbiome shifts from health to states of dysbiosis associated with different oral diseases.

In addition to differences in the microenvironments within the oral cavity that result in differences in niche specific community composition, there are also many hosts and environmental factors that play a large role in maintaining homeostasis as well onset and progression of oral diseases(17,18). For example, a diet rich in fermentable carbohydrates is strongly associated with a microbial community rich in acidogenic and aciduric species that facilitates the progression of dental caries. In addition, smoking, alcohol consumption, and medication use are risk factors that affect normal salivary function and composition which allows for enrichment of pathogenic species associated with periodontal disease(6).

1.1.2 *Next Generation Sequencing and the Oral Microbiome*

Nearly 30% of the identified bacterial species or phylotypes (an uncultivated taxa) detected within the oral cavity still remain uncultured and have only been detected through culture-independent molecular techniques, including next generation sequencing (NGS) strategies(11). With dramatic advances in NGS techniques, including strain level detection using amplicon sequencing (16S rRNA), Whole Genome Shotgun (WGS) metagenomic, and RNAseq metatranscriptomic sequencing, reduction in costs, and novel bioinformatic approaches, we now have the capacity and framework to investigate strain level variation, functional composition, and active gene expression of these very diverse microenvironments within the oral cavity in a culture-independent manner. These approaches used in a synchronous manner will provide the most robust characterization of the oral microbiome to date and highlight which

taxa are contributing, enabling, and/or preventing etiological processes associated with these different oral disease etiologies or aiding in homeostatic health.

To date, nearly 2,000 publications on PubMed.gov report using amplicon 16S rRNA sequencing methods (1997-2021) to investigate the oral microbiome, while only 152 report using whole genome (1997-2021) and 57 that report using RNAseq metatranscriptomic strategies (2012-2021) (**Table 1**). In addition to these approaches that aimed to investigate the oral microbiome, limited studies have applied similar techniques to investigate gingivitis and periodontitis. Although 16S rRNA sequencing strategies were dominant for investigating the oral microbiome, only 159 studies (1997-2021) report using 16S rRNA strategies to investigate gingivitis, whereas 421 studies (1997-2021) aimed to characterize periodontitis (**Table 1**).

Studies which aimed to investigate the oral microbiome using deeper NGS strategies, such as WGS and RNAseq, are even more limited. At the time of this dissertation, only 26 and 46 (1997-2021) studies applied whole genome sequencing strategies to investigate gingivitis and periodontitis respectively; whereas only 3 (2017-2021) and 30 (2014-2021) studies applied RNAseq metatranscriptomic approaches respectively (**Table 1**). Although this only provides a snapshot of the breadth of studies that have aimed to apply these culture-independent methods in order to investigate the oral microbiome and gingival diseases, a majority of our knowledge of the oral microbiome, gingivitis, and periodontitis seems to be based upon 16S rRNA studies.

Table 1. Research Articles on PubMed.gov using various Next Generation Sequencing (NGS) Techniques to investigate the Oral Microbiome, Gingivitis, and Periodontitis.

NGS Strategy	Focus	Search Terms	Number of Hits	Time Range
16S rRNA	Oral Microbiome	((16S rRNA) AND (microbiome)) AND (oral)	1824	1997-2021
16S rRNA	Gingivitis	((16S rRNA) AND (microbiome)) AND (gingivitis)	159	1997-2021
16S rRNA	Periodontitis	((16S rRNA) AND (microbiome)) AND (periodontitis)	421	1997-2021
WGS	Oral Microbiome	((whole genome) AND (microbiome)) AND (oral)	152	1997-2021
WGS	Gingivitis	((whole genome) AND (microbiome)) AND (gingivitis)	26	1997-2021
WGS	Periodontitis	((whole genome) AND (microbiome)) AND (periodontitis)	46	1997-2021
RNAseq	Oral Microbiome	((metatranscriptomics) AND (microbiome)) AND (oral)	57	2012-2021
RNAseq	Gingivitis	((metatranscriptomics) AND (microbiome)) AND (gingivitis)	3	2017-2021
RNAseq	Periodontitis	((metatranscriptomics) AND (microbiome)) AND (periodontitis)	30	2014-2021

16S rRNA sequencing, or amplicon sequencing, is a targeted approach that aims to amplify the 16S rRNA gene, which is a ubiquitous marker gene across all three domains of life(19). Although this technique is relatively inexpensive and applicable to many different sample types, 16S rRNA sequencing does have some key limitations that are often not accounted for when interpreting this type of data. The three major limitations for 16S studies include the inability to differentiate live bacteria from dead, as DNA does not rapidly degrade and can remain within the sample for extended periods of time. In addition, the number of 16S rRNA gene copy numbers vary across genera, thus a species within the *Streptococcus* genera, may have up to 8 copies of the 16S rRNA gene, compared to other genera that may only have 1 or 2 copies, and may inflate its overall relative abundance measure within that sample as its more likely to be amplified. Lastly, many 16S studies only amplify a specific hypervariable region of the 16S rRNA gene (V1-9), often with different regions being amplified across different studies. Thus,

it is hard to compare studies that utilize different hypervariable regions and come to a consensus of taxonomic assignment at the lowest levels (i.e. species). However, even with these limitations associated with 16S rRNA studies there remains a benefit for using 16S rRNA amplicon approach. As stated previously, this NGS strategy is widely applicable and dramatically cheaper than deeper sequencing methods, such as whole genome and metatranscriptomic sequencing – although one should keep these limitations in mind when inferring results from this type of data.

In addition to using 16S rRNA sequencing strategies to investigate the oral microbiome, it is essential to utilize the most representative database when assigning taxonomy. The expanded Human Oral Microbiome Database (*e*HOMD) is a curated database by the Forsyth Institute and funded by NIDCR (NIH) is one of the most robust oral microbiome database to date(20). In addition, incorporation of novel bioinformatic tools which have become available in recent years provides increased reliability and accuracy of 16S rRNA results. The application of the Divisive Amplicon Denoising Algorithm 2 (DADA2) allows for investigating exact amplicon sequence variants (ASVs) which represent strain level designations for 16S rRNA studies and provides the highest resolution of 16S rRNA data compared to previous operational taxonomic unit (OTU) clustering strategies(21,22). This newer approach offers better approximations of relative abundance and diversity measurements of microbial communities; however, few studies investigating the oral microbiome, gingivitis, and periodontitis have applied this newer bioinformatic approach and/or used the *e*HOMD database.

Lastly, many oral microbiome studies within the literature, including those that aimed to investigate gingivitis and periodontitis, have often relied on the use of saliva as the primary bio sample(1). Saliva has been shown to consist of a mixture of bacterial diversity that is predominantly associated with the composition of the posterior tongue and may not represent

the actual community composition found within the subgingival pocket(1). Although, it is possible to detect community members found within the subgingival pocket in saliva, this sample type should be interpreted in that context. Thus, studies that aim to use the most representative samples derived from specific microenvironments associated with the microbial niches in relationship with the targeted disease and/or condition, such as subgingival plaque for investigating periodontitis, aim to offer the highest resolution of the actual community composition and diversity associated with the tissues that those diseases and/or conditions impact. Studies that aim to apply NGS strategies with robust bioinformatic workflows and curated databases, such as the application of DADA2 and *e*HOMD, while using the most representative samples are of extreme value and needed to fill current knowledge gaps in microbially associated diseases within the oral cavity in humans, such as gingivitis and periodontitis.

1.1.3 *The Anatomy of the Periodontium in Relationship to the Oral Microbiome*

The periodontium is primarily comprised of gingiva, periodontal ligament, cementum, and alveolar bone which act together to maintain normal tooth function and structural health. These tissues are each unique in their role of maintaining periodontal homeostasis. However, recent research has shown that pathologic changes that occur in one of these major periodontal tissues may have significant effects for the maintenance, repair, and/or regeneration of other periodontium tissues – resulting in 4 major stages of periodontal diseases: Stage I (mild disease), Stage II (moderate disease), Stage III (severe disease), and Stage IV (very severe disease)(6).

With respect to investigating microbially associated diseases in association with the periodontium, such as gingivitis and periodontitis, it is essential to understand the differences in the microenvironments associated with the tooth and periodontium. The biofilm found above

the gingival margin is mostly comprised primarily of aerobic or facultative anaerobic bacterial species due to an environment rich in nutrients provided by the host and the hosts saliva. Whereas, the biofilm within the subgingival pocket, below the gingival margin, is more enriched in facultative and obligate anaerobic species that are bathed in a serum exudate known as gingival crevicular fluid (GCF) that contains host mediators as well as anti-oxidative properties that increases, as measured by GCF Flow Rate, during inflammation(23). It has also been proposed that as the supragingival plaque accumulates and the biofilm matures above the gingival margin, particular species are able to invade the gingival pocket and remain viable – resulting in an origin of infection or dysbiosis within the subgingival pocket (23). However, it remains unclear which species are able to translocate from supragingival plaque and survive in this very different microenvironment within the human oral cavity. Although key etiological agents, such as *Porphyromonas gingivalis*, have been identified in periodontitis(24), it remains unresolved regarding which bacterial species or strains are driving gingivitis as well as which are associated with the link between the reversible gingivitis and non-reversible periodontitis disease states. Thus, studies that are able to apply high resolution of the oral and subgingival microbiome during the transition from health to dysbiosis, associated with gingivitis and/or periodontitis, are critical in order to identify which bacterial species are able to survive and benefit from the induced inflammatory state and may help identify key etiological agents associated with gingivitis and potentially the transition from gingivitis to periodontitis.

1.1.4 *Periodontitis and Gingivitis*

Periodontitis is an inflammatory disease that is associated with group of gram negative microorganisms and dysbiosis of the host tissue homeostasis that results in the destruction of the supportive tissues surrounding the tooth and result in progressive and irreversible

attachment loss of the periodontal ligament and alveolar bone. Together over time, this can even result in tooth loss if left untreated(6). The most recent global burden of disease study indicated that nearly half of the global population suffered from some form of oral condition. Of those major oral conditions measured as part of this study, periodontitis was shown to affect nearly 796 million people globally(25). The same measures assessed by the most recent National Examination and Nutrition Health Survey (NHANES) indicate this trend is consistent in adults in the United States(26). This disease is also positively correlated with age; thus, with increases in modern medicine and access to care, we can expect that both the prevalence and incidence of periodontitis will continue to increase in the coming years and decades(6).

Gingivitis, a milder and reversible form of periodontal disease, is classified as the localized inflammation of the gingiva tissues surrounding the tooth without attachment loss of the periodontal ligament or alveolar bone degradation. Gingivitis associated with dental plaque, or plaque induced inflammation, is the most common form of gingival disease and is often considered to be a precursor to periodontitis(6); although, not every person who has plaque induced gingivitis will go on to develop periodontitis. Even though a direct link has yet to be established between either a microorganism(s) and/or host mediator(s) between these periodontal disease states, repeated studies have shown that bacteria play a major etiological role in gingivitis and periodontal disease(7,12,24,27–31). Many studies have focused on the etiology and the etiological agents of periodontitis and have even resulted in the identification of a keystone pathogen *Porphyromonas gingivalis*(24). However, our understanding of the etiology of plaque induced gingivitis remains less clear, and little information exists on the direct microbial relationship between periodontal disease and gingivitis. Due to the fact that gingivitis and periodontitis are inherently linked, further investigation into the temporal changes

that occur in microbial diversity between gingivitis and periodontitis are critical in order to understand both the key etiological agents and etiological processes for these disease states associated with periodontal tissues.

1.1.5 *Experimental Gingivitis Model*

The plaque induced experimental gingivitis (PI-EG) model was first introduced by Loe et al.(31). The focus of this landmark study was to identify relationships between the different types of microbes and the onset of clinical inflammatory measures associated with plaque induced gingivitis using the novel Gingival Index (GI) and Plaque Index (PI) measures over a period of oral hygiene cessation(31). This was the first reported characterization of how the oral microbial community shifted towards dysbiosis in the absence of oral hygiene. Interestingly, this was also the first observation of human variation associated with PI-EG as the onset of clinical measures varied among individuals, with peak inflammation occurring for some as early as 10 Days without oral hygiene and others at 21 Days(31).

Future studies would refine these clinical measures as well as provide additional surrogates, such as Bleeding on Probing (BOP), Pocket Depth (PD), and Gingival Crevicular Fluid (GCF) flow rate/volume, for gingival health status(12,29,30,32,33). Incorporation of next generation sequencing (NGS) techniques into this model in more recent years has also helped provide deeper resolution and characterization into the community composition in varied states of gingiva health and disease(6,7,9,34). Together, these foundational studies provide a framework for investigating gingival inflammation associated with PI-EG in humans. This model continues to serve as a framework for current and future studies that aim to understand the unique temporal microbial-host interactions working to maintain homeostasis in a controlled manner within the human gingiva.

1.2 Human Variation in Clinical Inflammation

1.2.1 *Clinical Responder Phenotypes (CRPs) associated with plaque-induced gingivitis*

Trombelli et al. was one of the first studies reported in the literature to greatly detail the variation in clinical parameters associated with plaque-induced experimental gingivitis (PI-EG)(29). The authors describe the two subpopulations of humans exposed to plaque-induced experimental gingivitis as eliciting different clinical response measures (gingival index (GI), bleeding on probing (BOP)): High and Low, even though plaque deposits and accumulation rates were similar between the two groups. Since then, this observation of clinical responder types has been validated in additional PI-EG studies(15,35).

This observation was most recently confirmed in a recent study conducted at the University of Washington(15) in which our group identified as well as characterized a novel third clinical responder type: Slow. These different responder types are now referred to as Clinical Responder Phenotypes (CRPs) and consist of High (High-CRP), Low (Low-CRP), and Slow (Slow-CRP). Within this same study the group highlight the temporal onset of clinical inflammation measures (BOP, GI, GCF) and can be seen in **Figure 1A-D,** while key differences in microbial alpha and beta diversity among the CRPs are shown in **Figure 2A and 2B**.

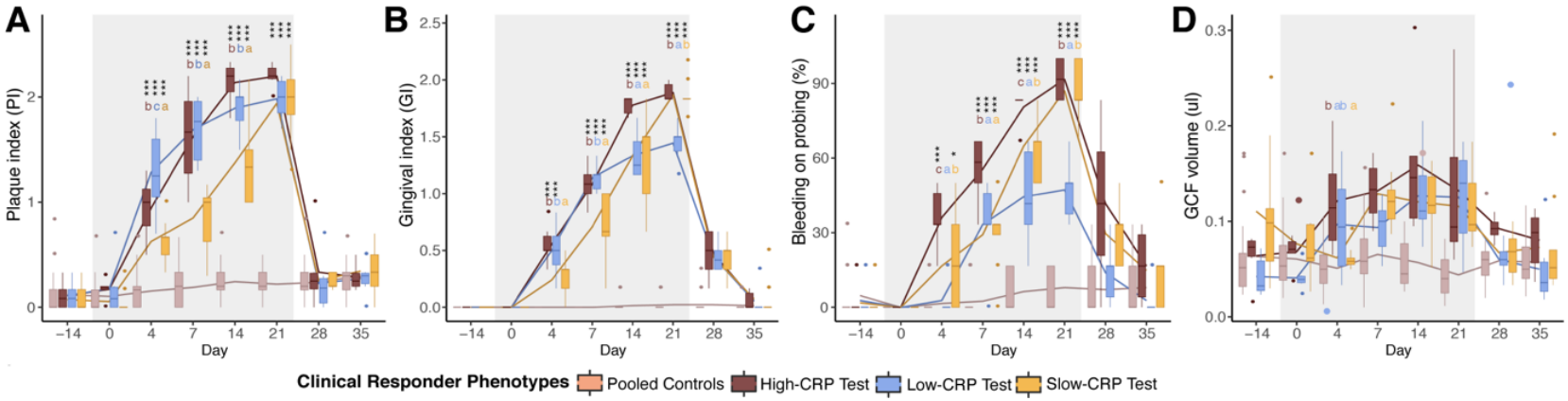

Figure 1 Clinical Measures for Gingivitis by Clinical Responder Phenotype. A) Visible Plaque Index. **B)** Gingival Index. **C)** Bleeding on Probing. **D)** Gingival Crevicular Fluid Volume. Grey Boxes indicate induction of inflammation phase (Day 0-21). Boxes represent data and medians ± interquartile ranges; whiskers and outliers > 1.5 IQR below (above) the 25th (75th) percentile. Statistics are between Clinical Responders by Day as well as between Respective Clinical Responders and Pooled Controls. Adapted from Previous Study: Figure 2, Human Variation in Clinical Inflammation by Bamashmous et al., (2021).

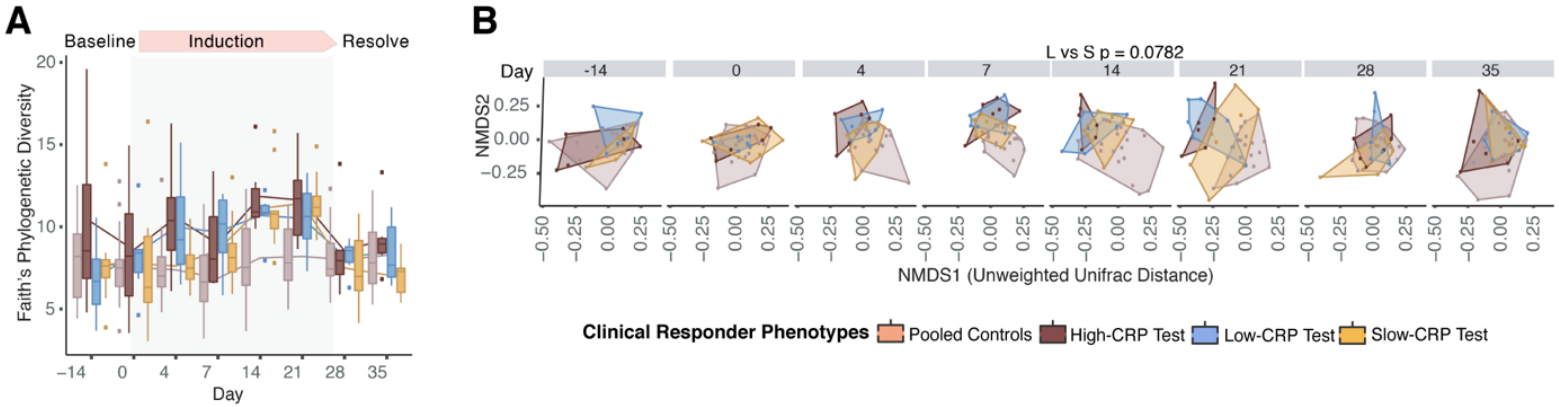

Figure 2 Microbiome Alpha and Beta Diversity by Clinical Responder Phenotype. A) Faiths Alpha Diversity by Clinical Responder Phenotype. Boxes represent 25% and 75% interquartile ranges with median values. Whiskers represent standard error. **B)** Principal coordinate analysis of beta diversity using unweighted NMDS distances. Adapted from Previous Study: Figure 5, Human Variation in Clinical Inflammation by Bamashmous et al. (2021).

A brief description of each CRP described in this study is provided:

- *High Clinical Responder Phenotype (High-CRP)*: During the induction phase of plaque induced inflammation (Day 0-21), clinical measures (BOP, PI, and GI) increased rapidly and were the highest among Responder types.
- *Low Clinical Responder Phenotype (Low-CRP)*: During the induction phase of plaque induced inflammation (Day 0-21), clinical measures (BOP, PI, and GI) were about half of the what the High Responders achieved, even though the rate of amount of plaque growth was very similar to the High Responder group.
- *Slow Clinical Responder Phenotype (Slow-CRP)*: During the induction phase of plaque induced inflammation (Day 0-21), clinical measures (BOP, PI, and GI) were similar to the High Responder group when peak inflammation was achieved (Day 21); however, there was a characteristic delay among clinical measures as well as in the rate of plaque growth and community maturation which is reflected in the observed delay of change in microbial community composition.

Results from Bamashmous et al. have greatly advanced our understanding of the changes in microbial diversity during the induction of inflammation associated with PI-EG(15). However, additional taxonomic characterization of the bacteria, specifically at the strain level, may help further elucidate unique and characteristic differences among Clinical Responder Phenotypes (CRPs) as well as identify associations between different strains and clinical response measures of gingival inflammation (BOP, GI, and GCF).

1.2.2 *Key Host Pro-Inflammatory Mediators during Gingival Inflammation*

The gingival crevicular fluid (GCF) within the subgingival pocket is rich in host immune and inflammatory mediators (chemokines, cytokines) that controls an immune-inflammatory state

that can maintain host-microbe homeostasis; however, in plaque induced gingivitis the rapid changes in host response to bacterial growth and maturation over time can be captured in humans through the experimental gingivitis model. Whereas in periodontitis, the host immune response has already become dysregulated and in turn likely further impacts bacterial growth and community composition within the subgingival plaque(36). In recent years, multiple biomarkers have been identified for assessing gingival health during microbially induced inflammation(37–42). Although there are some inconsistencies within the literature, interleukin-8 (IL-8), interleukin-6 (IL-6), tumor necrosis factor alpha (TNF-a), as well as interleukin-1 beta (IL-1b) are often seen as key pro-inflammatory host mediators that are indicative of active gingival inflammation associated with gingivitis and often also increased in periodontitis in addition to increased GCF volume and/or flow rate(43–45).

IL-8 is a potent chemoattractant cytokine and activator of neutrophils in inflammatory regions and is released from endothelial cells, gingival fibroblasts, neutrophils, monocytes, and phagocytes within the gingival crevice and facilitates the transit of neutrophils from the highly vascularized gingival tissue into the gingival crevice(46). IL-6 is a key regulatory cytokine that is involved in both in the acute innate immune response as well as recruitment of a more robust adaptive immune response which is often seen with chronic inflammation(47). TNF-a is produced by monocytes and macrophages in response to bacterial antigens and promotes the release of collagenases from gingival fibroblasts which results in localized tissue destruction(48). IL-1B also promotes osteoclastic activity and induction of tissue-degrading proteinases(49). Together these inflammatory host mediators elicit a pro-inflammatory response that affects the activities of leukocytes, osteoblast, and osteoclasts, and promotes tissue

remodeling process within the periodontium and are critical to assess when investigating the hosts immune response during plaque-induced inflammation within the oral cavity in humans.

1.2.3 *Machine Learning and the Oral Microbiome*

Machine Learning (ML) is a sub domain of artificial intelligence (AI) in which complex mathematical algorithms are automated in order to build mathematical models that are used to identify patterns in large data sets, predict outcomes, and/or make decisions with minimal human intervention or biases(50). The field of ML has been integral in healthcare AI in recent years by demonstrating impressive results in clinical decision support, patient monitoring, surgical assistance, patient care, and systems management(50). The application of ML in healthcare research, including dentistry, is also increasing as researchers aim to identify biomarkers for different diseases and/or conditions as well as factors associated with risk or severity of poor health outcomes. AI-based applications using ML in dentistry ultimately aim to streamline care, relieve the dental workforce from laborious routine tasks, increasing access to dental care at lower costs for the broader population, and eventually facilitate personalized, predictive, preventive, and participatory dentistry(51).

Given the variation in clinical inflammation associated with plaque-induced gingivitis in humans(15,29,31) is related to their severity and risk of inflammation and may have other unknown associations within an individual's systemic health, there is a need to be able to identify the different Clinical Responder Phenotypes (CRPs): High-CRP, Low-CRP, and Slow-CRP. Currently, the only method that exists for identifying the different CRPs is by temporally monitoring a patient's gingival health indices (i.e. BOP, GI) during oral hygiene cessation, usually for a period of 21 Days. This is both time consuming and costly research to perform. In addition, now that we have confirmed that there are these major differences in inflammatory

response to microbially-induced inflammation in humans, it is critical that the research community is able to account for this variation when testing products and or treatments as a patients CRP may be eliciting a confounding effect on the outcome being assessed and may even play a role in an individual's susceptibility to progress to more devastating disease states (i.e. gingivitis to periodontitis).

Lastly, ML can be applied to a variety of different data types from identifying patterns in written documents and radiographs to numerical measurements like the relative abundance of different taxonomy to clinical measures of different host mediators found in gingival crevicular fluid (GCF). Thus, the application of ML for identifying an individual's Clinical Responder Phenotype (CRP) may prove to be an essential tool in dentistry in order to identifying an individual's risk and severity of gingival inflammation and may even have broader implications on their overall systemic health.

Chapter 2. The Oral Contralateral Effect within the Human Oral Cavity During Experimental Gingivitis

2.1 Introduction

The link between oral and systemic health has become increasingly apparent from studies linking oral microbes found in dental plaque associated with oral diseases, specifically gingivitis and periodontitis, and systemic conditions such as endocarditis, bacterial pneumonia, type-2 diabetes, and even Alzheimer's(52,53). The most recent global burden of disease study indicated that nearly half of the global population suffered from some form of oral condition. Of those major oral conditions measured as part of this study, severe periodontitis was shown to affect nearly 796 million people globally(25). The same measures assessed by the most recent National Examination and Nutrition Health Survey (NHANES) indicate this trend is consistent in adults in the United States(26). Additionally, gingivitis, the less severe and reversible form of periodontal diseases and conditions, is considered a prerequisite for most forms of periodontal disease. Thus, as periodontal disease is positively correlated with age, we can predict that both the prevalence and incidence of gingivitis and periodontitis will continue to increase in the coming years and decades due to increases in modern medicine and access to care which are resulting in longer life expectancies(6). However, our understanding of the etiopathogenesis of these different gingival diseases, the transition from a single localized site of gingival inflammation to multiple sites within the mouth, as well as the progression from gingivitis to periodontitis, remain unresolved. Yet, by applying cutting edge next generation sequencing workflows and host mediator assays in order to investigate controlled microbial-induced inflammation and the hosts response in humans may help identify additional relationships and biomarkers associated with the onset and spread of gingivitis and subsequently periodontitis.

A recent study by Bamashmous et al.,(15) highlights that there are three major phenotypes that vary in host inflammatory response within humans revealed through a split-mouth plaque-induced experimental gingivitis (PI-EG) model. This model allows for the study of normal bacterial accumulation and maturation processes as well as the induced host inflammatory response in a controlled and reversible manner. Using robust host mediator data obtained from gingival crevicular fluid (GCF) (a serum exudate) and microbiome analysis using the most representative subgingival plaque samples, characterization of the temporal changes in microbial and host factors revealed key differential aspects of two distinct clinical inflammatory response phenotypes in humans that had been previously reported: High and Low, as well as uncovered and characterized a novel third responder phenotype: Slow. These host clinical responder phenotypes with varying degree and rates of inflammatory responses are now referred to as Clinical Responder Phenotypes (CRPs): High CRP (High-CRP), Low CRP (Low-CRP), and Slow CRP (Slow-CRP).

While our previous study focused on changes occurring within the test sites during plaque-induced inflammation over a period of 21 Days, the present study as part of this dissertation research project aimed to deeply characterize and investigate the longitudinal dynamics of observed contralateral changes on distant healthy teeth within the human oral cavity. Our analysis incorporates strain level microbiome analysis of subgingival plaque and host mediators (chemokines, cytokines) derived from GCF that highlight the highly coordinated, temporally delayed response between the inflamed test sites and healthy control sites in terms of host mediator alterations and microbial community shifts. Additionally, we determined this contralateral phenomenon varies accordingly with the onset of clinically observed inflammation observed within the three Clinical Responder Phenotypes respectively. Together

our data suggest that the observed contralateral changes in healthy sites are a result of the inflammatory changes that occur from microbial-induced inflammation occurring at distant test sites.

2.2 Study Design and Methods

2.2.1 *Human Induced Gingivitis Experiment*

The previous study methodology was established by Bamashmous et al.,(15) for the induction of reversible bacterial-induced inflammation via cessation of oral hygiene in humans. A study cohort made up of twenty-one generally healthy adults aged 18-35 years were consented and enrolled following the principles of the declaration of Helsinki. For inclusion, subjects had gingival health with no clinical signs of gingival inflammation at > 90% of sites at time of screening and had no signs of periodontal disease. The study included the following phases 1) Hygiene phase for two weeks prior to baseline (Day -14 – Day 0), 2) Gingivitis induction phase lasting for three weeks (Day 0 – Day 21), and 3) Resolution phase for two weeks (Day 21 – Day 35). In addition the incorporation of a split mouth design allowed for individual subjects to provide their own intra-oral controls over the duration of the study. During the experimental induction phase the subjects were given customized intraoral stents that prevented oral hygiene at the experimental (test) sites while regular brushing occurred across the entire time period on the control sites.

2.2.2 *Characterization of In Vivo Chemokine Responses during Experimental Gingivitis*

The previous study methodology was established by Bamashmous et al.,(15) in which local chemokine responsiveness was measured using gingival transudate, i.e. gingival crevicular fluid (GCF). Three test and control teeth were sampled without disrupting supragingival plaque by gentle insertion of sterile paper strips (Periopaper; Oraflow Inc., Smithtown, NY, USA) into the

gingival crevice. Samples from the test sites were pooled and placed immediately on ice and transported to the lab for processing. Samples from contralateral control teeth were also collected as controls for intra-individual comparisons. The volume of GCF samples was collected and immediately quantified as previously described(15). Concentrations of myeloperoxidase (MPO), an established marker of neutrophils (54), were quantified using a commercially available ELISA kit and simultaneous quantification of multiple chemokines was performed via a 40-plex chemokine bead-based multiplex assay (Bio-Plex Pro™ Human 40-plex Chemokine Panel; Bio-Rad Laboratories, Hercules, CA, USA) as previously described(15).

2.2.3 *Characterization of Microbial Changes in Response to Plaque Accumulation*

Subgingival plaque samples were collected in the previous study at each study visit from both control and test sides. Sterile paper points were inserted into the gingival sulcus of the six maxillary teeth for 30 seconds. At each study visit, a total of six samples per study side were collected and pooled and samples were transported to the lab on ice and then frozen at -80˚C until further analysis. DNA was extracted and 16S rRNA libraries as previously described(55,56). For DNA extraction negative controls were implemented by performing the DNA extraction protocol without plaque samples with either kit reagents only or kit reagents with the sterile paper points to assess for contamination. Quantitative real-time PCR was performed to determine the total bacterial load in each sequenced sample. A qPCR standard curve was generated from serially diluted *Fusobacterium nucleatum* ATCC 10953 genomic DNA as previously described(15).

Analysis of merged 300 bp paired-end reads (average length 450 bp) was performed as previously described(55,56) using the Quantitative Insights into Microbial Ecology 2

(QIIME2)(57) following the Divisive Amplicon Denoising Algorithm 2 (DADA2) pipeline workflow(21,22) to generate amplicon sequence variants (ASVs). Taxonomic assignment to classify ASVs was performed using the Human Oral Microbiome Database (HOMD 16S rRNA RefSeq v. 15.1)(11,20). Data were integrated into a single object using the "phyloseq" R package(58) and further analyzed.

2.2.4 *Variation in Clinical Gingival Inflammatory Responses*

Clinical data including plaque index (PI), gingival index (GI), bleeding on probing (BOP) were assessed at each timepoint as measures of clinical inflammation(31). All measurements were performed by a single, trained examiner using the same type of graded periodontal probes during the following study phases: health (Days -14 – 0), induction phase (Days 4, 7, 14 and 21), and resolution phase (Days 28, 35) as previously described(15). Inflammatory response phenotypes were determined using joint clinical data trajectories of gingivitis severity represented by GI and BOP in response to plaque accumulation represented by PI from Day 0 to Day 21 in the test sides using an implementation of k-means specifically design to cluster joint trajectories(59) with these three parameters as previously described(15).

2.2.5 *Statistical Analysis*

Statistical analysis was performed in the R suite using a variety of packages: including but not limited to: "ggpubr", "Rstatix", "Lme4", and "vegan" packages(60–63). The non-parametric Wilcoxon Rank Sum Test was used for pairwise comparisons of taxonomic levels and host mediators between Clinical Responder Phenotypes as well as over time. Linear regression was performed on sample means for both taxonomic levels and host mediators between Clinical Responder Phenotypes as well as over time. Adjusted P values were calculated using the False Discovery Rate (FDR) method.

2.3 Results

2.3.1 *Despite regular oral hygiene Control Sites Among Clinical Responder Phenotypes are not Static*

At the time of inclusion (Day -14) all study participants received a professional cleaning which aimed to normalize the oral health status across individuals. At baseline (Day 0), study subjects refrained from brushing on the test site of their mouth which were also were protected by a plastic stint, while the control site maintained regular oral hygiene with fluoride containing toothpaste for a period of 21 Days. Although no clinical inflammation was observed on the control sites among these generally healthy individuals over the induction period (Day 0-21), as measured by the Gingival Index (GI) and Bleeding on Probing (BOP) (**Figure 3C and 3E**), changes in both Gingival Crevicular Fluid (GCF) volume and Bacterial Load (**Figure 3G and 3I**) were observed on the control sites, although at a lower magnitude compared to test sites. Interestingly, bacterial load, which represents the number of 16S rDNA copies within a sample, increased among all Clinical Responder Phenotypes (CRPs) while Visible Plaque Index (VPI) (**Figure 3A**) remained rather stable over the induction period. These observations warranted further investigation into microbial diversity and host mediators changes previously reported among the different CRPs: High (High-CRP), Low (Low-CRP), and Slow (Slow-CRP)(15).

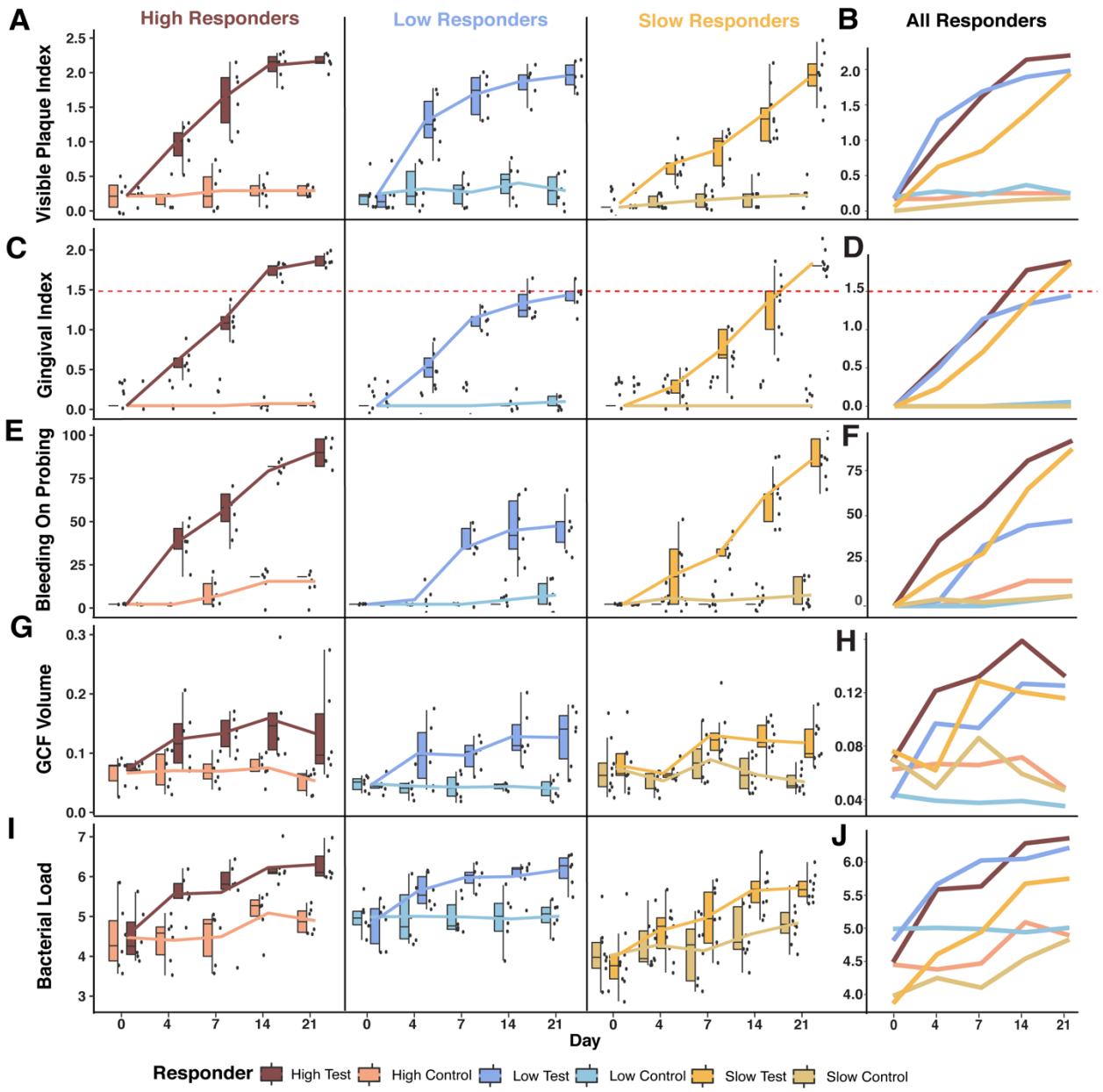

Figure 3 Clinical Parameters for Test and Control Sites During Experimental Gingivitis by Clinical Responder Phenotype. **A)** Visible Plaque Index (VPI) stratified by Clinical Responder Phenotype (CRP) over the induction phase (Day 0-21) with respective Controls. **B)** Linear Regression of mean VPI by CRP Test and Control over the induction phase. **C)** Gingival Index (GI) stratified by CRP over the induction phase with respective Controls. Red dashed line represents a GI value of 1.5 which represents significant clinical inflammation within gingiva tissues. **D)** Linear Regression of mean GI by CRP Test and Control over the induction phase. **E)** Bleeding on Probing (BOP) stratified by CRP over the induction phase with respective Controls. **F)** Linear Regression of mean BOP by CRP Test and Control over the induction phase. **G)** Gingival crevicular fluid (GCF) volume stratified by CRP over the induction phase with respective Controls. **H)** Linear Regression of mean GCF volume by CRP Test and Control over the induction phase. **I)** Bacterial Load (16S copies) stratified by CRP over the induction phase with respective Controls. **J)** Linear Regression of mean Bacterial Load by CRP Test and Control over the induction phase. Boxes represents data and medians ± interquartile ranges; whiskers and outliers > 1.5 IQR below (above) the 25th (75th) percentile. Trend lines represent loess regression mean values across all time points. Statistical analysis was performed using the non-parametric Wilcoxon-Rank Sum Test adjusted by FDR. Significance level indicated by asterisks. Significance levels: ns = non-significant, *P < 0.05, **P ≤ 0.01, and ***P ≤ 0.001.

2.3.2 *Changes in Subgingival Plaque Diversity is Observed in Healthy Control Sites and Varies by Clinical Responder Phenotype*

Microbial diversity was assessed for Clinical Responder Phenotypes (CRPs) in comparison to their respective controls. Alpha Diversity analysis measured by Observed Amplicon Sequence Variants (ASVs) and Shannon Indices (**Figure 4A**) illustrate changes occurring on the control and test side among CRPs. Bray Curtis dissimilarity index was also assessed for each CRP with respect to the baseline (Day 0) and highlights a detectable increase in dissimilarity over the induction period among all CRPs control sites (**Figure 4C**) their respective test sites (**Figure 4B**). Principle coordinate analysis using Weighted Unifrac distances indicates a more gradual shift in beta diversity within the control sites among High-CRPs and Slow-CRPs in comparison with the changes observed among their respective test sites, with Low-CRP having a more stable community across control sites. (**Figure 4D**).

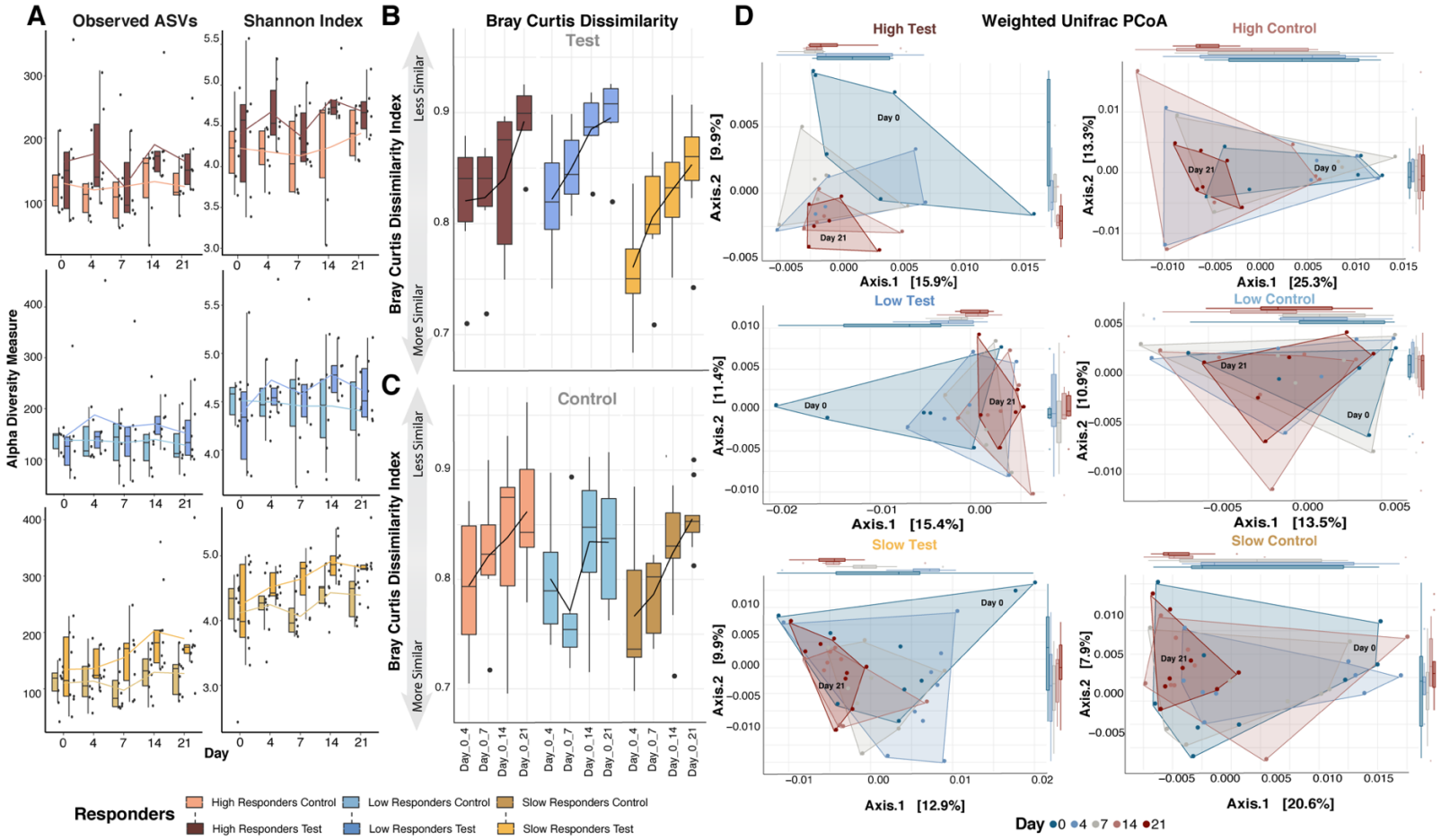

Figure 4 Microbiome Diversity Shifts in Healthy Controls. A) Alpha diversity measured by Observed Amplicon Sequence Variants (ASVs) and Shannon Indices. Statistical Significance calculated by Wilcoxon Rank Sum Test Adjusted by FDR. **B)** Bray-Curtis Dissimilarity Index for each Responder Type Test compared to Day 0 over the Induction phase (Day 0-21). **C)** Bray-Curtis Dissimilarity Index for each Responder Type Controls compared to Day 0 over the Induction phase (Day 0-21). **D)** Beta Diversity calculated using Weighted Unifrac Distances and visualized by Principal Coordinate Analysis for each Responder Type with Test and Controls. Marginal Boxplots indicate PC1 and PC2 over the induction phase (Day 0-21). Boxes represents data and medians ± interquartile ranges; whiskers and outliers > 1.5 IQR below (above) the 25th (75th) percentile. Trend lines represent loess regression mean values across all time points. Dashed lines represent test sites and solid lines represent control sites. Statistical analysis was performed using the non-parametric Wilcoxon-Rank Sum Test adjusted by FDR. Significance level indicated by asterisks. Significance levels: ns = non-significant, *P < 0.05, **P ≤ 0.01, and ***P ≤ 0.001.

2.3.3 *A Unique Responder Dependent Microbiome Composition Shift is Evident within Healthy Control Sites*

Relative abundance at the phylum level was assessed by Clinical Responder Phenotype (CRP) with their respective controls (**Figure 5**). The mean relative abundance for the top six major phyla which were assigned to the most amplicon sequence variants are highlighted (**Figure 6A**). Differences in the general trends across phyla, specifically increase in gram-negative associated Bacteroidetes and decrease in gram-positive associated Firmicutes, and CRPs between the test and control sites are observed and indicate these changes among control sites are not universal nor normal maturation of the subgingival biofilm community after a deep cleaning as Actinobacteria increase over the induction phase (Day 0-21). A z-scored heatmap of relative abundance at the genus level was stratified by Gram stain designation (positive and negative) as well as by members of the candidate phyla radiation (CPR) (**Figure 6B**). Here we observe that during maturation of the community on the test side a number of genera are enriched resulting in induced inflammation on the test sites among the various CRPs are also observed within the respective controls during the Induction phase (Day 0-21), specifically: Selenomonas, Aggregatibacter, Porphyromonas, Treponema, Tannerella, Alloprevotella, Prevotella, and Saccharibacteria. Most of these members are within the Firmicutes and Bacteroidetes phyla. Thus, we implemented the inverse Firmicutes/ Bacteroidetes Ratio (*i*FBR) as a measure of dysbiosis of subgingival plaque where increased Bacteroidetes are associated with disease and increased Firmicutes are associated with homeostatic health. We observed a decrease in Firmicutes across all CRPs test and control sites over the induction period, while Bacteroidetes increased across all CRPs test and control sites (**Figure 6C**). In addition, we observed that the *i*FBR shift on the test sites among High- and Low-CRPs occurs by Day 4 of

the Induction phase (Day 0-21); whereas the test site among Slow-CRPs is delayed and does not occur until Day 7 – which is characteristic of this responder phenotype as previously reported(15). Interestingly, we observed that the *i*FBR shift on the control sites among High-CRPs had a similar shift at Day 7 of the induction phase, whereas control sites among Low- and Slow-CRPs had a similar *i*FBR shift, but not until Day 14. However, when comparing the *i*FBR for each of the CRPs with their respective controls (**Figure 7**) we observed that only the High- and Slow-CRPs control sites significantly changed over the Induction phase.

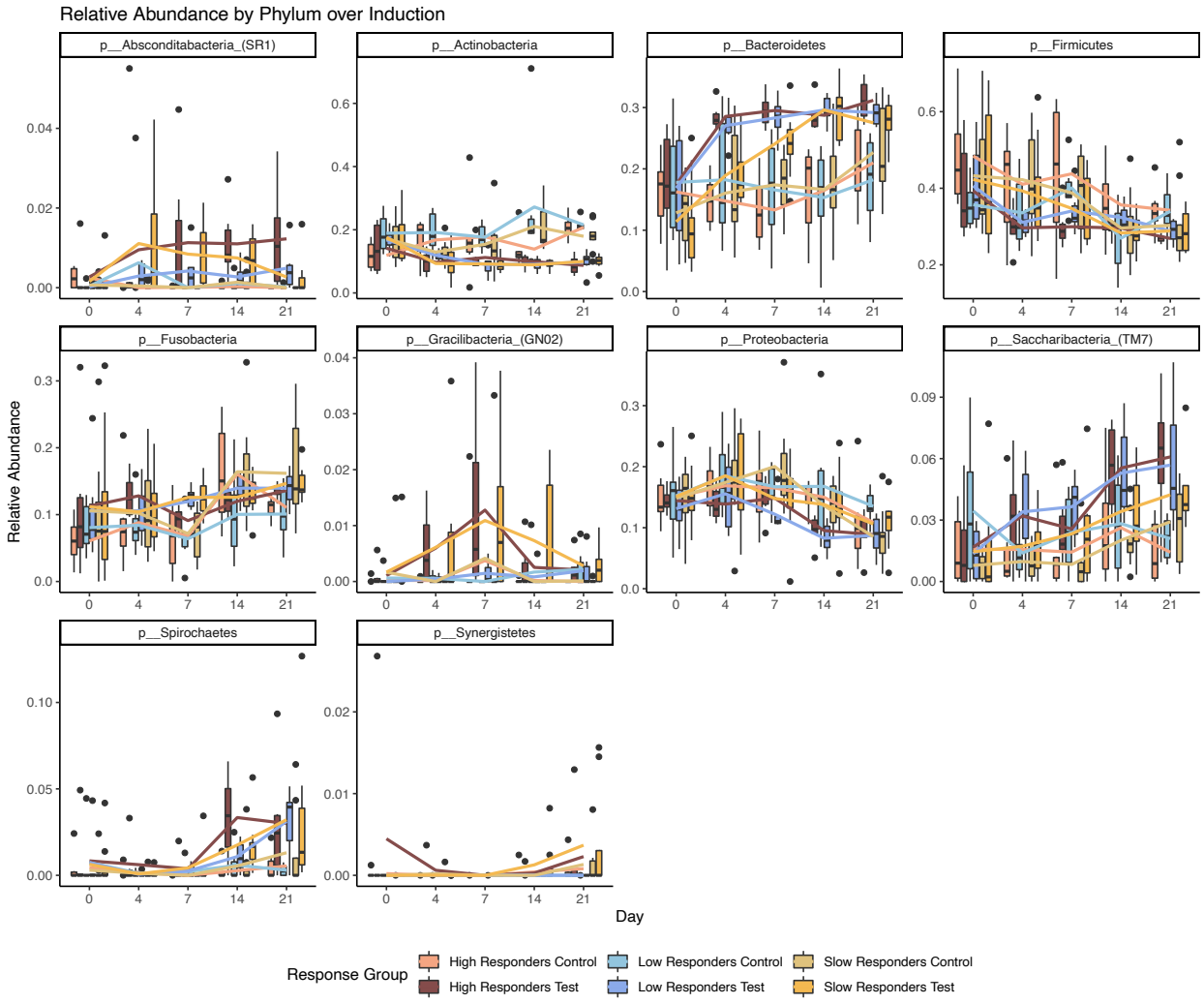

Figure 5. Relative abundance by Phylum Over the Induction Phase (Day 0-21) by Clinical Responder Phenotype with Respective Controls. Boxes represents data and medians ± interquartile ranges; whiskers and outliers > 1.5 IQR below (above) the 25th (75th) percentile. Trend lines represent loess regression mean values across all time points. Dashed lines represent test sites and solid lines represent control sites. Statistical analysis was performed using the non-parametric Wilcoxon-Rank Sum Test adjusted by FDR (Data not shown).

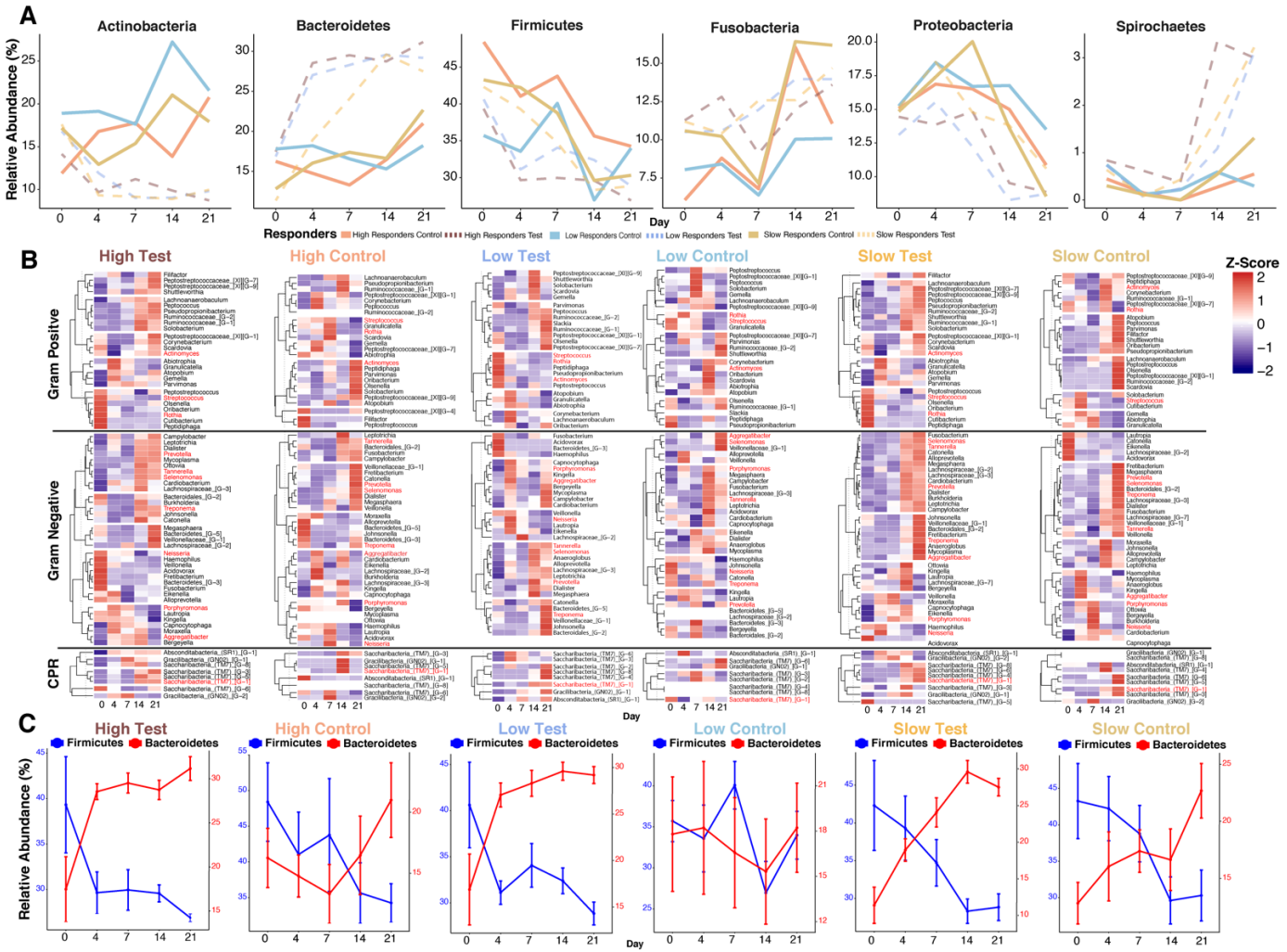

Figure 6. Phylum and Genus Level Relative Abundance by Clinical Responder Phenotype. A) Percent relative abundance of agglomerated count data at the phylum level for the 6 most abundant phyla. Dashed lines represent test sites and solid lines represent control sites by clinical responder phenotype (CRP). **B)** Z-scored heatmaps of relative abundance using agglomerated data at the genus level. Heatmaps were then organized and grouped based off gram stain designation including Gram-positive, Gram-negative, as well as by members of the Candidate Phyla Radiation (CPR). Key bacteria from each gram classification are highlighted in red to compare across different responder test and control sites. Most are members of the Firmicutes and Bacteroidetes phyla or are associated with periodontal disease. **C)** Percent relative abundance of agglomerated data at the phylum level grouped by Responder test and control sites over the induction period. Trend lines represent mean values across all time points. Whiskers represent standard error.

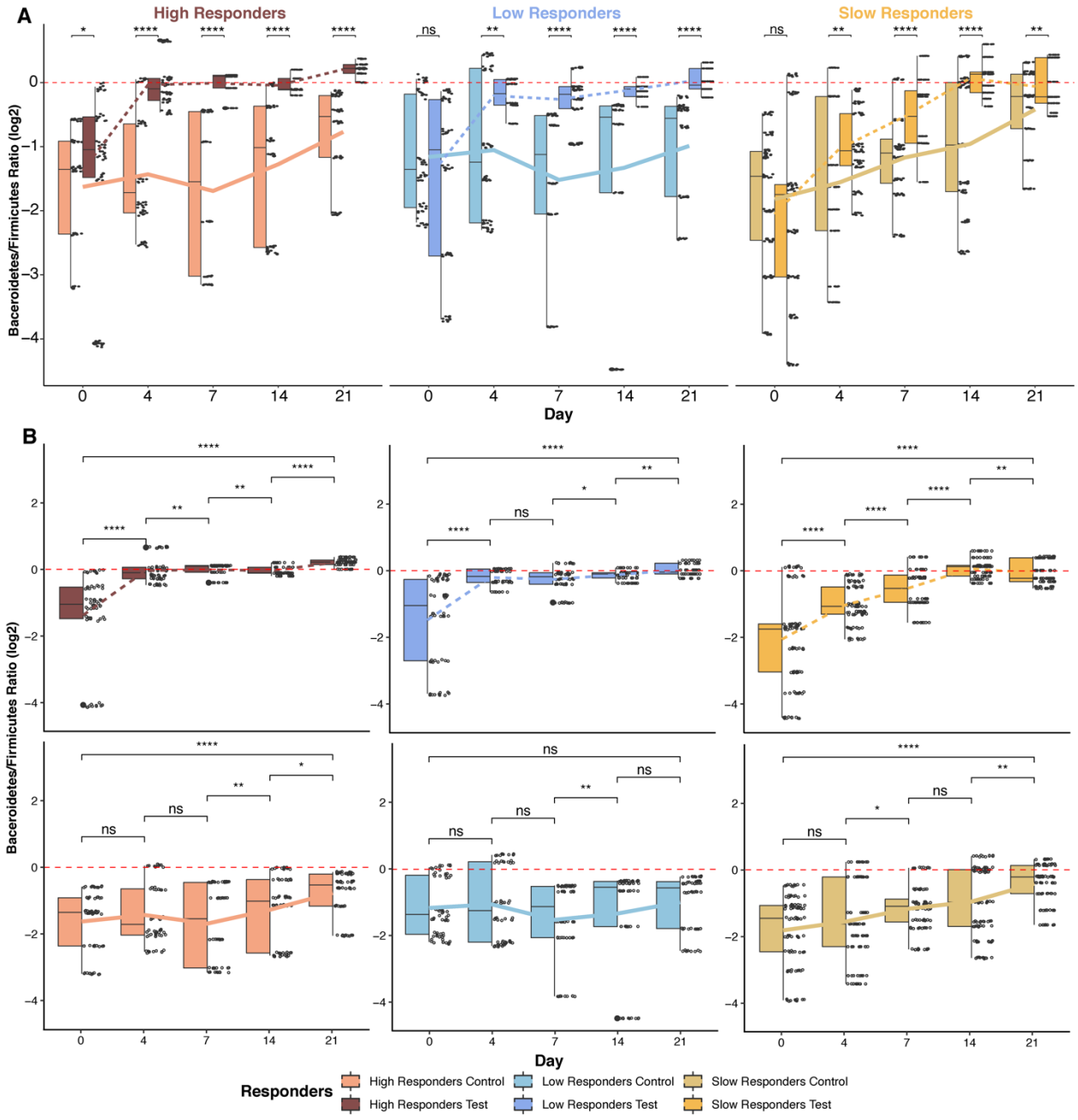

Figure 7. The Inverse Firmicutes/Bacteroidetes Ratio (iFBR) by Clinical Responder Phenotype. The inverse Firmicutes/Bacteroidetes Ratio (*i*FBR) was generated using relative abundance data agglomerated to the phylum level. The dashed red line represents 0 on the Log2 scale as a reference across plots. **A)** Represents the *i*FBR for test and control sites among the different Clinical Responder Phenotypes (CRPs) with their respective controls. **B)** Represents the *i*FBR for test and control sites stratified by CRP. The dashed red line represents 0 on the Log2 scale as a reference across plots. Boxes represent data and medians ± interquartile ranges; whiskers and outliers > 1.5 IQR below (above) the 25th (75th) percentile. Trend lines represent loess regression mean values across all time points. Dashed lines represent test sites and solid lines represent control sites. Statistical analysis was performed using the non-parametric Wilcoxon-Rank Sum Test adjusted by FDR. Significance level indicated by asterisks. Significance levels: ns = non-significant, *P < 0.05, **P ≤ 0.01, and ***P ≤ 0.001.

2.3.4 *Amplicon Sequence Variants are Detected Contralaterally between Test and Control Sites among Study Subjects*

Amplicon sequence variants (ASVs) represent strain level diversity for 16S rDNA gene sequencing data(21). A total of 3,509 ASVs from enriched genera identified on the test sites during induced inflammation were examined for contralateral detection at the strain level, including: Selenomonas (19 Species, 433 ASVs), Aggregatibacter (7 Species, 155 ASVs), Porphyromonas (10 Species, 414 ASVs), Treponema (23 Species, 233 ASVs), Tannerella (3 Species, 118 ASVs), Alloprevotella (7 Species, 285 ASVs), Prevotella (38 Species, 1602 ASVs), and Saccharibacteria (8 Species, 269 ASVs) (**Figure 8D**). Using a presence/absence heatmap of the 3,509 ASVs of enriched genera, 29 (0.83%) ASVs were contralaterally detected among High-CRPs with 6/6 subjects having had a contralaterally detected ASV (**Figure 8A**). 15 (0.43%) ASVs were detected with 3/6 Subjects among Low-CRPs having had a contralaterally detected ASV (**Figure 8B**). 89 (2.5%) ASVs were contralaterally detected in 8/9 Subjects among Slow-CRPs having had a contralaterally detected ASV (**Figure 8C**). Thus, there is variation in the contralateral detection of ASVs among different CRPs; however, H- and Slow-CRPs seem to have higher rates of contralaterally detected ASVs, which corresponds with the observed VPI and Bacterial Load (**Figure 3A and 3I**) as well as with the characterization of the different CRP previously reported(15).

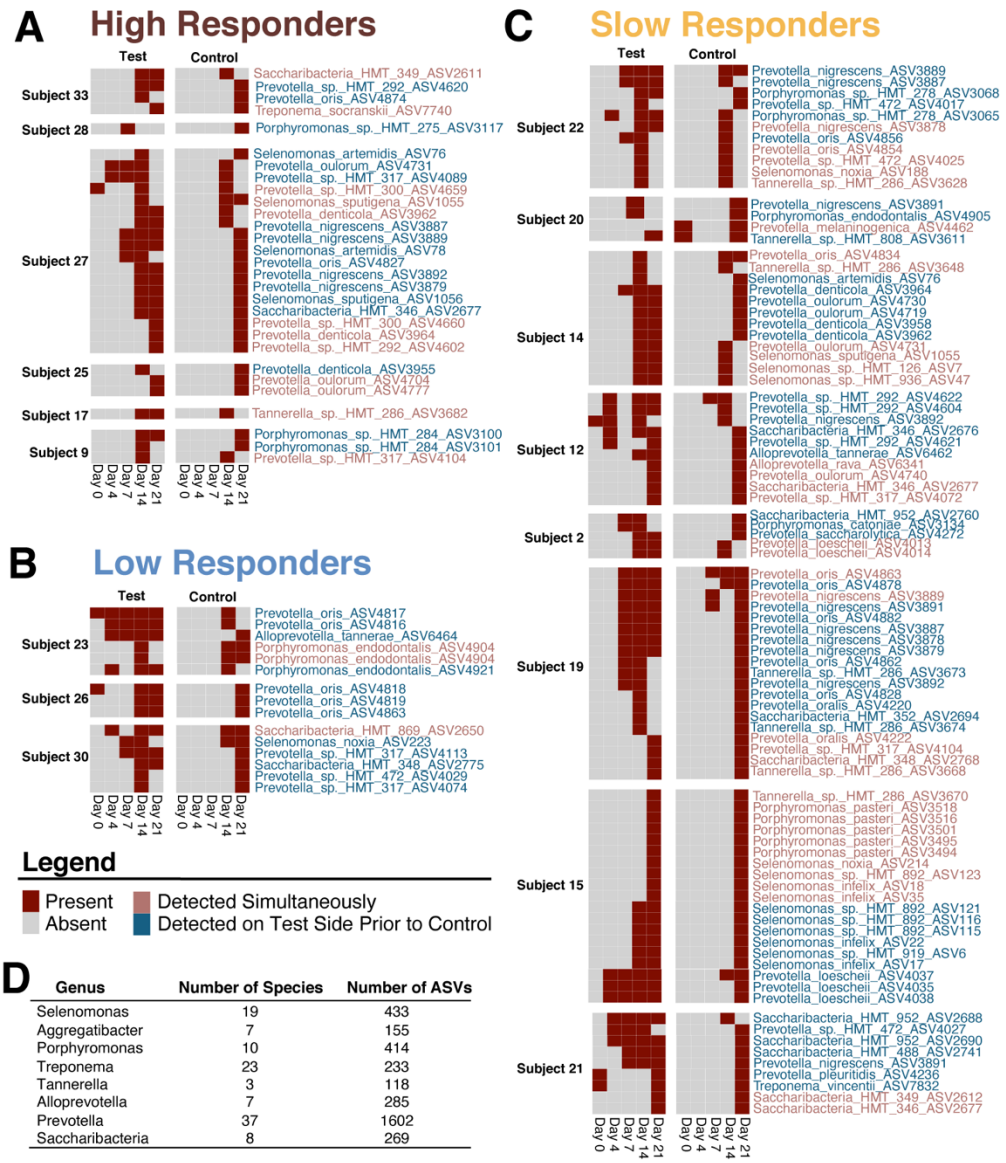

D

Genus	Number of Species	Number of ASVs
Selenomonas	19	433
Aggregatibacter	7	155
Porphyromonas	10	414
Treponema	23	233
Tannerella	3	118
Alloprevotella	7	285
Prevotella	37	1602
Saccharibacteria	8	269

Figure 8. Contralaterally Detected Amplicon Sequence Variants (ASVs) within Subgingival Plaque during Induced Inflammation. ASV level data was converted to a presence-absence matrix and plotted as a heatmap in order to identify contralateral detection between test and control sites over the induction period (Day 0-21) by Clinical Responder Type (CRT). Gram negative and CPR genera that were enriched in test sites were selected for this analysis resulting in a total of 3,509 ASVs. Red text represents ASVs that were detected simultaneously between test and control sites by subject. Blue text represents ASVs that were detected in test sites prior to any detection in control sites by subject. **A)** High CRT by subject resulted in 29 (0.83%) ASVs that were contralaterally detected. 6/6 subjects had a contralaterally detected ASV. **B)** Low CRT by subject resulted in 15 (0.43%) ASVs that were contralaterally detected. 3/6 subjects had a contralaterally detected ASV. **C)** Slow CRT by subject resulted in 89 (2.5%) ASVs that were contralaterally detected. 8/9 subjects had a contralaterally detected ASV. **D)** A Table of the Gram negative and CPR genera used in this analysis, the number of species detected within those genera as well as the number of corresponding ASVs for each genus.

2.3.5 *Amplicon Sequence Variants by Subjects among Clinical Responder Phenotypes during Experimental Gingivitis*

The number of Amplicon Sequence Variants (ASVs) varies greatly by study subject; however, we observe trends in the number of ASVs between test and control sites by subject and Clinical Responder Phenotypes (CRPs). We for the first time report the number of ASVs within subgingival plaque over an entire experimental gingivitis study stratified by CRP – including the hygiene phase (Day -14-0), induction phase (Day 0-21), and resolution phase (Day 21-35) for (**Figure 9A-C**). We observed that the High-CRPs had an average of 166 ASVs at inclusion in the study (Day -14), an average of 191 and 141 on test and control sites respectively over the Induction phase (Day 0-21), and 117 ASVs on average during the Resolution phase (Day 28-35). Low-CRPs had an average of 125 ASVs at inclusion in the study (Day -14), an average of 169 and 102 on test and control sites respectively over the Induction phase (Day 0-21), and 115 ASVs on average during the Resolution phase (Day 28-35). Slow-CRPs had an average of 135 ASVs at inclusion in the study (Day -14), an average of 159 and 107 on test and control sites respectively over the Induction phase (Day 0-21), and 113 ASVs on average during the Resolution phase (Day 28-35). Interestingly, the Slow-CRPs (**Figure 9C**) had the highest number of ASVs on average over the Induction phase, despite having a delayed VPI, Bacterial Load, and community maturation as measured by Bray-Curtis dissimilarity (**Figure 3A and 3I, Figure 4B and 4C**).

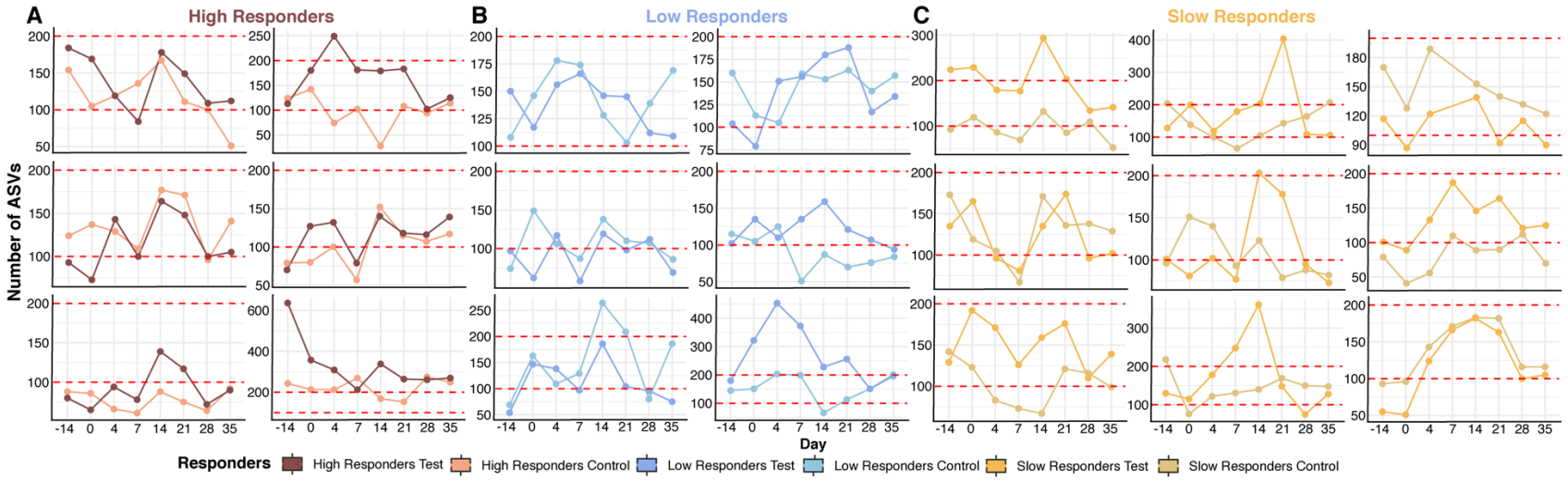

Figure 9. Amplicon Sequence Variant Trajectories for Test and Control Sites by Clinical Responder Phenotypes. The number of ASVs was calculated for the test and control sites respectively and plotted by individual subject over the duration of the experiment (Day -14- 35). Red dashed lines at 100 and 200 are for reference. **A)** High Clinical Responder Type (CRT), (N=6). **B)** Low CRT (N=6). **C)** Slow CRT (N=9).

2.3.6 *Induced Inflammation in Test Sites Results in Changes in Chemokine Profiles in Control Sites across Clinical Responder Phenotypes*

A panel of 41 host mediators within gingival crevicular fluid (GCF) were examined among Clinical Responder Phenotypes (CRPs) test and control sites over the Induction phase (Day 0-21). A row-wise z-scored heatmap of chemokines by CRP test and control sites (**Figure 10A**) was clustered using the k-means algorithm and resulted in 12 unique clusters. Individual clusters, which represent the trajectories of the standard deviation from the mean, were then plotted by CRP test and control sites in order to investigate the temporal dynamics and similarly behaving chemokines over the Induction phase (**Figure 10B**). Here it was again evident that the control side was not static and not randomly changing as there were multiple mediators showing similar patterns that varied by responder types and time compared to the test side. Of particular interest is cluster 5 which contains several pro-inflammatory mediators (TNFa, IL-6, and IL8) and seem to share similar trajectories over the induction phase among the different CRPs – peaking by Day 4 in the High- and Low-CRP controls yet delayed in the Slow-CRP which doesn't peak until Day 7 in the control sites (**Figure 10A and 10B**). A limited number of these mediators however were detected to significantly change on the control sites among Slow- and Low-CRPs despite no signs of clinical inflammation being observed on these brushed sites (**Figure 3C and 3E**). Slow-CRP showed significant decrease in CCL1 over the Induction phase and this trend was observed in 7 out of 9 individuals within this group (**Figure 10C**). Slow-CRP also showed a significant decrease in MIF over the Induction phase among 8 out of 9 individuals within this group despite increasing significantly on the test side across CRPs as previously shown by Bamashmous et al.(15)(**Figure 10D**). Low-CRPs showed significant decrease in IL-10, among 4 out of 6 individuals within this group, while 6 out of 6 individuals

showed a decrease in TNF-a over the Induction phase (**Figure 10E and 10F**). Thus, we were able to detect subclinical changes in host mediators in healthy control sites in the absence of localized inflammation as well as revealing the variation of these changes among CRPs.

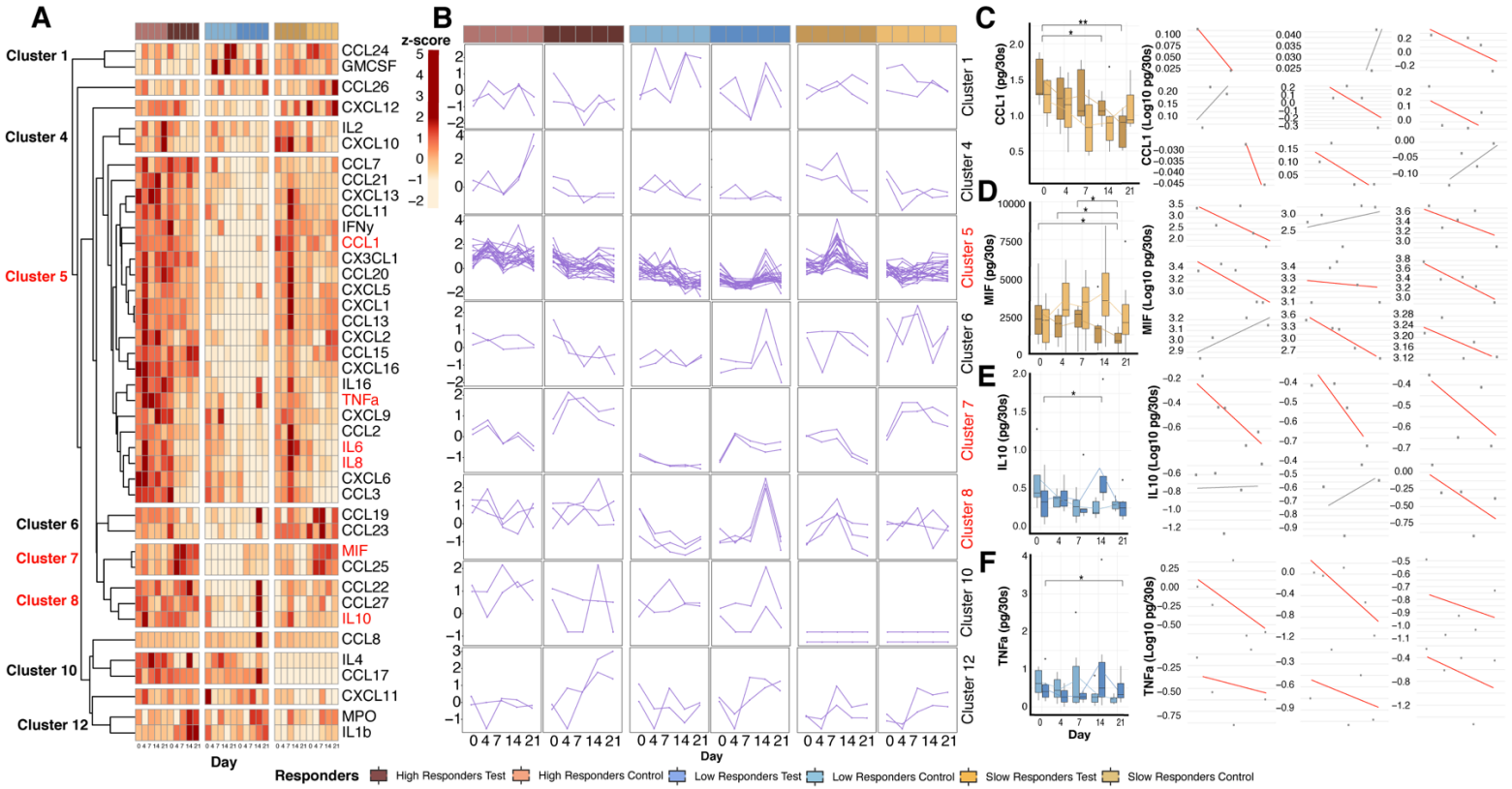

Figure 10. Host Mediators Dynamics Among Clinical Responder Phenotypes. A) Z -scored heatmap of host inflammatory mediators (41) clustered using the k-means algorithm for Clinical Responder Phenotypes (CRP) test and control sites over the Induction phase (Day 0-21). Chemokines that change on the control side with statistical significance are highlighted in red. **B)** Standard deviation from the mean chemokine value within respective clusters were plotted over the Induction phase (Day 0-21). **C)** CCL1 in Slow Responders showed similar patterns to changes occurring on the test side within the control side and 7 out of 9 individual subjects had the same negative trend in decreasing CCL1 concentrations over Induction (Day 0-21). **D)** IL10 in Low Responders showed similar patterns to changes occurring on the test side within the control side and 4 out of 6 individual subjects had the same negative trend in decreasing IL10 concentrations over Induction (Day 0-21). **E)** MIF in Slow Responders showed similar patterns to changes occurring on the test side within the control side and 7 out of 9 individual subjects had the same negative trend in decreasing MIF concentrations over Induction (Day 0-21). **F)** TNF-a in Low Responders showed similar patterns to changes occurring on the test side within the control side and 6 out of 6 individual subjects had the same negative trend in decreasing TNF-a concentrations over Induction (Day 0-21). Boxes represent data and medians ± interquartile ranges; whiskers and outliers > 1.5 IQR below (above) the 25th (75th) percentile. Trend lines represent loess regression mean values across all time points. Trendlines for Chemokines by subject represent the linear regressed mean over the induction phase (Day 0-21). Statistical analysis was performed using the non-parametric Wilcoxon-Rank Sum Test adjusted by FDR. Significance level indicated by asterisks. Significance levels: ns = non-significant, *P < 0.05, **P ≤ 0.01, and ***P ≤ 0.001.

2.3.7 *Temporal Resolution of Subgingival Microbiome and Host Mediator Shifts by Clinical Responder Phenotype*

Having established both microbial and host mediators are changing in the control sites and these changes are related to their respective responder types, we sought to investigate if there were any temporal coordination of these changes within healthy control and test sites. A z-scored heatmap of log-fold change of a filtered panel of 37 chemokines was examined among Clinical Responder Phenotype (CRP) control sites over the induction phase (Day 0-21) (**Figure 11A-C**). We observed that a majority of chemokines had the greatest change among High-CRPs by Day 4; whereas L- and Slow-CRPs had the greatest change by Day 7 over the Induction phase. IL-8, IL-6, and TNF-a, which are potent inflammatory mediators identified to have a significant effect within test sites during induced inflammation during experimental gingivitis(15), were investigated within control sites among the different CRPs (**Figure 11D-F**). Here we observe that the peak response on the control site is by Day 4 among High-CRPs and Day 7 among L- and Slow-CRPs. This corresponds to the start of clinically observed inflammation (**Figure 3C and 3E**) as well as elevated GCF volume (**Figure 3G**) among the test sites of the different CRPs, which is the result of plaque accumulation and community maturation (**Figure 3A and 3I, Figure 4B and 4C**). The contralateral shift in host mediators among control sites within the different CRPs precedes a contralateral shift in the microbial diversity (**Figure 11G-I**) and taxonomic structure. The inverse Firmicutes Bacteroidetes ratio (*i*FBR) highlights the dysbiotic shift within the test sites among the different CRPs with the shift occurring by Day 4 in High- and Low-CRPs and by Day 7 in Slow-CRP during the Induction phase (Day 0-21). However, we observed that the contralateral shift in the *i*FBR among High-CRPs occurs at Day 14; whereas Low- and Slow-CRPs do not see a shift until Day 21. Together, this data represents the

subgingival contralateral effect that highly likely results from locally induced inflammation occurring elsewhere in the mouth and having a subclinical effect on the hosts mediators and microbiome within healthy sites and varies among the different Clinical Responder Phenotypes associated with plaque-induced experimental gingivitis.

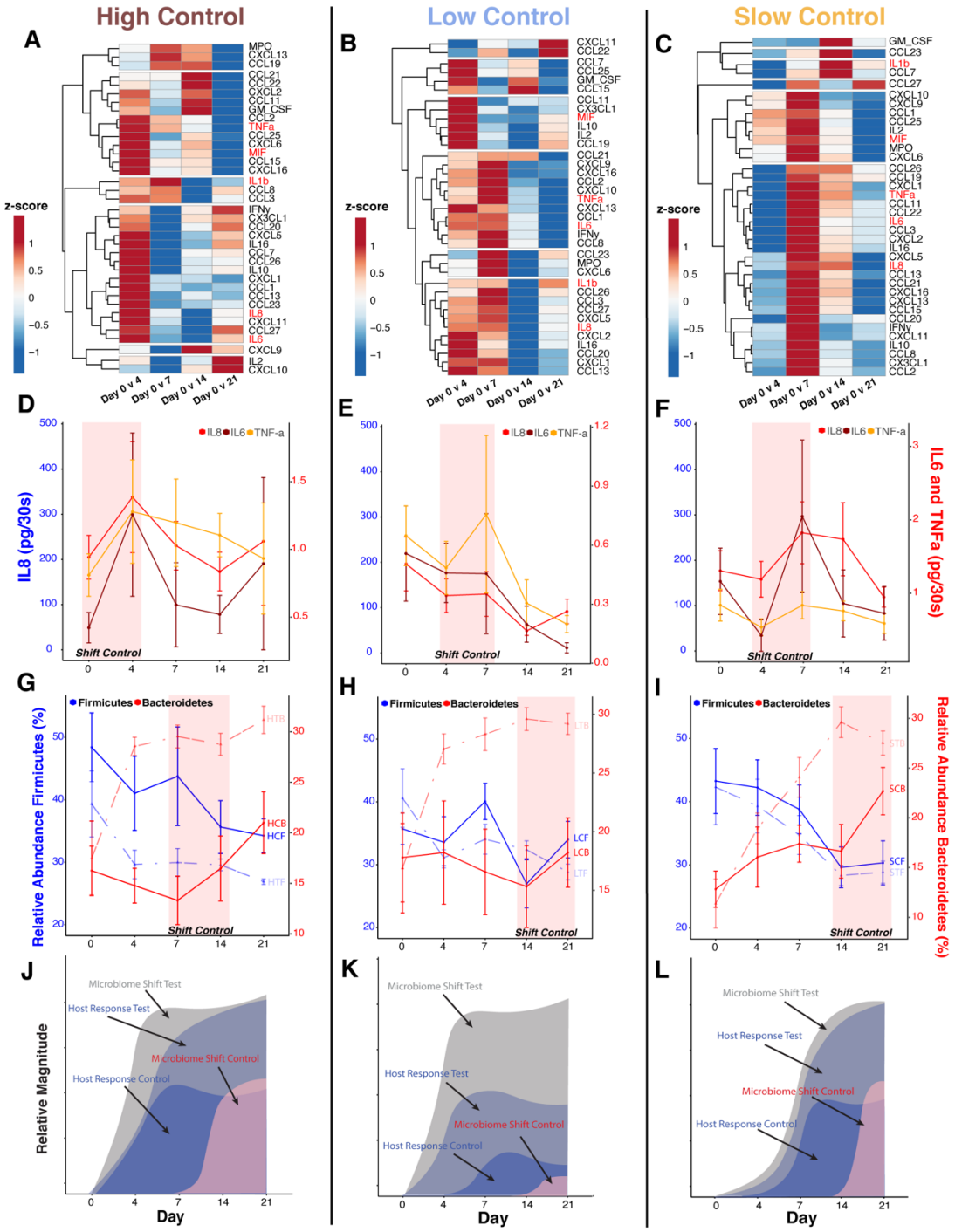

Figure 11. Temporal Resolution of the Oral Contralateral Effect. A-C) Z-scored heatmap of log fold change of chemokines compared to baseline (Day 0) among different Clinical Responder Phenotype (CRP) control sites. Key inflammatory mediators are highlighted in red text. D-F) IL-8 (Left y-axis), IL-6, and TNF-a (Right y-axis) among CRP control sites. Red box highlights shift in host mediators in control site. **G-I)** Percent Relative Abundance of Firmicutes (Left y-axis) and Bacteroidetes (Right y-axis) using agglomerated data at the phylum level. Trendlines represent the mean value. Solid lines represent control sites and dashed lines represent test sites. Labels represent CRP test and control sites by Phylum (i.e. HTF – High Test Firmicutes, HCF – High Control Firmicutes). Red boxes represent the dysbiotic shift in control sites. **J-L)** Graphical interpretation of the temporal relationships of the microbiome and host mediators between test and control sites over the induction phase (Day 0-21).

2.4 Discussion

The plaque-induced experimental gingivitis model provides a robust and controlled way to investigate host-microbe interactions in association with microbial-induced inflammation within humans. A recent study by Bamashmous et al.,(15) provided the most comprehensive look at these interactions within the human oral cavity by investigating host responses through visible clinical parameters and host mediators to normal plaque accumulation and community maturation of the subgingival plaque microbiome. The present study aims to build upon the recent characterizations which highlight the variation among different Clinical Responder Phenotypes (CRPs), including the previously identified High (High-CRP) and Low (Low-CRP) responders in addition to the novel Slow responder (Slow-CRP), by focusing on the changes observed within intra-oral healthy control sites across individuals among the respective responder groups during plaque-induced inflammation associated with experimental gingivitis.

Visible Plaque Index (VPI or PI) is a relative measure of plaque accumulation occurring above the supragingival margin and serves as a clinical surrogate marker for plaque accumulation occurring within the subgingival pocket(31) which is not readily measurable by clinicians. In the present study, healthy control sites maintained normal oral hygiene throughout the duration of the study and VPI remained rather stable with only a significant increase observed at later time point within the Slow-CRP during the Induction phase (Day 0-21) (Day 14 $p_{adj} = 0.014$; Day 21 $p_{adj} = 0.004$) (**Figure 3A**). Additionally, we observed significant changes in the Slow-CRP control sites with respect to the total number of 16S rDNA copies ($p_{adj} = 0.012$), which serve as a quantitative measure of the subgingival Bacterial Load (**Figure 3I**). We also observed significant changes with respect to clinical inflammatory indices, specifically BOP, at later timepoints within the High-CRP (Day 14 $p_{adj} = 0.001$; Day 21 $p_{adj} = 0.001$) on the

control side during the Induction phase (**Figure 3E**). Although no statistically significant changes in Gingival Crevicular Fluid (GCF) volume were detected, we observed increasing trends within the High- and Slow-CRPs control sites during the inflammatory Induction phase (Day 0-21) (**Figure 3G**) which is indicative of a response by the host(64). Together these significant changes observed within healthy control sites, albeit at a lower magnitude than test sites, warranted a deeper investigation in order to better understand how or why contralateral healthy sites that had maintained normal oral hygiene, showed detectable and significant increase in BOP, VPI, and Bacterial Load with trends of increasing GCF volume.

We initially sought to investigate the alpha and beta diversity measures between test and control sites in more detail since we had observed fluctuations in microbial richness across CRPs (**Figure 4A**) as well as similar shifts in community composition (**Figure 4D**) between test and control sites over the Induction phase. These changes within the subgingival microbiome are most evident when investigating the Bray-Curtis Dissimilarity index across test and control sites among the different CRPs. This dissimilarity index highlights the relative change in community composition over the Induction phase (Day 0-21) compared to baseline (Day 0) (**Figure 4B and 4C**). Together, multiple measures of microbial diversity highlight that the subgingival microbiome community within healthy control sites are changing despite maintained normal hygiene and seem to be correlated to changes in diversity observed with respective test sites among the different CRPs. Thus, we can speculate that these changes in diversity within healthy control sites may somehow be a result of changes that are being induced within test sites occurring contralaterally in the mouth.

In order to understand these observed changes in microbial diversity among the different CRPs we completed a taxonomic analysis by stratifying CRPs with their respective controls

over the Induction phase. Using the mean relative abundance measures for the top 6 most abundant phyla we plotted relative abundance trajectories between test and control sites over the Induction phase (**Figure 6A**). The behavior observed across most of these phyla indicate similar patterns in relative abundance between test and control sites among different CRPs, although in a delayed manner within healthy control sites. Investigation of the Actinomyces phyla observed within the healthy control sites indicates that this was not merely normal maturation of the subgingival biofilm community as these changes were opposite of what was observed within contralateral test sites (**Figure 6A)**. Most evident were trends observed among the two most abundant phyla observed in this study – Firmicutes and Bacteroidetes. Interestingly, we observed a decrease in Firmicutes, which are normally associated with commensalism and health within the human oral cavity, within test and control sites across CRPs during the Induction phase. We also observed the simultaneous increase in Bacteroidetes, which are normally associated with dysbiosis and disease within the human oral cavity, over the same time period (**Figure 6A and 6C**). These results suggest that subgingival plaque within healthy control sites undergo similar shifts in community composition and taxonomic diversity in a delayed manner as observed in localized sites of inflammation occurring contralaterally in the mouth, despite maintained normal oral hygiene.

Additionally, it has been well established within gut microbiome research in humans that the Firmicutes/Bacteroidetes ratio (FBR) is a useful indicator of health and microbial dysbiosis within the human gut, with an increased ratio of Bacteroidetes being associated with health and an increased ratio of Firmicutes being associated with dysbiosis (65–67). As previously discussed, most taxonomic assignments identified in the present study belonged to two major phyla, Firmicutes and Bacteroidetes. However, in the oral cavity, Firmicutes are generally

associated with commensalism or health, while Bacteroidetes are associated with dysbiosis or disease(11). Thus, applied an inverse Firmicutes/Bacteroidetes ratio (*i*FBR) as an index for subgingival community health/dysbiosis in humans in which a Firmicutes dominant community (*i*FBR < 0) is representative of health and a Bacteroidetes dominant community (*i*FBR $\geq$ 0) is representative of dysbiosis (**Figure 7**). Our results indicate the *i*FBR is indicative of a major community shift when investigating the subgingival plaque community as we observed a rapid increase in *i*FBR within High- and Low-CRP test sites over the Induction phase, with a delayed increase in *i*FBR among Slow-CRP test sites – all of which correlate with the temporal increase in supragingival plaque accumulation (VPI) and clinical inflammatory markers (GI, BOP) among the different CRPs test sites (**Figure 1A-C**).

Interestingly, when we applied this *i*FBR index to healthy control sites we observed significant changes and similar shifts towards dysbiosis as observed in test sites among the different CRPs (**Figure 7**). This was most evident in the High- and Slow-CRPs in which both groups show a significant increase in Bacteroidetes and decrease in Firmicutes over the Induction phase compared to baseline (High-CRP $p_{adj} > 0.001$; Slow-CRP $p_{adj} > 0.001$) with the High-CRP eliciting a rapid increase in *i*FBR while the Slow-CRP had a delayed increase in *i*FBR within respective healthy control sites (**Figure 7**). Notably, there was no significant increase in *i*FBR within the Low-CRP control sites, which may be related to the fact that this responder phenotype does not have a significant increase in clinical indices (GI, BOP) or VPI and does not illicit the same level of inflammation within test sites in comparison to the other Clinical Responder Phenotypes (**Figure 1B and 1C**).

Investigating the taxonomic changes using relative abundance measures among the different CRPs and their respective controls indicates that there are non-universal changes

occurring within the subgingival communities between test and control sites over the Induction phase (Day 0-21) (**Figure 5, Figure 6A**). Since all study participants received a professional cleaning at the time of inclusion (Day -14), we sought to ensure that these observed taxonomic and diversity changes within healthy control sites were not just normal maturation of the subgingival plaque community. Although our results indicate there are some shared trends over time in between test and control sites among the different CRPs at the phylum level (i.e. Firmicutes and Bacteroidetes), not all observed changes track between test and control sites – specifically with respect to the Actinobacteria phyla (**Figure 6A**). Additionally, the 2-week Hygiene phase (Day -14-0) where all teeth were brushed likely allowed for the normal maturation of the subgingival plaque community after a professional cleaning which is supported by the non-significant differences we observed in both alpha and beta diversity measures between CRPs at baseline (Day 0) (**Figure 2A and 2B**). Together, these taxonomic and diversity microbiome data suggest that the observed changes in relative abundance within healthy control sites are not just normal community maturation after a professional cleaning as we would expect these changes to be consistent across all Clinical Responder Phenotypes over the same period as observed with respect to the Hygiene phase.

Due to the fact that we observed contralateral changes in microbial (**Figure 4**) and taxonomic diversity, at both the phylum and genus levels (**Figure 5**, **Figure 6A and 6B**), within healthy control sites across the different CRPs, we aimed to investigate if these changes in diversity are a linked to changes occurring contralaterally in the mouth within the test sites of the different CRPs. It has even been proposed in the literature that a particular strains of bacteria can be associated with different levels of disease severity (68,69). Thus, we aimed to identify if a particular strain represented by an amplicon sequence variant (ASV), which represents strain

level diversity in 16S rDNA sequence data, could be identified within individuals among the different CRPs test and control sites over the Induction phase. We detected nearly 12,000 ASVs across 21 individuals over a 7-week study. This enabled tracking of an individual's total strain level dynamics between test and control sites over the induction phase for the first time (**Figure 9**). We then aimed to narrow our focus on gram-negative bacteria which are often associated with oral disease, including genera like Porphyromonas and Prevotella within the Bacteroidetes phylum, during the Induction phase. This analysis revealed several strains that were either simultaneously detected between test and control sites (**Figure 8A-C,** *Red*) or were detected in the test site prior to detection on the control site (**Figure 8A-C,** *Blue*) over the Induction phase within individuals across all CRPs. This further supports the notion that the increases in microbial diversity observed in healthy control sites among the different CRPs over the Induction phase may be a direct result of plaque accumulation occurring within test sites and provides a unique signature for detecting dysbiotic associated strains for the first time in association with development of gingivitis. Although we highlight the detection of strains in test sites prior to or simultaneously in healthy control sites, we also detected strains that were detected in healthy control sites prior to detection in test sites. Ultimately, these results highlight the dynamics of subgingival microbial colonization within the human oral cavity. Future studies that aim to apply deeper sequencing strategies, such as whole-genome shotgun (WGS) DNA sequencing, may help further elucidate strain level differences between strains detected in dysbiotic test and contralateral healthy sites.

In addition to the contralateral changes detected within the subgingival microbiome, we sought to identify if any host mediators were significantly changing within healthy control sites over the Induction phase. This resulted in only a few host mediators that were identified to

significantly change within healthy control sites from the 41 that were assessed (See Methods). Interestingly, statistically significant changing host mediators were only detected in Low- and Slow-CRP control sites and none within the High-CRP group (**Figure 10C-F)**. We then applied an alternative strategy to look at temporal trends in host mediators utilizing a row-wise-z-scored changes of host mediator values over the Induction phase within test and control sites for the different CRPs (**Figure 10A**). This analysis highlights High-CRPs who have a high host mediator response within test sites also have a high host mediator response within their respective controls; Low-CRPs who have a low host mediator response within test sites also have a low host mediator response within their respective controls; and Slow-CRPs who have similar levels of host mediators within test sites approaching that of the High-CRP also have a host mediator response within their respective controls. Interestingly, control sites for the different CRPs show some of the largest deviations in host mediator values(**Figure 3G**).

Understanding how different host mediators change during induced inflammation was of interest as the panel of 41 host mediators assessed in the previous study included multiple pro- and anti-inflammatory markers (IL-6, IL1-B, MIF, IL-10, IL-4) as well as some markers for neutrophil migration (TNF-a, IL-8) and bone homeostasis (CCL5, CCL20, CCL3, CCL2). Thus, we sought to identify if any of these host mediators behaved similarly over the Induction phase within the different CRPs. To assess this, we applied the k-means clustering algorithm which independently clustered chemokines based on their measured values over the Induction phase. This resulted in 12 unique clusters, with 8 of those clusters containing more than one host mediator. To better investigate the dynamics of these clusters we plotted the standard deviation from the mean host mediator value (**Figure 10B**). This revealed several host mediators that shared similar patterns over the Induction phase. Of particular interest is cluster

5 which contains potent pro-inflammatory mediators, including: IL-6, IL-8, and TNF-a. When we investigated the cluster 5 dynamics for the different CRP control sites over the Induction phase, we observed that cluster 5 peaks as early as Day 4 in the High-CRP and by Day 7 in the Slow-CRP control sites (**Figure 10B**). Additionally, macrophage migration inhibitory factor (MIF), within cluster 7, was observed to peak by Day 4 across all CRP test sites yet is only observed to peak by Day 4 in the High-CRP and Day 7 in the Slow-CRP control sites, with no notable variation observed within the Low-CRP controls sites. In addition MIF was clustered with CCL25 which has also been shown to drive the migration of immune cells to sites of mucosal inflammation(70). Interestingly, cluster 8 contains the anti-inflammatory chemokine IL-10, which peaks at Day 14 on the test site within Low-CRPs (**Figure 10B**) and may be a mechanism in which the Low-CRP are able to modulate their inflammatory response (15). Ultimately, this analysis revealed that there are groups of host mediators that seem to be coordinated within the respective CRP test and control sites and warrants further investigation in order to better understand why and how these host mediators behave in similar manner during plaque induced inflammation.

Logically, we then tried to identify what may be driving the contralateral changes within healthy control sites among the different CRPs between the microbiome and the host mediators. Because our stratified host mediator analysis revealed several host mediators that seem to share similar dynamics over the Induction phase, we implemented a z-scored heatmap of log-fold-change host mediator values compared to baseline (Day 0) to better highlight when these host mediators were changing within control sites among the respective CRPs (**Figure 11A**). Surprisingly, these results show that most host mediators that were assessed as part of this study show the greatest level of change from Day 0 to Day 4 within the High-CRP and Day 0 to Day

7 within the Slow-CRP which is consistent with the overall delay in the slow responders. However, distinct temporal changes are less evident within the Low-CRP control sites with major changes being observed between baseline and Day 4 as well as Day 7 (**Figure 11A**). This analysis also revealed that key pro-inflammatory mediators IL-6, IL8, and TNF-a peak within control sites among the High-CRP by Day 4, whereas they do not peak in the Low- and Slow-CRP until Day 7. This was unexpected as there was no significant plaque accumulation (VPI) nor clinical inflammation (GI, BOP) observed within any healthy control sites early on within the Induction phase across all CRPs (**Figure 3**). However, there were significant changes in VPI, GI, and BOP occurring within test sites within the respective CRPs as early as Day 4 in the High- and Low-CRP and as early as Day 7 in the Slow-CRP. This suggests that the host response to plaque-induced inflammation occurring within test sites is likely resulting in a increase of pro-inflammatory mediators within healthy control sites contralaterally in the mouth and is correlated with the degree of gingival inflammation in observed within test sites among the different CRP, despite maintained normal oral hygiene. This would suggest that localized sites of inflammation may have effects beyond observable sites of inflammation in the human oral cavity. This is of great interest as multiple studies in the literature have continued to identify links between oral gingival diseases, like periodontitis, and other systemic conditions, such as endocarditis, in humans. This may offer a novel way to investigate the non-localized effects of plaque-induced inflammation and host-microbe interactions in humans and warrants further investigation.

Lastly, we sought to determine if a shift within the subgingival microbiome community among test and control sites, represented by the inverse Firmicutes/Bacteroidetes ratio (*i*FBR), was at all related to shift in host mediators we observed within contralateral healthy control

sites. This analysis highlights a significant shift in *i*FBR towards dysbiosis (increase Bacteroidetes) within all test sites across CRPs between Day 0 and Day 4, although delayed in magnitude within the Slow-CRP until later during the Induction phase (**Figure 7B**). A significant shift in the *i*FBR was also observed between Day 7 and Day 14 within the High- and Low-CRP and a similar shift between Day 14 and Day 21 within the Slow-CRP control sites (**Figure 7B**). This is further evident when we look at the relative abundance of the Firmicutes and Bacteroidetes phyla over the Induction phase within the different CRP control sites (**Figure 11G-I**). This suggest that a shift within the subgingival microbiome towards dysbiosis among different CRP test sites results in an induced host-response that is detected simultaneously in healthy control sites contralaterally in the mouth- - although most evident in the High- and Slow-CRP and less evident in the Low-CRP. This host response detected in healthy control sites precedes a similar dysbiotic shift within healthy control sites among CRPs that occurs later during the Induction phase, despite maintained normal oral hygiene. A graphical interpretation of the magnitude and temporal relationship between the shift in microbiome and host mediators within test and control sites for each CRP is shown in **Figure 11** (**J-L**). This illustrates that the observed oral contralateral effect seems to be correlated with the temporal severity associated with CRP test sites: High-CRPs have an increased host response with rapid increase in GI and BOP by day 4 and results in an increased contralateral effect, Low-CRPs have a low host response modulating their GI and BOP by Day 7 and results in a less evident contralateral effect, and Slow-CRP have a delayed response but by Day 14 have an elevated GI and BOP and results in an increased but delayed contralateral effect.

When we look at the totality of our results from this recent plaque-induced experimental gingivitis study we can make several conclusions: First, there are significant changes in both

microbial diversity and host mediators occurring in contralateral healthy control sites in the mouth among all CRPs during the Induction phase (Day 0-21). Second, contralateral changes in host mediators occurring in the control sites among the CRPs occur in the absence of significant plaque accumulation (VPI) and or any significant signs of clinical inflammation as measured by Gingival Inflammation (GI) and Bleeding on Probing (BOP) (**Figure 3**). Third, we can conclude that changes being induced due to plaque accumulation and community maturation results in a shift in *i*FBR within test sites and is driving the host changes in the test sites. We can then observe changes in in host mediators within healthy control sites contralaterally in the mouth. Importantly, this analysis highlights that a contralateral shift in host mediators within healthy control sites precedes a similar dysbiotic shift (*i*FBR) within healthy control sites that is correlated with the different CRPs during the Induction phase. Together indicating that localized plaque-induced inflammation associated with experimental gingivitis may have broader subclinical effects on otherwise healthy tissues elsewhere in the human oral cavity beyond the visibly inflamed site(s).

In conclusion, we provide multiple layers of evidence of a contralateral effect within the human oral cavity, specifically in which microbial-induced inflammation results in changes in both host mediators and microbial diversity in the absence of clinically detectable inflammation and plaque accumulation in otherwise generally healthy tissues. Although reported in other human systems, this EG model in has allowed the controlled induction of inflammation and temporal monitoring of the contralateral changes to. Characterization of this contralateral effect indicates this is not just normal subgingival plaque maturation and that the magnitude of the contralateral effect varies by Clinical Response Phenotype (CRP), which is correlated with observations in clinical indices, subgingival microbiome diversity, and host mediators observed

within respective CRP test sites. Most notably, we for the first time show how healthy tissues are temporally affected, with respect to host mediators and subgingival microbiome, due to localized plaque accumulation and maturation that triggers gingival inflammation elsewhere in the human mouth – representing a major advance in oral health research.

Chapter 3. Using Machine Learning to Predict Risk and Severity of Microbially-Induced Inflammation

3.1 Introduction

Identifying a patient's risk of disease allows healthcare professionals to develop and implement effective screening, prognosis, and treatment planning for their patients. For example, individuals with a family history of cancer are considered to be at a higher risk of getting cancer at some point in their lifetime compared to those without incidence of cancer within their family health history(71). Thus, individuals who are considered high risk of getting cancer are often screened earlier in life and with greater frequency in order to identify the cancer as early as possible. This is of extreme importance for improving patient health outcomes as survival rates associated with cancer are often the highest when the cancer is detected and treated in the earliest stages in comparison to later stages and metastasis(72). In addition to family history, biomarkers, such as host mediators like chemokines, are also widely used to assess a patient's risk of developing cancer as well as predict the severity of the disease if they were to get it (73,74). Advances in technology and public health research in recent years have rapidly improved our ability to identify these different biomarkers as well as additional risk factors for a variety of human associated diseases. Although the application of predicting an individual's likelihood or risk of developing a particular disease has been limited to more devastating disease types, such as cancer, prediction strategies has begun to become incorporated across the healthcare spectrum in recent years(75).

Machine Learning (ML) is a sub domain of artificial intelligence (AI) in which complex mathematical algorithms are automated in order to build mathematical models that are used to identify patterns in large data sets, predict outcomes, and/or make decisions with minimal human intervention or biases(50). The field of ML has been integral in healthcare AI with

respect to clinical decision support, patient monitoring, surgical assistance, patient care, and systems management(50). Most recently, ML strategies have played a critical role in identifying disease severity and outcomes for individuals infected with SARS-CoV-2 as well as identifying important host mediators that differ among those who died and those who survived infection – helping pinpoint key host factors to monitor during diagnosis and treatment(76,77). The application of ML across healthcare research, including dentistry, has increased in recent years as researchers aim to identify biomarkers for different diseases and/or conditions as well as risk factors associated with disease severity and poor health outcomes. AI-based applications in dentistry using ML will ultimately streamline care, relieving the dental workforce from laborious routine tasks, increase health at lower costs for the broader population, and eventually help facilitate personalized, predictive, preventive, and participatory dentistry(51).

There are a variety of mathematical models and bioinformatic tools that are publicly available and reported to identify risk of disease and severity and/or predict health outcomes within literature(78–80). However, these all generally follow the same overall approach and is summarized as follows: First, a dataset must have a powered sample size in which results represents the entire study population. If this key criterion is met, the dataset is then split into two separate data sets in which the first training set and often larger set is used to train the model, while the second often smaller test set is used to test the model. The training and testing of a model can go through a number of iterations in which the model is refined based on a number of mathematical assessments unique to each approach in order to improve its overall sensitivity and specificity in identifying the desired outcome of interest, such as risk of developing cancer or inflammation associated with plaque-induced gingivitis. Finally, once a model is trained, refined, and tested an additional data set, ideally from another independent

study and/or population, is used to validate the model and its ability to confidently predict the desired outcome of interest.

One of the most robust ML models used in prediction is the Random Forest Machine Learning algorithm(81). This approach, like others, relies on the use of rich datasets that contains a large enough number of samples in order to represent an entire study population. However, in reality these types of data sets contain large variability, or imbalanced data, as well as are limited in oral health research due to the challenges, expense, and time associated with studying humans. The Random Forest ML algorithm aims to specifically improve prediction using these types of imbalanced data sets by applying random sampling and variable selection (i.e. species, chemokines) using unweighted voting via a random network of decision trees. These decision tree networks are repeated hundreds to thousands of times - eventually growing a "forest". As the forest grows, eventually becoming stable, variables within these decision trees are identified as part of the algorithm and are assessed in their ability to predict the desired outcome of interest also known as classification within for the Random Forest model. This helps identify or narrow the focus on significant variables within the data set being used to train the model. These significant variables are then referred to as Variables of Importance (VOI) and are identified by the Random Forest algorithm, usually by assessing a multi-way importance plot of the Mean Decrease Accuracy, which represents an estimate in loss in prediction performance when a variable is omitted from the training set, and Mean Decrease Gini, which represents node impurity and highlights how important a variable is across the decision tree network. The model can then be refined to exclude extraneous variables that are not identified as VOI in order to improve accuracy and reduce misclassification within the model (i.e. prediction of the desired outcome, such as risk and or severity of plaque-induced inflammation).

Reducing misclassification improves the predictive power of the model and is often assessed by investigating the bootstrapping variable represented by the out-of-bag (OOB) estimate of error rate(82).

To begin to develop a Random Forest model, a data set is partitioned in which some of the data is used to train the model and the remaining data is used to evaluate the model. Once the model is trained and refined as previously discussed, the model then uses the remaining partitioned data set to test the accuracy of the model. This results in an output known as a receiver operator characteristic (ROC) curve that assess sensitivity over specificity. The area under the curve (AUC) for the ROC curve represents a single value between 1.0 and 0.0 in which the accuracy of the model is obtained. A Random Forest model with an AUC value of 1.0 is ideal as this suggest that the model is able to predict the desired outcome 100% of the time. While an AUC value of 0 is not ideal and suggest that the Variables of Importance are reciprocating the actual outcomes 100% of the time. The worst-case scenario is a Random Forest model with an AUC of 0.5 which is indicative that the model has no discriminatory capacity and is often used as an empirical benchmark. Although there is no hardline of what a successful predictive model AUC value for a ROC curve is, the following is a general consensus within the literature: AUC 0.50-0.60 = failure, 0.60-0.70 = poor, 0.70-0.80 = fair, 0.80-0.90 = good, and 0.9-1.0 = excellent(83).

ML strategies can also be applied to a variety of different data types from written documents to radiographs as well as numerical values, including: the relative abundance of different taxonomic measures, clinical measures, and host mediators found within gingival crevicular fluid (GCF). In a recent experimental gingivitis study at the University of Washington by Bamashmous et al.(15), the group robustly and temporally characterize the

variation in gingival inflammation within the human population based on these variables. These differences in variation and risk of gingival inflammation are now referred to as Clinical Responder Phenotypes (CRPs): High-CRP, Low-CRP, and Slow-CRP, and result in different levels of severity of gingival inflammation, temporal onset of gingival inflammation, and have even been confirmed with similar rates in additional experimental gingivitis data sets (Unpublished). Some individuals are at a higher risk of eliciting an inflammatory response to dental plaque accumulation and have even shown signs of clinical inflammation as early as 4 days without brushing (High-CRP). While other individuals can accumulate significant amounts of dental plaque, yet they are able to modulate their inflammatory response (Low-CRP) – representing a lower risk of gingival inflammation severity. Currently, the only way to diagnose an individual's CRP is to subject them to the experimental gingivitis protocol. Thus, we sought to use microbiome and host mediator data collected at time of inclusion (Day -14) in order to evaluate if we could predict an individual's CRP using the most representative samples from their natural oral health state as would likely be used in future diagnostic strategies. There is a need to incorporate ML-based strategies, such as the Random Forest model, in order to predict the risk and severity of gingival inflammation within the human population as this may help identify an individual's risk of progressing to the more severe diseases state associated with gingival inflammation, periodontitis, as well as be used to dictate preventative care and treatment planning – representing an exciting new area of research in the field of dentistry and oral health.

3.2 Study Design and Methods

3.2.1 *Human Induced Gingivitis Experiment - EG-1*

The previous study methodology was established by Bamashmous et al.(15) for the induction of reversible bacterial-induced inflammation via cessation of oral hygiene in humans. With approval by the University of Washington's Human Subjects Review Committee (HSD# 50151) twenty-one generally healthy adults aged 18-35 years were consented and enrolled following the principles of the declaration of Helsinki. For inclusion, subjects had gingival health with no clinical signs of gingival inflammation at > 90% of sites at time of screening and had no signs of periodontal disease. The study included the following phases 1) Hygiene phase from time of inclusion (Day -14) to baseline (Day 0), 2) Gingivitis induction phase (Day 0 – Day 21), and 3) Resolution phase (Day 21 – Day 35). During the experimental induction phase the subjects were given customized intraoral stents that prevented oral hygiene for the experimental sites. In addition, each subject provided their own internal controls using contralateral teeth, throughout the duration of the study. Fidelity monitoring of the intervention was conducted at each timepoint throughout the experiment by clinical assessment of the plaque index. An overview of this study is shown in **Figure 12A.**

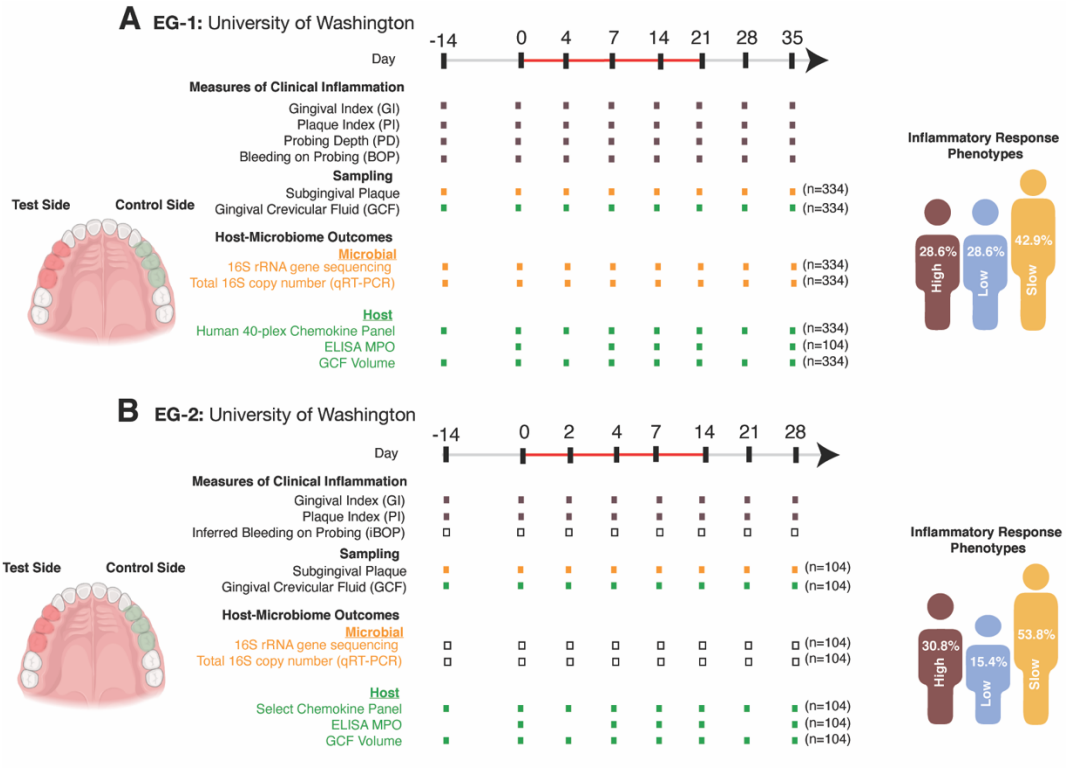

Figure 12. Overview of Experimental Gingivitis Studies EG-1 and EG-2. Two individual experimental gingivitis studies were completed at the University of Washington. **A)** EG-1 (N=21) was the foundational study done by Bamashmous et al. (2021). **B)** EG-2 (N=13) was a follow up study focused on angiogenesis biomarkers during experimental gingivitis. White boxes are currently being investigated for the EG-2 study.

3.2.2 *Variation in Clinical Gingival Inflammatory Responses - EG-1*

Clinical data including plaque index (PI), gingival index (GI), and bleeding on probing (BOP) were assessed at each timepoint as measures of clinical inflammation as part of the previous study design (15,31,84). All measurements were performed by a single, trained examiner using the same type of graded periodontal probes during the following study phases: health (Days -14 – 0), induction phase (Days 4, 7, 14 and 21), and resolution phase (Days 28, 35) (**Figure 12A**). To identify clusters of inflammatory responses among participants we assessed joint clinical data trajectories of gingivitis severity represented by GI and BOP in response to plaque accumulation represented by PI from Day 0 to Day 21 in the test sides by implementing the k-means algorithm using the "kml" and "kml3d" packages within the R suite in order to specifically design cluster joint trajectories(59,85).

3.2.3 *Human Induced Gingivitis Experiment - EG-2*

The study methodology for this independent clinical study was based on the established protocols outlined by Bamashmous et al., (15) for induction of reversible bacterial-induced inflammation via cessation of oral hygiene in humans. Thirteen generally healthy adults aged 20-33 years were consented and enrolled following the principles of the declaration of Helsinki. For inclusion, subjects had gingival health with no clinical signs of gingival inflammation at > 90% of sites at time of screening and had no signs of periodontal disease. The study included the following phases 1) Hygiene phase from time of inclusion (Day -14) to baseline (Day 0), 2) Gingivitis induction phase (Day 0 – Day 21), and 3) Resolution phase (Day 21 – Day 35). During the experimental induction phase the subjects were given customized intraoral stents that prevented oral hygiene for the experimental sites. In addition, each subject provided their own internal controls using contralateral teeth, throughout the duration of the study. An

overview of this study is shown in **Figure 12B.** This study was only used to validate if three Clinical Responder Phenotypes (CRPs) could be identified in an additional experimental gingivitis study: High-CRP, Low-CRP, and Slow-CRP.

3.2.4 *Variation in Clinical Gingival Inflammatory Responses -EG-2*

Clinical data, including plaque index (PI) and gingival index (GI), were assessed at each timepoint as measures of clinical inflammation(31,84). All measurements were performed by a team of trained examiners using the same type of graded periodontal probes during the following study phases: health (Days -14 – 0), induction phase (Days 2, 4, 7 and 14), and resolution phase (Days 21, 28) (**Figure 12B**). To identify clusters of inflammatory responses among participants we assessed joint clinical data trajectories of gingivitis severity represented by GI in response to plaque accumulation represented by PI from Day 0 to Day 14 in the test sides by implementing the k-means algorithm using the "kml" and "kml3d" packages within the R suite in order to specifically design cluster joint trajectories(59,85).

3.2.5 *Developing a Predictive Model to Identify Clinical Responder Phenotypes using Relative Abundance Microbiome Data from EG-1*

A recent experimental gingivitis study (EG-1) was carried out at the University of Washington(15) in which three Clinical Response Phenotypes (CRPs) were identified. Subgingival plaque samples were obtained at time of inclusion into the EG-1 study (Day -14) and were used as a proxy for the natural oral health state for study subjects that were relatively young and otherwise generally healthy. Subgingival plaque samples underwent amplicon 16S rRNA sequencing as part of EG-1 using methods previously described(15,55,56). Relative abundance values for taxonomic assignments agglomerated to the species level were then used as feature classifiers, variables, in the Random Forest model. This relative abundance data set

was partitioned using the “split.sample” function as part of the “caTools” package within the R suite, in which 75% (3/4) of the data was used to train the model and 25% (1/4) was used as a subset to test the model in later steps. Training the model was performed using the “randomForest” package within the R suite was performed with the following settings: mtry=3, ntree = 5001, importance = TRUE. A multi-way importance plot was generated using the “plot_multi_way_importance” function as part of the randomForest package within R using the following settings: x_measure = “accuracy_decrease”, y_measure = “gini_decrease”, size measure = “p_value”. The model was then re-trained using a Mean Decrease Gini cutoff of 0.5 for Variables of Importance. Testing the model was performed using the “predict” function as part of the “randomForest” package in R. Receiver operator characteristic (ROC) curves with area under the curve (AUC) measures were generated using the “prediction” and “performance” functions as part of the “ROCR” package in R using the following settings: measure = "sens", x.measure = "fpr", and measure = “auc”.

3.2.6 *Developing a Predictive Model to Identify Clinical Responder Phenotypes using Host Mediators Data from EG-1*

A recent experimental gingivitis study (EG-1) was carried out at the University of Washington(15) in which three Clinical Response Phenotypes (CRPs) were identified. Gingival crevicular fluid (GCF) samples were obtained at time of inclusion into the EG-1 study (Day -14) and were used as a proxy for the natural oral health state for study subjects that were relatively young and otherwise generally healthy. The host mediator data was generated using methods previously described(15). Values for 41 chemokines obtained from GCF were then used as feature classifiers, variables, in the Random Forest model. This chemokine data set was partitioned using the “split.sample” function as part of the “caTools” package within the R suite,

in which 75% (3/4) of the data was used to train the model and 25% (1/4) was used as a subset to test the model in later steps. Training the model was performed using the "randomForest" package within the R suite was performed with the following settings: mtry=3, ntree = 5001, importance = TRUE. A multi-way importance plot was generated using the "plot_multi_way_importance" function as part of the randomForest package within R using the following settings: x_measure = "accuracy_decrease", y_measure = "gini_decrease", size measure = "p_value". The model was then re-trained using a Mean Decrease Gini cutoff of 0.5 for Variables of Importance. Testing the model was performed using the "predict" function as part of the "randomForest" package in R. Receiver operator characteristic (ROC) curves with area under the curve (AUC) measures were generated using the "prediction" and "performance" functions as part of the "ROCR" package in R using the following settings: measure = "sens", x.measure = "fpr", and measure = "auc".

3.2.7 *Developing a Comprehensive Predictive Model to Identify Clinical Responder Phenotypes Incorporating Microbiome and Host Mediator Data*

Variables of Importance that were identified using the relative abundance values for the relative abundance microbiome data as well as the values for the host mediator data from the previous EG-1 study were isolated and used to train a comprehensive predictive Random Forest model. After initial assessment, the model was then re-trained using a Mean Decrease Gini cutoff of 0.5 for Variables of Importance. In total, 54 Variables of Importance (37 species and 17 chemokines) were used to re-train the comprehensive Random Forest model. Training the model was performed using the "randomForest" package within the R suite was performed with the following settings: mtry=3, ntree = 5001, importance = TRUE. A multi-way importance plot was generated using the "plot_multi_way_importance" function as part of the

randomForest package within R using the following settings: x_measure = “accuracy_decrease”, y_measure = “gini_decrease”, size measure = “p_value”. Testing the model was performed using the “predict” function as part of the “randomForest” package in R. Receiver operator characteristic (ROC) curves with area under the curve (AUC) measures were generated using the “prediction” and “performance” functions as part of the “ROCR” package in R using the following settings: measure = "sens", x.measure = "fpr", and measure = “auc”.

3.2.8 *Validating the Predictive Model to Identify Clinical Responder Phenotypes.*

At time of inclusion (Day -14) into a recent experimental gingivitis study by Bamashmous et al.,(15) subjects provided subgingival plaque and gingival crevicular fluid (GCF) samples. These samples were then used as a proxy for the natural oral health state as these subjects were relatively young and otherwise generally healthy. After receiving a professional cleaning at the time of inclusion (Day -14), subjects then participated in wash-out period in which whole-mouth normal oral hygiene was maintained until baseline (Day 0). After sampling of subgingival plaque and GCF at baseline, subjects began the 21-Day induction phase. Thus, for purposes of validating the comprehensive model that we have developed, the baseline data (Day 0) was used due to the fact it was the most similar to the time of inclusion data (Day -14) obtained during this experiment and was most reflective of the subject’s natural oral health state. Validating the model was performed using the “predict” function as part of the “randomForest” package in R. Receiver operator characteristic (ROC) curves with area under the curve (AUC) measures were generated using the “prediction” and “performance” functions as part of the “ROCR” package in R using the following settings: measure = "sens", x.measure = "fpr", and measure = “auc”.

3.3 Results

3.3.1 *Identifying Clinical Responder Phenotypes within a Second Experimental Gingivitis Study*

The first experimental gingivitis study outlined by Bamashmous et al.,(15) is now referred to as Experimental Gingivitis study #1 (EG-1) and was the first study to temporally characterize the High and Low Clinical Responder Phenotypes with high resolution in addition to discovering a novel clinical response type, Slow. In order to validate if these observations hold true across the human population, a second experimental gingivitis study using the same methodology as EG-1 was subsequently performed at the University of Washington and is now referred to as Experimental Gingivitis study #2 (EG-2). Clinical data, visible plaque index (VPI or PI), and gingival index (GI) were used in order to identify CRPs in EG-2 in addition to the implementation of a clustering algorithm using the "kml" and "kml3d" packages within the R suite. This resulted in the identification of an optimal clustering of 3 distinct groups (Calinski-Harabasz), similarly to the EG-1 study results. Within these three clusters, we were able to investigate their joint trajectories based on additional clinical measures, including VPI and GI. These clusters are shown in **Figure 13.** Based on these clinical trajectories, we indicate that cluster A (red) represents the Slow-CRP (53.3%), cluster B (green) represents High-CRP (30.8%), and cluster C (blue) represents Low-CRP (15.4%). We therefore validated the EG1 findings and were able to delineate the three Clinical Responder Phenotypes with clinical parameters from an independent clinical study which also agreed with the percentages of each group found in the previous study, thus further justifying the development of a predictive model to classify subjects into one of the three phenotypes.

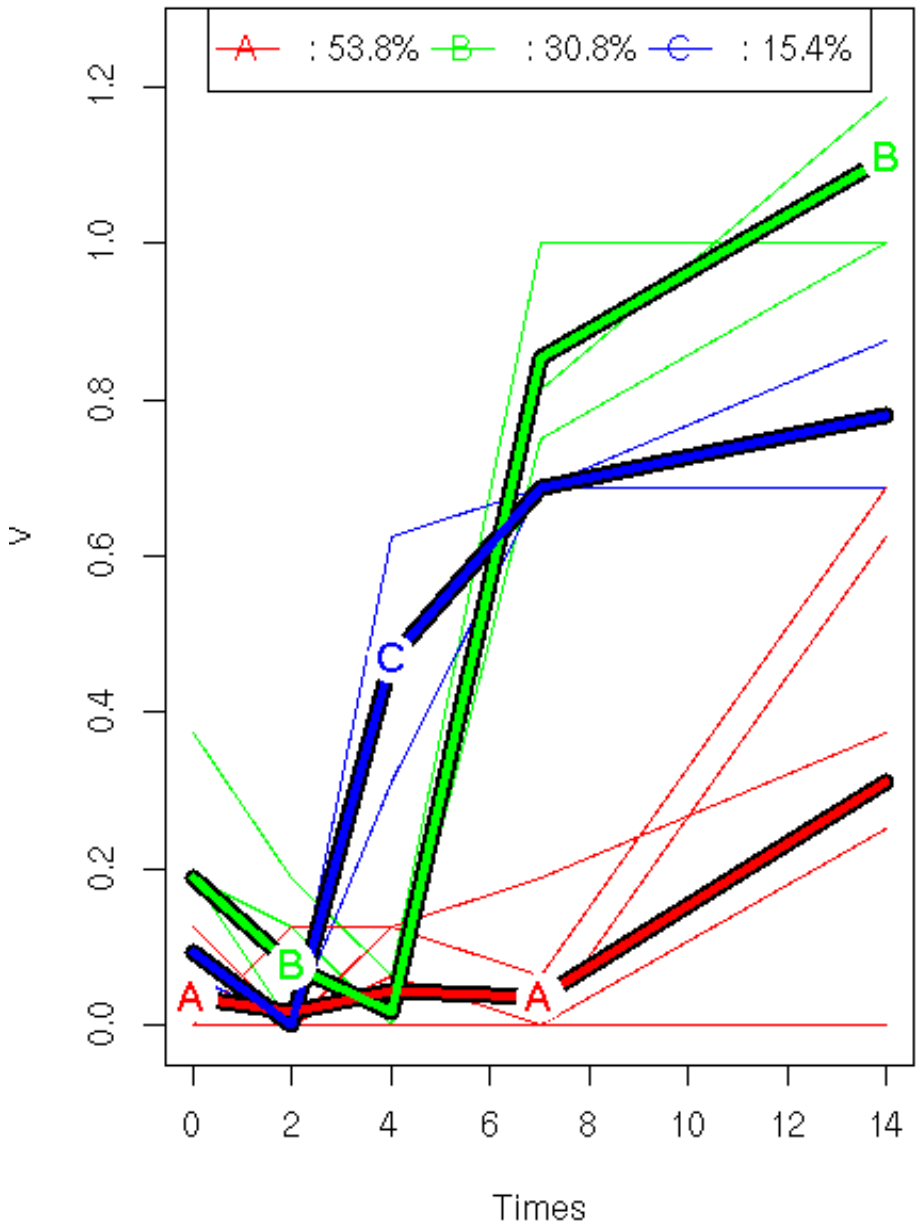

Figure 13. Identifying Clinical Responder Phenotypes within EG-2. Joint clinical data trajectories of gingivitis severity represented by gingival index (GI) on the y axis (V) in response to plaque accumulation represented by PI from Day 0-14 on the x axis (Times) was used to predict Clinical Responder Phenotypes (CRPs) for 13 Study Subjects using the kml algorithm within a second experimental gingivitis study (EG-2). A (red) represents the Slow-CRP (53.3%), B (green) represents High-CRP (30.8%), C (blue) represents Low-CRP (15.4%).

3.3.2 *Developing a Predictive Model to Identify Clinical Responder Phenotypes using Relative Abundance Microbiome Data from EG-1*

Subgingival plaque from test and control sites (n=42) obtained at the time of inclusion into the EG-1 Study (Day -14) were informatically pooled and used as a surrogate for the natural oral health state for 21 subjects whose Clinical Responder Phenotype (CRP) had been previously determined (High-CRP, Low-CRP, Slow-CRP). The data was randomly partitioned into a training data set (75%, n = 31) and test data set (25%, n =10). Species level relative abundance values obtained from 16S rRNA microbiome data generated by the EG-1 study resulted in the identification 336 species after filtering contaminants and singletons. Of the 336 species, 136 were identified as Variables of Importance ($p < 0.01$) by the Random Forest algorithm (Mean Accuracy Decrease v Mean Gini Decrease) (**Figure 14**) with an initial an out-of-box (OOB) estimate error rate of 46.88%. The next iteration of the model used only these 136 species that were identified as Variables of Importance in order to re-train the model and resulted in an improved model with an OBB estimate error rate of 40.62%. The performance of these 136 Variables of Importance is shown in **Table 2.** The test data set (25%, 21 Subjects) was then used to evaluate the model and resulted in an area under the curve (AUC) value, for the receiver operator characteristic (ROC) curve, of 0.95 for High-CRP, 0.95 for Low-CRP, and 0.83 for Slow-CRP (**Figure 15**).

Figure 14. Multi-way Importance Plot of Variables of Importance Identified within Subgingival Plaque at Time of Inclusion for EG-1. Subgingival plaque samples from time of inclusion (Day -14) were obtained for Test and Control sites. Relative abundance values agglomerated at the species level were and informatically pooled and evaluated using the Random Forest algorithm. Significance was determined by comparing Mean Gini Decrease versus Mean Accuracy Decrease. The most significant Variables of Interest are shown in red ($p < 0.01$), with the top 10 Variables of Interest being labeled.

Table 2. Performance of Variables of Importance Identified from Subgingival Plaque Isolated at Time of Inclusion for EG-1

Variable	Mean Min Depth	Number of Nodes	Accuracy Decrease	Gini Decrease	Number of Trees	Times a Root	p value
Granulicatella.adiacens	3.516	164	0.000669	0.186587	153	18	4.22E-49
Streptococcus.intermedius	3.506	154	0.001274	0.220720	148	17	4.82E-43
Veillonella.parvula	3.439	149	0.002295	0.199987	144	17	4.04E-40
Streptococcus.cristatus_clade_578	3.563	148	0.002515	0.202432	141	17	1.52E-39
Porphyromonas.pasteri	3.699	140	0.000175	0.156148	137	9	4.84E-35
Veillonella.dispar	3.782	137	0.000370	0.176176	130	19	2.10E-33
Corynebacterium.durum	3.952	136	0.002335	0.185997	133	17	7.27E-33
Streptococcus.sanguinis	3.795	135	0.002924	0.178533	133	16	2.50E-32
Rothia.mucilaginosa	3.583	135	0.001663	0.167654	135	18	2.50E-32
Abiotrophia.defectiva	3.915	135	0.000918	0.161338	134	13	2.50E-32
Granulicatella.elegans	3.627	134	0.002675	0.174299	131	19	8.54E-32
Fusobacterium.nucleatum_subsp._animalis	3.924	134	0.000257	0.150547	132	10	8.54E-32
Haemophilus.parainfluenzae	4.181	133	0.000692	0.165069	127	17	2.89E-31
Pseudopropionibacterium.propionicum	4.321	131	0.000215	0.113993	125	7	3.25E-30
Actinomyces.naeslundii	4.175	130	0.000530	0.127822	127	15	1.08E-29
Capnocytophaga.gingivalis	4.022	129	0.000684	0.131976	123	15	3.53E-29
Gemella.haemolysans	3.754	128	0.001133	0.135167	123	11	1.15E-28
Prevotella.melaninogenica	3.576	127	0.001965	0.157801	125	17	3.73E-28
Fusobacterium.nucleatum_subsp._polymorphum	4.001	122	0.000548	0.133965	119	11	1.18E-25
Prevotella.oulorum	4.093	121	0.000277	0.126419	119	14	3.63E-25
Actinomyces.gerencseriae	4.090	119	0.001194	0.150135	118	13	3.37E-24
Prevotella.nigrescens	4.019	118	0.001338	0.124911	115	16	1.01E-23
Streptococcus.oralis_subsp._tigurinus_clade_071	4.277	118	0.001269	0.140839	107	9	1.01E-23
Fusobacterium.sp._HMT_204	4.274	116	0.000177	0.138483	115	11	8.95E-23
Neisseria.mucosa	4.235	115	0.000311	0.111508	112	6	2.63E-22
Eikenella.corrodens	4.420	112	0.000492	0.092522	110	3	6.30E-21
Parvimonas.sp._HMT_110	4.307	111	0.000689	0.138037	109	8	1.78E-20
Tannerella.sp._HMT_286	4.231	109	0.000846	0.122382	107	14	1.39E-19
Neisseria.flavescens	4.333	108	0.000702	0.105022	106	17	3.84E-19
Actinomyces.sp._HMT_169	4.549	106	0.001654	0.128805	103	12	2.84E-18
Haemophilus.haemolyticus	4.541	105	0.000739	0.113588	102	8	7.63E-18
Oribacterium.sp._HMT_078	4.471	105	0.000147	0.086952	103	8	7.63E-18
Fusobacterium.sp._HMT_203	4.312	103	0.001985	0.119869	102	15	5.33E-17
Aggregatibacter.aphrophilus	4.164	103	0.000664	0.106689	103	16	5.33E-17
Bacteroidales_.G.2..bacterium_HMT_274	4.077	102	0.001359	0.117334	96	17	1.39E-16
Acidovorax.temperans	4.872	102	0.000690	0.084255	98	7	1.39E-16
Neisseria.cinerea	4.718	101	0.001087	0.106340	99	14	3.59E-16
Streptococcus.vestibularis	4.524	101	0.000563	0.109854	97	8	3.59E-16
Alloprevotella.tannerae	4.580	101	0.000058	0.080359	99	8	3.59E-16
Dialister.invisus	4.764	96	0.000309	0.084507	93	10	3.55E-14
Cardiobacterium.valvarum	4.385	94	0.002061	0.105233	90	13	2.08E-13
Prevotella.saccharolytica	4.845	89	0.000343	0.083199	88	8	1.43E-11
Actinomyces.massiliensis	4.686	88	0.000842	0.096686	87	15	3.23E-11
Peptostreptococcus.stomatis	4.464	87	0.001310	0.104180	84	15	7.21E-11
Saccharibacteria_.TM7._.G.3..bacterium_HMT_351	4.765	86	0.000858	0.080937	84	8	1.59E-10
Haemophilus.parahaemolyticus	5.098	85	0.000904	0.072778	84	3	3.47E-10
Lachnospiraceae_.G.3..bacterium_HMT_100	4.649	82	0.000489	0.089472	82	9	3.37E-09
Neisseria.oralis	5.007	82	0.000198	0.077483	81	9	3.37E-09
Veillonella.rogosae	5.088	79	0.000474	0.069746	79	8	2.94E-08
Saccharibacteria_.TM7._.G.1..bacterium_HMT_349	4.624	78	0.000400	0.055129	76	12	5.90E-08
Capnocytophaga.granulosa	4.580	77	0.001011	0.083976	77	13	1.17E-07
Parvimonas.micra	5.068	77	0.000403	0.061816	76	5	1.17E-07
Selenomonas.noxia	4.990	76	0.000217	0.069497	76	8	2.29E-07
Actinomyces.oris	5.042	76	0.000216	0.067404	76	6	2.29E-07
Saccharibacteria_.TM7._.G.6..bacterium_HMT_870	4.901	75	0.001983	0.097276	74	9	4.44E-07
Saccharibacteria_.TM7._.G.1..bacterium_HMT_346	4.920	75	0.000459	0.065626	74	10	4.44E-07
Haemophilus.sp._HMT_036	5.149	75	0.000160	0.062461	74	9	4.44E-07
Treponema.socranskii	4.833	73	0.000790	0.078550	73	16	1.60E-06
Prevotella.sp._HMT_317	5.132	73	0.000020	0.049089	72	5	1.60E-06
Leptotrichia.sp._HMT_392	4.796	71	0.001033	0.079139	71	17	5.46E-06
Porphyromonas.sp._HMT_275	4.851	69	0.001111	0.074663	69	9	1.77E-05
Campylobacter.showae	5.086	69	0.000585	0.069816	69	11	1.77E-05
Neisseria.subflava	5.398	68	0.000084	0.056361	65	10	3.12E-05
Prevotella.nanceiensis	5.259	67	0.000309	0.080278	67	10	5.43E-05
Alloprevotella.sp._HMT_473	5.451	66	0.000633	0.058224	65	5	9.31E-05
Fusobacterium.naviforme	5.032	65	0.000488	0.062847	65	12	0.0002
Streptococcus.sinensis	5.074	64	0.000990	0.069172	63	9	0.0003

Variable	Mean Min Depth	Number of Nodes	Accuracy Decrease	Gini Decrease	Number of Trees	Times a Root	p_value
Tannerella.sp._HMT_808	5.250	64	0.000647	0.049377	63	8	0.0003
Veillonella.sp._HMT_780	5.233	64	0.000637	0.065562	64	8	0.0003
Actinomyces.meyeri	5.126	64	0.000176	0.057545	63	10	0.0003
Prevotella.loescheii	5.139	63	0.000628	0.064465	63	10	0.0004
Capnocytophaga.sp._HMT_864	5.477	62	0.000362	0.048233	62	4	0.0007
Actinomyces.sp._HMT_180	5.366	62	0.000051	0.047224	62	10	0.0007
Bacteroidetes_.G.5..bacterium_HMT_511	4.845	61	0.001417	0.083844	60	14	0.0011
Treponema.maltophilum	4.978	61	0.001068	0.075198	61	8	0.0011
Actinomyces.georgiae	5.316	60	0.000103	0.051160	60	5	0.0017
Bergeyella.sp._HMT_422	5.534	58	0.001250	0.053034	58	4	0.0041
Streptococcus.australis	5.495	58	0.000137	0.039571	58	2	0.0041
Porphyromonas.sp._HMT_930	5.329	57	0.000307	0.047470	57	7	0.0062
Streptococcus.sp._HMT_074	5.264	57	0.000300	0.050050	57	10	0.0062
Saccharibacteria_.TM7._.G.1..bacterium_HMT_352	5.338	56	0.000345	0.041314	55	5	0.0091
Prevotella.veroralis	5.491	56	0.000254	0.035423	56	5	0.0091
Treponema.sp._HMT_231	5.144	56	0.000124	0.055881	56	12	0.0091
Olsenella.sp._HMT_807	5.312	55	0.000961	0.044701	55	3	0.0133
Fretibacterium.fastidiosum	5.199	54	0.000447	0.064981	54	10	0.0190
Prevotella.sp._HMT_472	5.546	52	0.000090	0.039256	51	4	0.0370
Selenomonas.sp._HMT_892	5.476	52	0.000008	0.040450	52	3	0.0370
Selenomonas.infelix	5.310	51	0.000373	0.044212	51	10	0.0505
Prevotella.micans	5.337	48	0.001178	0.060275	48	10	0.1157
Johnsonella.ignava	5.511	48	0.000138	0.041175	47	5	0.1157
Streptococcus.gordonii	5.572	48	0.000011	0.028616	48	6	0.1157
Treponema.denticola	5.276	47	0.000503	0.047427	47	12	0.1476
Streptococcus.parasanguinis_clade_411	5.503	47	0.000337	0.049071	46	8	0.1476
Actinomyces.sp._HMT_877	5.629	47	0.000193	0.037913	47	6	0.1476
Mycoplasma.salivarium	5.424	46	0.000154	0.039561	46	9	0.1852
Burkholderia.cepacia	5.566	45	0.000033	0.038469	45	7	0.2286
Porphyromonas.catoniae	5.660	44	0.000215	0.027243	43	4	0.2776
Prevotella.scopos	5.627	43	0.000094	0.039454	43	6	0.3316
Prevotella.buccae	5.882	41	0.000280	0.029938	40	4	0.4511
Actinomyces.sp._HMT_170	5.832	41	0.000104	0.034001	41	2	0.4511
Aggregatibacter.sp._HMT_898	5.950	41	0.000094	0.025978	41	1	0.4511
Alloprevotella.sp._HMT_912	5.662	41	0.000042	0.033493	41	7	0.4511
Peptostreptococcaceae_.XI..G.1..sulci	5.553	40	0.000010	0.030187	39	8	0.5141
Absconditabacteria_.SR1._.G.1..bacterium_HMT_875	5.769	39	0.000125	0.034394	39	7	0.5773
Prevotella.sp._HMT_475	5.726	37	0.000096	0.027732	37	5	0.6979
Bergeyella.sp._HMT_206	5.837	37	0.000001	0.026382	37	3	0.6979
Haemophilus.paraphrohaemolyticus	5.793	35	0.000543	0.033131	35	4	0.8017
Actinomyces.sp._HMT_175	5.826	35	0.000195	0.024490	35	5	0.8017
Actinomyces.timonensis	5.813	35	0.000003	0.027055	35	6	0.8017
Cutibacterium.acnes	5.974	34	0.000400	0.020139	34	4	0.8448
Fretibacterium.sp._HMT_360	5.857	34	0.000198	0.032737	34	7	0.8448
Aggregatibacter.actinomycetemcomitans	5.885	32	0.000087	0.030062	32	4	0.9121
Filifactor.alocis	5.731	30	0.000452	0.034244	30	7	0.9554
Gracilibacteria_.GN02._.G.1..bacterium_HMT_872	5.859	30	0.000083	0.021146	29	7	0.9554
Peptostreptococcaceae_.XI..G.6..minutum	5.787	29	0.000201	0.030460	29	10	0.9696
Shuttleworthia.satelles	6.068	29	0.000112	0.018773	29	4	0.9696
Atopobium.rimae	5.996	29	0.000057	0.019896	29	4	0.9696
Actinomyces.sp._HMT_525	5.750	27	0.000242	0.029837	27	12	0.9872
Tannerella.forsythia	5.860	26	0.000291	0.025295	26	3	0.9921
Desulfobulbus.sp._HMT_041	5.857	25	0.000228	0.027074	25	9	0.9953
Leptotrichia.sp._HMT_219	5.857	25	0.000213	0.025694	25	10	0.9953
Saccharibacteria_.TM7._.G.1..bacterium_HMT_347	6.093	25	0.000075	0.016110	25	5	0.9953
Bacteroidetes_.G.3..bacterium_HMT_281	6.078	24	0.000290	0.021258	24	3	0.9973
Gracilibacteria_.GN02._.G.1..bacterium_HMT_871	6.030	24	0.000084	0.013514	23	4	0.9973
Selenomonas.flueggei	5.999	24	0.000003	0.013885	24	4	0.9973
Erysipelotrichaceae_.G.1..bacterium_HMT_905	5.984	23	0.000030	0.016275	23	4	0.9985
Streptococcus.anginosus	6.152	22	0.000127	0.013664	22	5	0.9992
Alloprevotella.sp._HMT_913	6.043	20	0.000185	0.018433	20	6	0.9998
Prevotella.marshii	6.180	20	0.000164	0.013563	20	2	0.9998
Leptotrichia.sp._HMT_498	6.220	20	0.000133	0.013083	20	3	0.9998
Bacteroidetes_.G.3..bacterium_HMT_899	6.239	20	0.000067	0.016115	20	2	0.9998
Selenomonas.sp._HMT_937	6.113	19	0.000191	0.015717	19	3	0.9999
Anaeroglobus.geminatus	6.202	18	0.000122	0.014847	18	1	1.0000
Ruminococcaceae_.G.2..bacterium_HMT_085	6.268	15	0.000056	0.011262	15	1	1.0000
Porphyromonas.gingivalis	6.273	11	0.000118	0.011128	11	5	1.0000

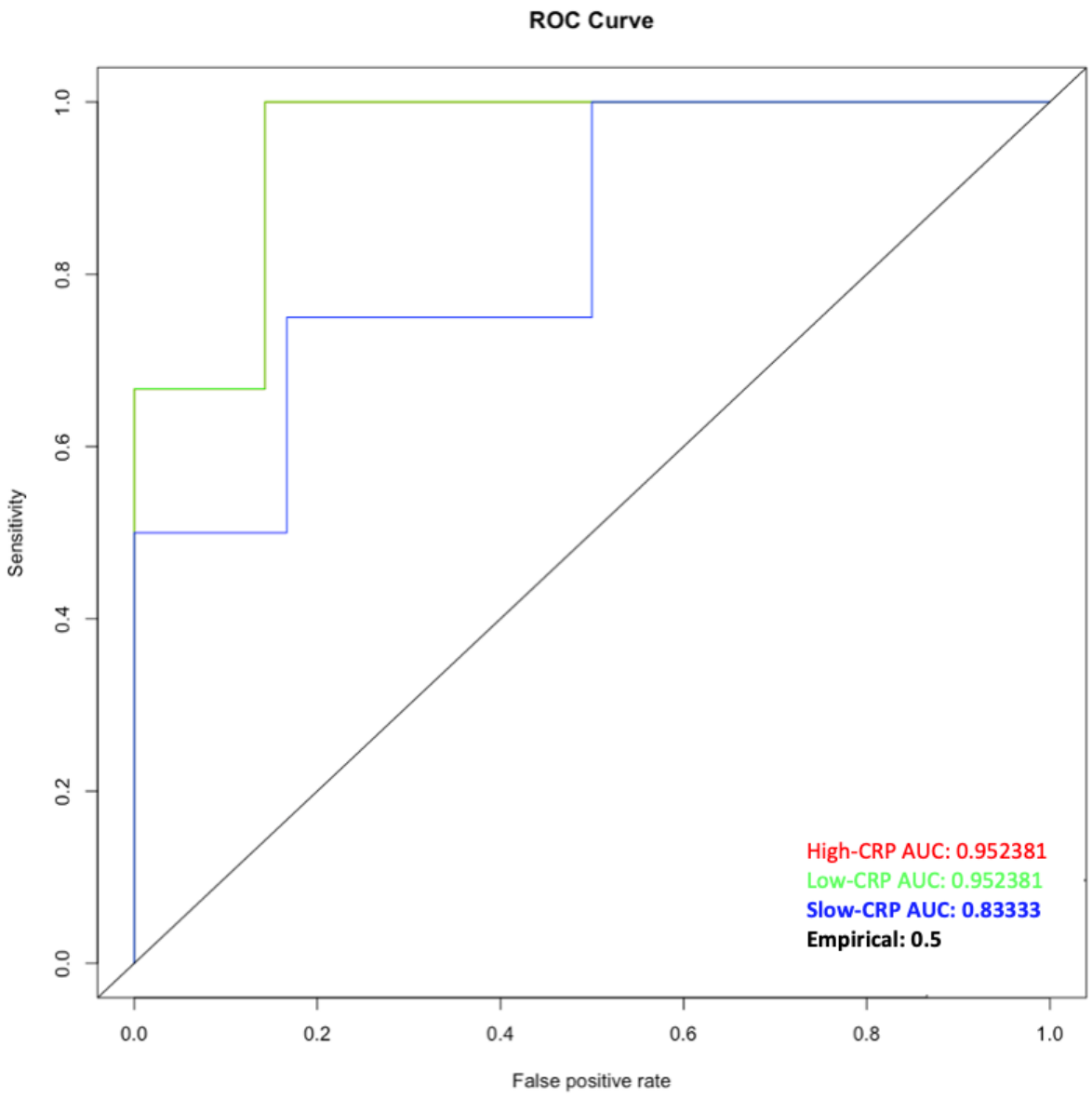

Figure 15. Evaluation of the Predictive Model to Identify Clinical Responder Phenotypes using Species Level Microbiome Data from EG-1. Relative abundance values agglomerated at the species level were used to test the Random Forest model. A receiver operator characteristic (ROC) curve was plotted comparing sensitivity and specificity (represented by the false positive rate). An area under the curve (AUC) value was calculated for each Clinical Responder Phenotype (CRP) with a value of 0.95 for High-CRP (red, overlapped by green), 0.95 for Low-CRP (green), and 0.83 for Slow-CRP (blue). The black line represents the empirical sensitivity over specificity.

3.3.3 *Developing a Predictive Model to Identify Clinical Responder Phenotypes using Host Mediator Data from EG-1*

A panel of 41 host mediators detected in gingival crevicular fluid (GCF) from test and control sites obtained at the time of inclusion into the EG-1 Study (Day -14) were informatically pooled and used as a surrogate for the natural oral health state for 21 subjects whose Clinical Responder Phenotype (CRP) had been previously determined (High-CRP, Low-CRP, Slow-CRP). The data was randomly partitioned into a training data set (75%, n = 31) and test data set (25%, n =10). Of the 41 host mediators (chemokines and cytokines), 17 were identified as Variables of Importance ($p < 0.01$) by the Random Forest algorithm (Mean Accuracy Decrease v Mean Gini Decrease) (**Figure 16**) with an initial an out-of-box (OOB) estimate error rate of 56.25%. The next iteration of the model used only these 17 chemokines that were identified as Variables of Importance in order to train the model and resulted in an OOB estimate error rate of 46.88%. The performance of these 17 Variables of Importance is shown in **Table 3.** The test data set was then used to evaluate the model and resulted in an AUC of 0.86 for High-CRP, 0.95 for Low-CRP, and 1.00 for Slow-CRP (**Figure 17**).

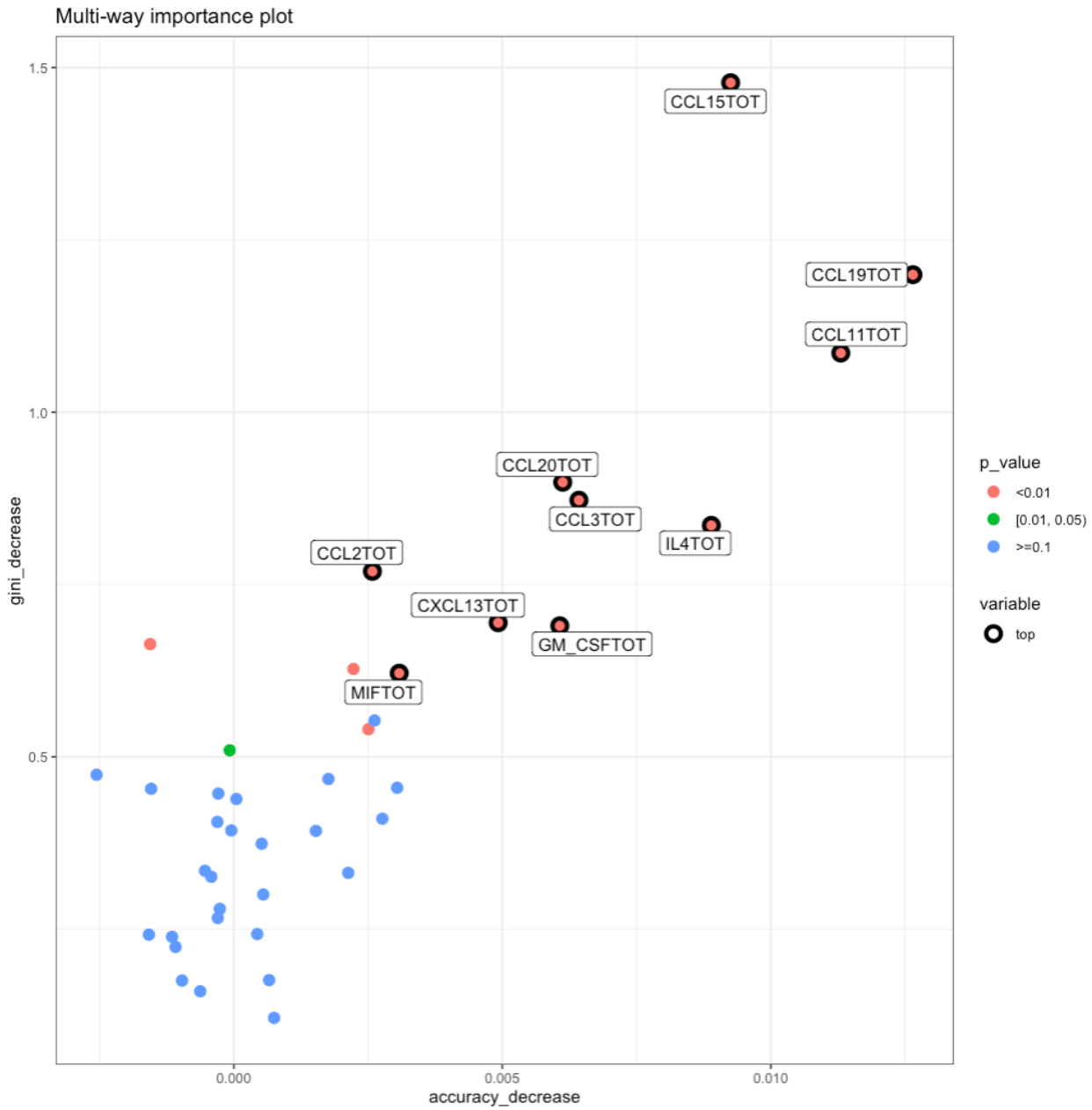

Figure 16. Multi-way Importance Plot of Variables of Importance Identified within Gingival Crevicular Fluid at Time of Inclusion for EG-1. Gingival crevicular fluid samples from time of inclusion (Day -14) were obtained for Test and Control sites and informatically pooled and evaluated using the Random Forest algorithm. Significance was determined by comparing Mean Gini Decrease versus Mean Accuracy Decrease. The most significant Variables of Interest are shown in red ($p < 0.01$), with the top 10 Variables of Interest being labeled.

Table 3. Performance of Variables of Importance Identified from Gingival Crevicular Fluid Isolated at Time of Inclusion for EG-1

Variable	Mean Min Depth	Number of Nodes	Accuracy Decrease	Gini Decrease	Number of Trees	Times a Root	p value
CCL15	1.2732175	1865	0.0092523	1.47803639	1669	533	4.69E-232
CCL19	1.88252272	1602	0.01264711	1.19954193	1481	253	1.19E-140
CCL11	2.01743174	1495	0.01130337	1.08577994	1347	265	6.03E-109
CCL20	2.18552898	1335	0.00612524	0.89834383	1235	308	4.16E-68
CCL3	2.41930104	1143	0.00642658	0.87233244	1050	354	1.22E-30
GM_CSF	2.70907257	1103	0.00606983	0.69012965	1024	165	1.41E-24
CCL2	2.5897579	1099	0.0025803	0.76907336	1001	233	5.23E-24
CXCL13	2.70007472	1068	0.00492254	0.69452799	977	183	8.38E-20
CCL7	2.76335146	1010	-0.0015585	0.66352508	955	203	5.13E-13
IL4	2.45983482	996	0.00889251	0.83580806	969	368	1.35E-11
MIF	2.85610715	915	0.00307972	0.62137862	842	237	4.33E-05
CCL22	3.04020239	897	0.00250607	0.54006578	841	103	0.00047168
IFNy	2.85929129	872	0.00222638	0.62743609	829	252	0.00732575
TNFa	3.09018041	865	-7.77E-05	0.50953833	808	87	0.01401205
CXCL16	3.11225592	831	0.00176028	0.46782369	789	74	0.15797067
CXCL6	3.19156912	825	-0.0002908	0.44669853	764	51	0.21462751
CXCL2	3.15349273	821	-0.0025571	0.47393355	774	91	0.25829513

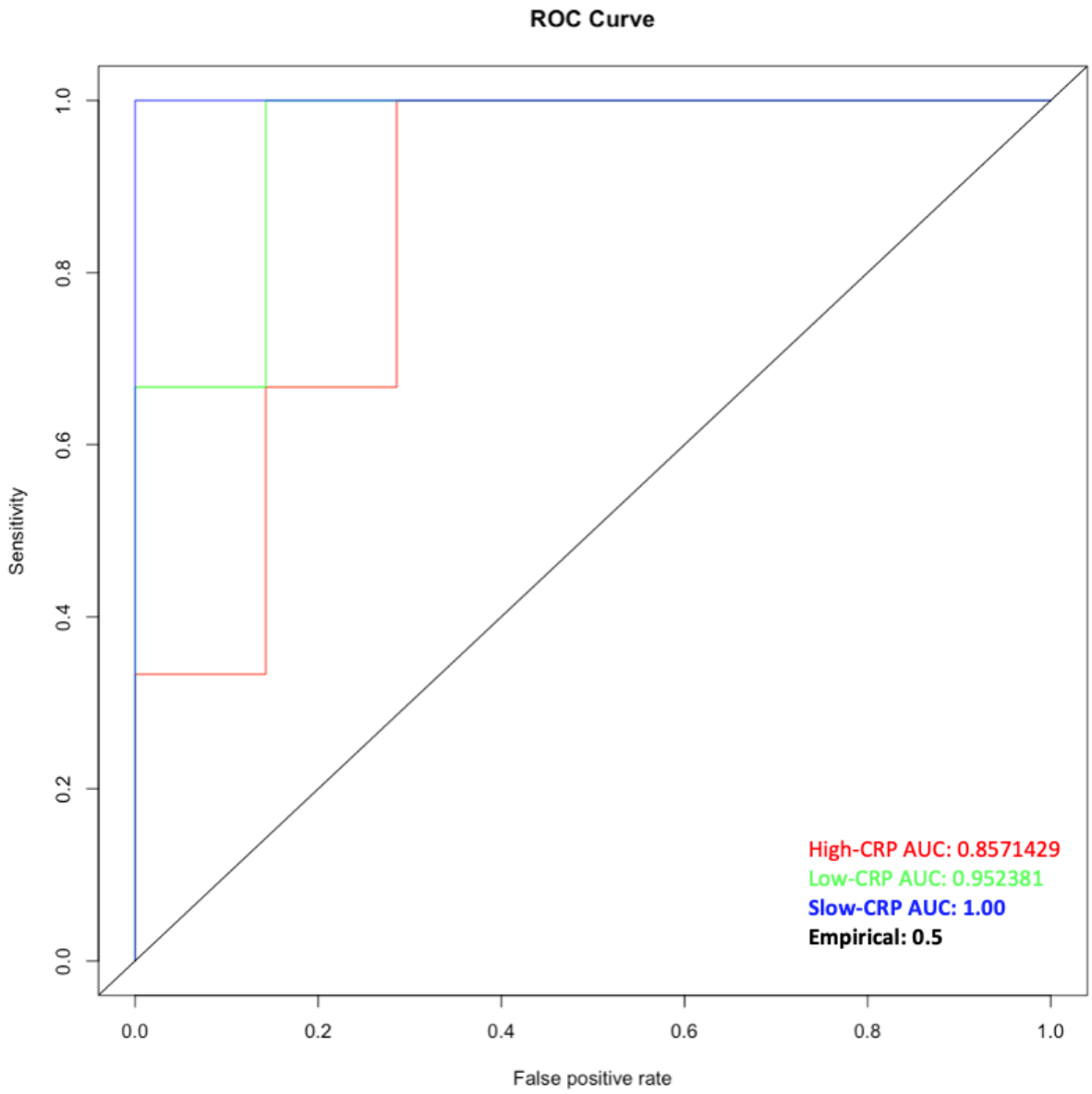

Figure 17. Evaluation of the Predictive Model to Identify Clinical Responder Phenotypes using Host Mediator Data from EG-1. Host mediators isolated from gingival crevicular fluid (GCF) were used to test the Random Forest model. A receiver operator characteristic (ROC) curve was plotted comparing sensitivity and specificity (represented by the false positive rate). An area under the curve (AUC) value was calculated for each Clinical Responder Phenotype (CRP) with a value of 0.86 for High-CRP (red), 0.95 for Low-CRP (green), and 1.00 for Slow-CRP (blue). The black line represents the empirical sensitivity over specificity.

3.3.4 *Developing a Comprehensive Random Forest Model to Predict Clinical Responder Phenotypes Incorporating Microbiome and Host Mediator Data*

Subgingival plaque and gingival crevicular fluid (GCF) mediators from test and control sites were obtained at the time of inclusion into the EG-1 Study (Day -14) and informatically pooled respectively. These samples represent surrogates for the natural oral health state for 21 subjects whose Clinical Responder Phenotype (CRP) had been previously determined (High-CRP, Low-CRP, Slow-CRP). A comprehensive model was developed using Variables of Importance identified from Random Forest models that were trained on relative abundance values using species level microbiome data isolated from subgingival plaque (**Table 2**) and host mediators isolated from GCF (**Table 3**) as part of EG-1. Training the comprehensive model on these combined Variables of Importance (136 species and 17 Chemokines) resulted in an OOB estimate error rate of 34.38%. The performance of the top 54 Variables of Importance (37 Species and 17 Chemokines) are shown in **Table 4.** The test data set was then used to evaluate the model and resulted in an AUC of 0.86 for High-CRP, 0.95 for Low-CRP, and 1.00 for Slow-CRP (**Figure 19**). Statistical comparison of the top 5 Variables of Importance for both host mediators and species between CRP at time of inclusion (Day -14) are shown in **Figure 18.**

Table 4. Performance of Variables of Importance Identified from Subgingival Plaque and Gingival Crevicular Fluid Isolated at Time of Inclusion for EG-1

Variable	Mean Min Depth	Number of Nodes	Accuracy Decrease	Gini Decrease	Number of Trees	Times a Root	p value
Granulicatella.adiacens	1.2519780	1767	0.0214939	1.5747431	1643	415	0
Veillonella.parvula	1.8514732	1228	0.0095354	1.15287036	1170	456	9.00E-169
CCL20	2.5732260	912	0.0034827	0.70828517	872	207	3.57E-62
Parvimonas.sp._HMT_110	2.6043610	906	0.0033273	0.7074898	879	145	1.40E-60
Actinomyces.gerencseriae	2.4719087	874	0.0038176	0.80340317	851	243	2.21E-52
Streptococcus.cristatus_clade_578	2.6222931	826	0.0049662	0.69411489	803	187	4.53E-41
Cardiobacterium.valvarum	2.4222381	826	0.0082285	0.80371218	817	332	4.53E-41
Streptococcus.intermedius	2.7412227	799	0.0014284	0.60302013	763	157	3.00E-35
Haemophilus.parainfluenzae	2.7789513	716	0.0015363	0.60457449	672	196	5.99E-20
CCL3	2.8125395	693	0.0003708	0.58617161	661	199	1.93E-16
CCL15	2.9521443	689	-0.000409	0.49669657	639	121	7.29E-16
Fusobacterium.nucleatum_subsp._animalis	2.8480415	689	0.0020113	0.53817448	663	161	7.29E-16
CCL19	3.0046946	665	0.0021464	0.45518019	635	78	1.27E-12
Tannerella.sp._HMT_286	2.887446	632	0.0017048	0.54245143	619	165	8.8073E-09
Streptococcus.sanguinis	2.9458881	629	0.0023313	0.50751726	607	120	1.8093E-08
Streptococcus.oralis_subsp._tigurinus 071	3.1425925	616	-0.000385	0.37436268	596	48	3.4751E-07
Corynebacterium.durum	2.9044186	607	0.0047996	0.53866409	588	182	2.2954E-06
CCL2	3.1177064	559	0.0001323	0.39312617	530	87	0.00581737
Neisseria.flavescens	3.0742982	535	0.0003705	0.40987021	522	105	0.07058982
Veillonella.dispar	3.1648100	531	0.0011240	0.37485185	496	71	0.09772112
Gemella.haemolysans	3.1453210	522	0.0017439	0.37213394	508	80	0.18530942
MIF	3.1956561	521	0.0002831	0.34987394	488	69	0.19743868
IL4	3.0680482	489	0.0028248	0.42232525	484	165	0.72196177
CCL7	3.2349353	481	0.0001496	0.32231635	467	44	0.82978448
CXCL16	3.2858729	475	-0.000185	0.28366876	453	42	0.89029341
GM_CSFT	3.3183442	462	-1.587e-05	0.2578492	443	40	0.96617663
CXCL2	3.2804075	454	-0.001500	0.28027994	441	52	0.98605597
Prevotella.melaninogenica	3.1681099	450	-0.000109	0.34574158	444	110	0.99146988
CCL11	3.2916892	441	0.0018474	0.30321271	420	40	0.9975007
Fusobacterium.nucleatum_polymorphum	3.2761657	440	-0.001796	0.2986134	423	64	0.99784241
CXCL13	3.3363333	421	-0.000182	0.24337561	410	31	0.99991312
CCL8	3.3065160	419	0.0010909	0.2877615	404	61	0.99994092
Rothia.mucilaginosa	3.2698908	414	0.0020021	0.30002201	409	65	0.99997837
IFNy	3.3155515	407	0.0003434	0.26611601	397	50	0.9999952
Granulicatella.elegans	3.3843529	376	0.0015566	0.24689047	373	26	1
CCL22	3.3561607	374	0.0006026	0.24408156	365	68	1
Prevotella.oulorum	3.3895357	372	0.0013712	0.2354331	364	26	1
TNFa	3.4311428	352	-0.000200	0.19875622	348	19	1
Neisseria.mucosa	3.4202059	337	0.0002400	0.21633537	330	35	1
Aggregatibacter.aphrophilus	3.7130985	101	-4.415e-05	0.04893039	101	12	1
Peptostreptococcus.stomatis	3.7003926	128	-3.321e-05	0.0598065	126	3	1
Haemophilus.haemolyticus	3.7009950	133	-0.000311	0.06403151	132	2	1
Capnocytophaga.gingivalis	3.6450568	179	0.0002557	0.09158423	175	4	1
Neisseria.cinerea	3.6453642	179	0.0001668	0.09220996	172	3	1
Streptococcus.vestibularis	3.6305312	198	0.0003009	0.10278442	194	4	1
Bacteroidales_.G.2..bacterium_HMT_274	3.6461303	219	-0.000258	0.10353797	216	4	1
Actinomyces.naeslundii	3.6103269	213	-0.000956	0.1049308	211	9	1
Abiotrophia.defectiva	3.6015171	200	-0.000191	0.11080502	196	10	1
Actinomyces.sp._HMT_169	3.5864139	189	-0.000434	0.12609615	185	39	1
Porphyromonas.pasteri	3.5310409	281	-0.000309	0.15665209	270	14	1
Prevotella.nigrescens	3.5247661	261	0.0003893	0.16339593	256	27	1
Pseudopropionibacterium.propionicum	3.4878087	293	-0.000238	0.175682	288	29	1
Fusobacterium.sp._HMT_204	3.4623585	281	-0.000232	0.19146536	277	46	1
Fusobacterium.sp._HMT_203	3.4077318	329	0.001749	0.20837956	327	33	1

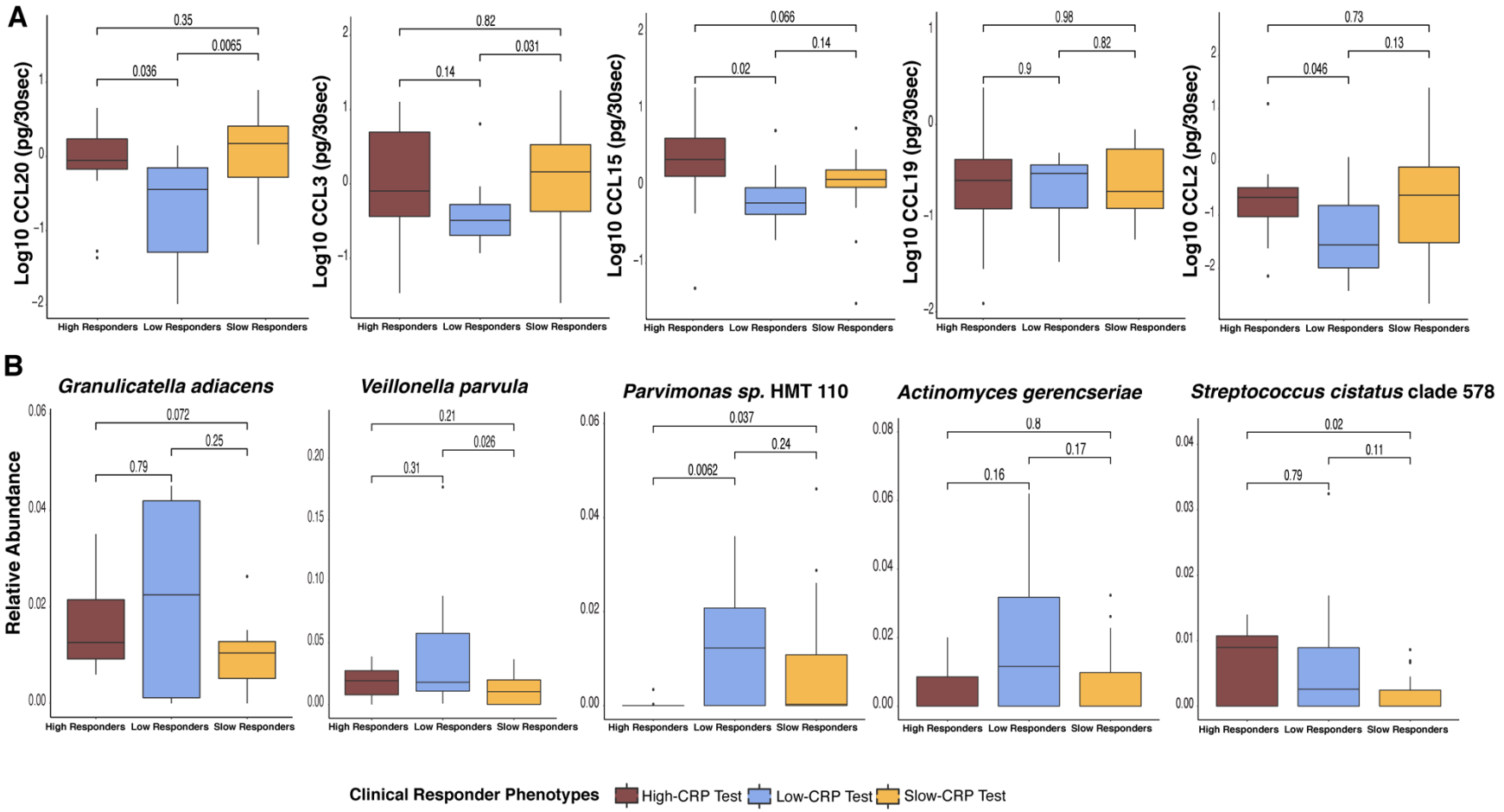

Figure 18. Top 5 Variables of Importance for Species and Chemokines Identified by the Random Forest Model for Predicting Clinical Responder Phenotypes. **A)** Top 5 Host mediators identified as Variables of Importance isolated from gingival crevicular fluid between Clinical Responder Phenotypes at time of inclusion (Day -14) in the EG-1 study. **B)** Top 5 Species identified as Variables of Importance isolated from subgingival plaque. Boxes represents data and medians ± interquartile ranges; whiskers and outliers > 1.5 IQR below (above) the 25th (75th) percentile. Trend lines represent loess regression mean values across all time points. Statistical analysis was performed using the non-parametric Wilcoxon-Rank Sum Test adjusted by FDR. Significance level indicated by asterisks. Significance levels: ns = non-significant, *P < 0.05, **P ≤ 0.01, and ***P ≤ 0.001.

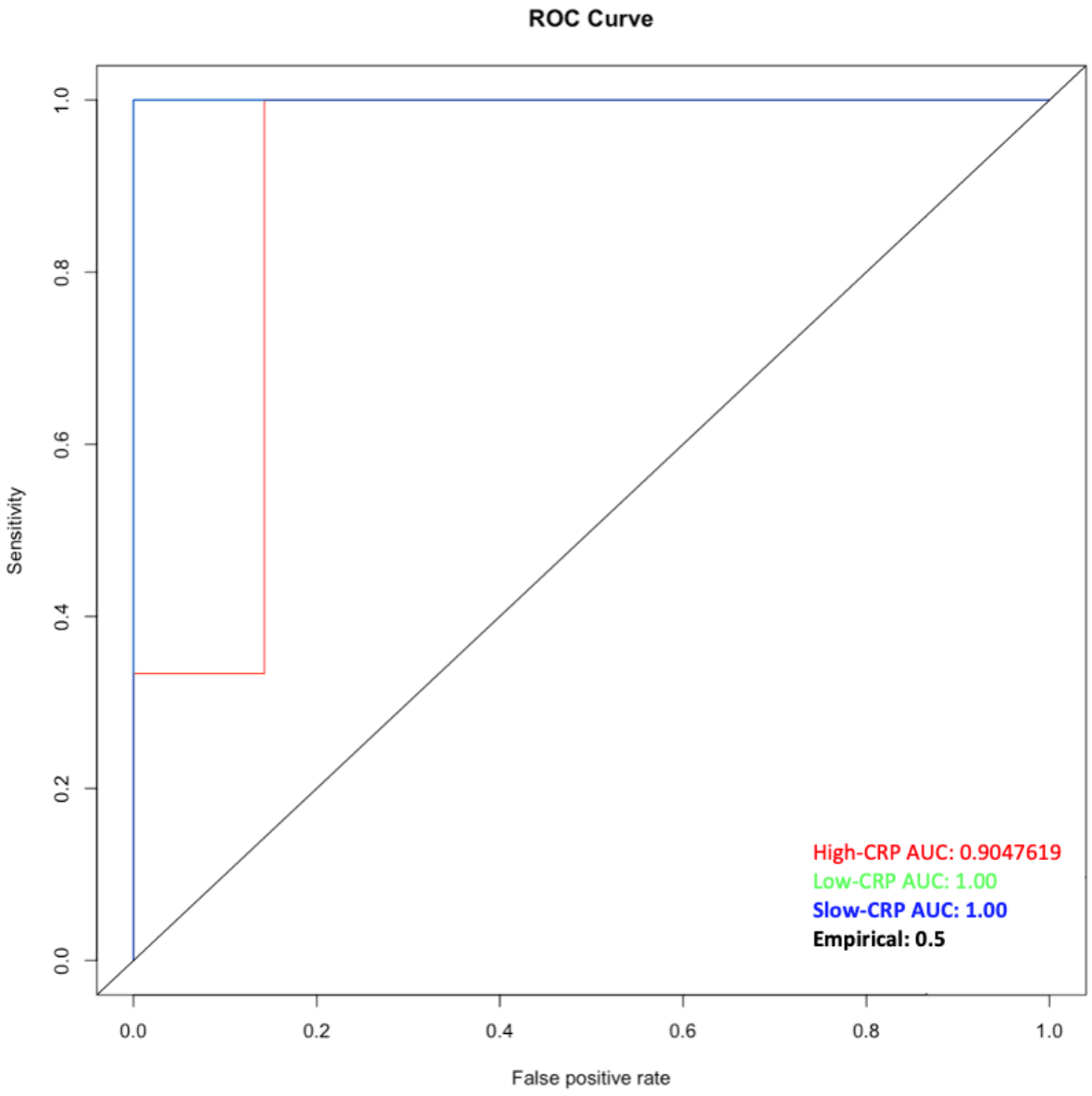

Figure 19. Evaluation of the Comprehensive Predictive Model to Identify Clinical Responder Phenotypes using Species Level Microbiome and Host Mediator Data from EG-1. Host mediators isolated from gingival crevicular fluid (GCF) were used to test the Random Forest model. A receiver operator characteristic (ROC) curve was plotted comparing sensitivity and specificity (represented by the false positive rate). An area under the curve (AUC) value was calculated for each Clinical Responder Phenotype (CRP) with a value of 0.86 for High-CRP (red), 0.95 for Low-CRP (green), and 1.00 for Slow-CRP (blue). The black line represents the empirical sensitivity over specificity.

3.3.5 *Validating the Random Forest Model for Predicting Clinical Responder Phenotypes*

At time of inclusion into this recent experimental gingivitis study (Day -14) for EG-1, subjects provided subgingival plaque and gingival crevicular fluid (GCF) samples. These samples were then used as a proxy for the natural oral health state as these subjects were relatively young and otherwise generally healthy. After receiving a professional cleaning at the time of inclusion (Day -14), subjects then participated in wash-out period in which whole-mouth normal oral hygiene was maintained until baseline (Day 0). After sampling of subgingival plaque and GCF at baseline, subjects began the 21-Day induction phase. Thus, for purposes of validating the comprehensive model that we have developed, the baseline data (Day 0) was used due to the fact it was the most similar to the time of inclusion data (Day -14) obtained during this experiment and was most reflective of the subject's natural oral health state two weeks following professional cleaning.

Host mediators (chemokines and cytokines) and species level microbiome data from EG-1 were then used to validate the comprehensive Random Forest model that was previously trained and tested using Day -14 data in order to determine its broader application. Pooled Test and Control data for Day 0, which represents the baseline measure for the induction phase, was used to validate the model and resulted in an AUC of 0.73 for High-CRP, 0.81 for Low-CRP, and 0.71 for Slow-CRP (**Figure 20**).

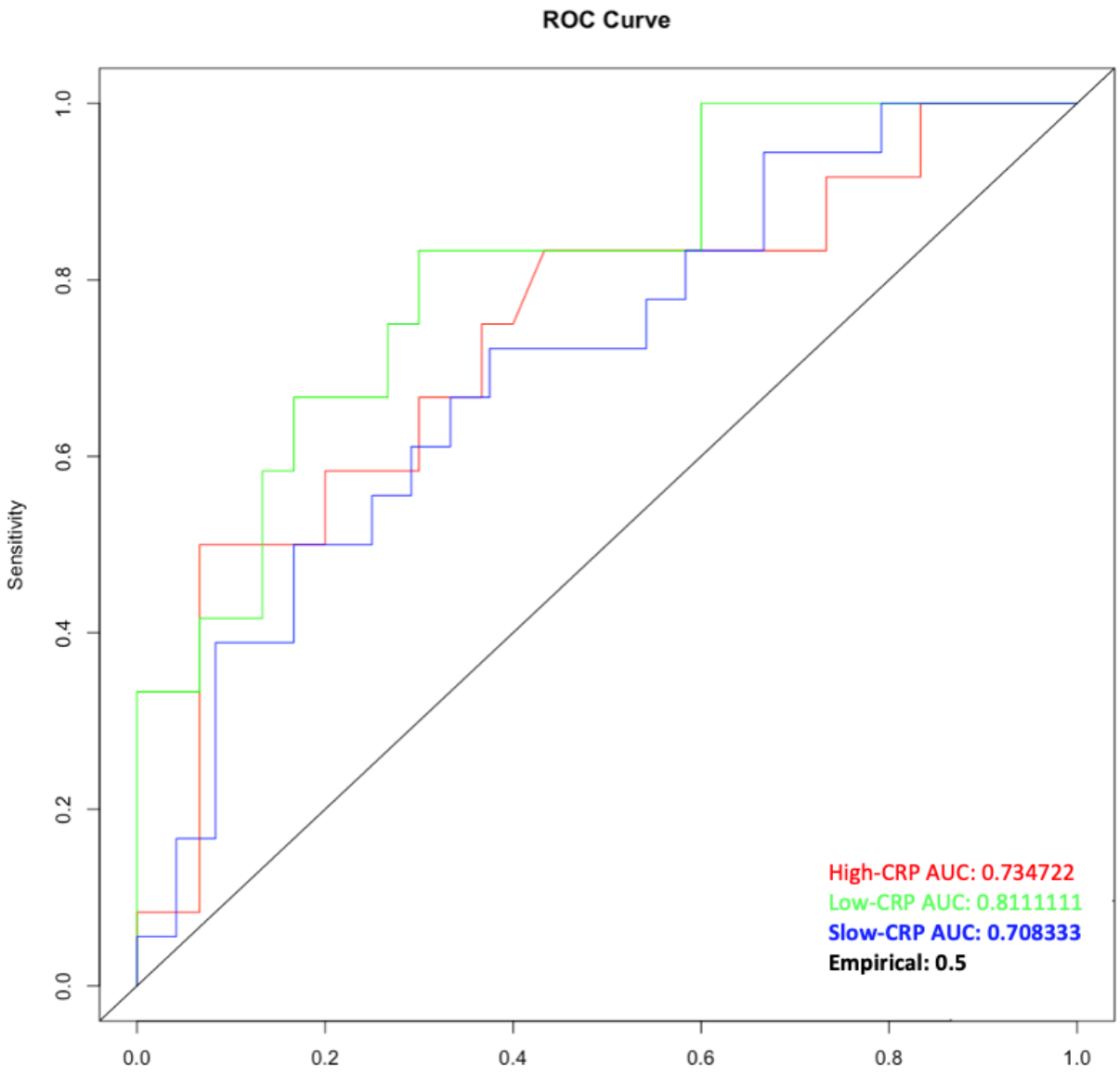

Figure 20. Validating of the Comprehensive Predictive Model to Identify Clinical Responder Phenotypes using Species Level Microbiome and Host Mediator Baseline Data from EG-1. Host mediators isolated from gingival crevicular fluid (GCF) were used to test the Random Forest model. A receiver operator characteristic (ROC) curve was plotted comparing sensitivity and specificity (represented by the false positive rate). An area under the curve (AUC) value was calculated for each Clinical Responder Phenotype (CRP) with a value of 0.73 for High-CRP (red), 0.81 for Low-CRP (green), and 0.71 for Slow-CRP (blue). The black line represents the empirical sensitivity over specificity.

3.4 Discussion

It has been well established within the literature that there is variation in gingival inflammation within the human population with respect to plaque-induced inflammation that results during experimental gingivitis (15,29). This variation has long been characterized by two major groups, High and Low clinical responses which were derived by various clinical indices: including, gingival index (GI) and bleeding on probing (BOP)(29). However, it wasn't until recently that this variation in gingival inflammation within the human population was temporally analyzed with high resolution while incorporating additional clinical measures: including, visible plaque index (VPI or PI) and gingival crevicular fluid (GCF) flow rate. This resulted in a novel response phenotype referred to as the Slow (15). This Slow response group has a characteristic delayed plaque growth rate represented by the visible plaque index (VPI) which subsequently resulted in a delayed onset of gingival inflammation and clinical indices (GI, BOP, GCF volume) within Slow responder test sites; however, eventually reaching the inflammatory level similar to the High responder test sites (15). This group had a discernable difference in microbiome profile with a high level of Firmicutes at the time of inclusion which was restored again at the resolution phase(15). Additionally, the low response group exhibited a distinct host mediator phenotype exhibiting lower levels of many host mediators compared to the other groups. These response types, now referred to as Clinical Responder Phenotypes (CRPs), which consist of High (High-CRP), Low (Low-CRP), and Slow (Slow-CRP), have been identified in additional experimental gingivitis studies, including a second experimental gingivitis study completed at the University of Washington which followed the same protocols as the recent study by Bamashmous et al.,(15) with minor variations based on study aims (**Figure 12B**). Due to the fact that this variation in gingival inflammation exists within the

human population and has now been confirmed in multiple experimental gingivitis studies (15,29), there is a need to be able to identify an individual's Clinical Response Phenotype in order to predict their risk of microbially-induced inflammation as well as severity of inflammation within the human oral cavity as this may provide an essential tool for oral health researchers and clinicians.

At the time of this dissertation, application of Machine Learning (ML) and Artificial intelligence (AI) using clinical, microbiome, and host mediator data is limited in the field of dentistry and within the dental research literature. Here we present an initial application of the Random Forest Machine Learning algorithm in order to identify Clinical Responder Phenotypes (CRPs) using the time of inclusion (Day -14) data from the EG-1 study (15), which is most representative of the study subject's natural oral health state. In addition to applying this strategy to highly relevant clinical data (VPI, GI, BOP, GCF), we also applied three unique approaches in order to evaluate the different predictive models using a variety of data types collected in EG-1: including relative abundance of species level microbiome data, host mediator levels derived from gingival crevicular fluid (GCF), as well as a comprehensive model which combined both species level relative abundance microbiome data and host mediator data. This provided multiple strategies to develop and evaluate predictive models in order to identify CRPs using a variety of experimental gingivitis data types used in previous, current, and future experimental gingivitis studies.

Amplicon 16S rRNA sequencing is one of the most inexpensive and robust sequencing strategies for investigating microbial taxonomy within the human microbiome, including dental plaque. Thus, developing a predictive model in order to identify CRPs using 16S rRNA microbiome data seems highly feasible and relies on an accessible and less invasive sample

type. In order to train our predictive model using the Random Forest algorithm, we first aimed to use species level agglomerated data from the taxonomic classified amplicon sequence variants (ASVs), which represent a strain level taxonomic designation for 16S rDNA data, as they were rarely observed across individuals (**Figure 8**). The initial subgingival microbiome data at time of inclusion (Day -14) resulted in 336 species after filtering (See Methods). This analysis identified 136 species as being important in differentiating the different CRP. The most influential species to this model are highlighted in **Figure 14**, with the most important species to the model to classify subjects into all three CRP were: *Streptococcus sanguinis*, *Granulicatella elegans*, *Streptococcus cristatus* clade 578, *Corynebacterium durum*, and *Veillonella parvula* (**Table 2**). Interestingly, previously identified perio-pathogenic species associated with Periodontitis, like *Porphyromonas gingivalis* were not identified as important features within our model, which suggests that this keystone pathogen did not help differentiate CRPs using samples derived from study subjects' natural oral health state. This may be due to the fact that the study population was made up of young healthy individuals and that the relative abundance of *Porphyromonas gingivalis* was consistently low across healthy individuals, being most abundant within the High-CRP group.

These 136 species were then used to retrain the model which reduced the out-of-bag (OOB) estimate of misclassification error from 46.88%. to 40.62%. This re-trained model was then tested using the partitioned test data set (See Methods) in which a receiver operator characteristic (ROC) curve was evaluated using the area under the curve (AUC) measurement, representing the model's effectiveness at predicting the desired outcome – in this case correctly identifying an individual's CRP using species level 16S rRNA data obtained from subgingival plaque. The AUC values for CRPs using the 16S rRNA relative abundance data agglomerated

to the species level resulted in the model successfully predicting the High-CRP and Low-CRP 95.2% of the time, while the Slow-CRP was successfully predicted 83.3% of the time. Although there is no definitive AUC value that represents a successful predictive model, it is generally accepted that this is an excellent model for predicting High- and Low-CRPs and good model for predicting Slow-CRP. When we look at the top bacterial species (**Figure 18B**) we can see why some of they were chosen in differentiating the different CRPs at time of inclusion (Day -14). For Example, *Parvimonas sp.* HMT 110 (Firmicutes) was mostly present in the Low- and Slow-CRP and was significantly greater than the High-CRP, which is likely why this species is important to our model as it is likely helping differentiate the Low- and Slow-CRP from the High-CRP. Although *Parvimonas spp*. are generally not associated with health it may not be associated with the most rapid onset of inflammation observed during experimental gingivitis in young healthy individuals.

Gingival crevicular fluid (GCF) is a serum exudate that bathes the gingival tissues within the subgingival pocket, creating a barrier to the external environment within the oral cavity. GCF is also composed of both host and microbial factors, including host mediators that are secreted by various gingival epithelial cells and immune cell types. A robust chemokine panel that measures 41 different host mediators were then used to train the predictive Random Forest model (See Methods). Our analysis resulted in the identification of 17 host mediators that were the most influential to this predictive model are highlighted in **Figure 18A**, with the most important chemokines to the model being CCL2, MIF, CXCL13, CCL20, and GM_CSF (**Table 3**). Using these 17 host mediators to retrain the model reduced the OOB estimate of misclassification error from 56.25% to 46.88%. This re-trained model was then tested using the partitioned test data set (See methods) in which a ROC curve was evaluated using the AUC

measurement, representing the model's effectiveness at predicting the desired outcome – in this case correctly identifying an individual's CRP using host mediators isolated from GCF. The AUC values for CRPs using the chemokines isolated from GCF resulted in the model successfully predicting the High-CRP 85.7% of the time, Low-CRP 95.2% of the time, while the Slow-CRP was successfully predicted 100% of the time. Thus, it is generally accepted that this is an excellent model for predicting Low- and Slow-CRPs and good model for predicting High-CRP. Although we are not focused on the function of these host mediators at this time, it is interesting to see that CCL15, which provides a potent chemotactic effect, was significantly higher in the High-CRP in comparison to the Low- and Slow-CRP which may suggest that the High-CRP is more primed to recruit neutrophils when a response is triggered in comparison to the other responder phenotypes.

Due to the fact that we were able to train and test two predictive models using species level relative abundance values from amplicon sequence data as well as host mediators isolated from GCF, we logically aimed to evaluate if combining these two data types would result in an even more accurate model. We then used the 136 species and 17 Host mediators identified within each respective model and used them to retrain the Random Forest model. This resulted in the identification of 37 Species and 17 Host mediators which were important in differentiating the CRPs and reduced the OOB estimate of misclassification error to 34.38%, which was the lowest we observed in any of the models we had developed. The most influential species and chemokines identified in this model are highlighted in **Table 4**, with the most important variables to the model being *Granulicatella adiacens*, *Veillonella parvula*, CCL20, *Parvimonas sp*. HMT 110, *Actinomyces gerencseriae*, and *Cardiobacterium valvarum*. This re-trained model was then tested using the partitioned test data set in which a ROC curve was evaluated

using the AUC measurement, representing the model's effectiveness at predicting the desired outcome – in this case correctly identifying an individual's CRP using both species level 16S rRNA data obtained from subgingival plaque and host mediators isolated from GCF. The AUC values for CRPs using the 16S rRNA relative abundance data agglomerated to the species level in addition to the chemokines isolated from GCF resulted in the model successfully predicting the High-CRP 90.4% of the time, while the Low- and Slow-CRP were successfully predicted 100% of the time (**Figure 19**). Thus, it is generally accepted that this is an excellent model for predicting all CRPs and is the most robust predictive model we were able to generate.

Due to the fact that our comprehensive model trained using both species level relative abundance and host mediator data, we sought to validate this model. However, at the time of this dissertation, there are no publicly available host mediator or 16S rRNA data sets in which the investigators stratified by the 3 different Clinical Responder Phenotypes within the respective studies. Thus, we determined that the baseline data (Day 0) from EG-1 was the most representative and most like the time of inclusion (Day -14) data that was used to train and test our predictive models with the only major difference between the two time points was the application of a professional cleaning after sampling at time of inclusion (Day -14). We then used the complete baseline data set from Day 0, species level relative abundance (383) and host mediator values (41) and ran it against our comprehensive model. This resulted in AUC values for the comprehensive model successfully predicting the High-CRP 73.4% of the time, the Low-CRP 81.1% of the time, and Slow-CRP 70.8% of the time (**Figure 20**).

Although the AUC values for the comprehensive model reduced the ability to successfully predict the different Clinical Responder Phenotypes in comparison to the comprehensive test data set, we believe some of these differences are due to the fact that the model is more

influenced by species level abundance values in comparison to host mediator measurements and that the professional cleaning, which was implemented as part of the study design in order to normalize all the study subject's oral health status, may have influenced these results as all subjects subgingival microbiome became more similar by Day 0 (**Figure 2A and 2B**). In addition, since we could not find a comprehensive public data set to validate our model, this supports the notion that there is a clear need to develop additional and comparable experimental gingivitis data sets in order to continue to refine and bolster our machine learning approaches in order to successfully identify an individual's risk and severity of inflammation associated with plaque-induced gingivitis by predicting their Clinical Responder Phenotype which may have implications with respect to an individual's oral and systemic health.

Chapter 4. Summary and Future Directions

Experimental gingivitis using a split-mouth design provides a robust model for investigating host-microbial interactions during normal plaque accumulation and maturation as well as the resulting inflammatory processes within the oral cavity. As a result of continuing to mine data sets generated from recent experimental gingivitis studies (EG-1 and EG-2) carried out at the University of Washington, we have continued to uncover new and exciting results that aim to fill knowledge gaps in gingivitis and oral health research. In summary, work outlined as part of this dissertation research project has provided new knowledge of an oral contralateral effect observed within the human oral cavity that is a direct result of localized inflammation stemming from plaque-induced experimental gingivitis occurring in distant sites within the mouth. In addition, this work has also resulted in the development of a number of predictive models – microbiome-based, host mediator-based, and a comprehensive microbiome and host mediators-based model – for identifying the different Clinical Responder Phenotypes (CRP): High-CRP, Low-CRP, and Slow-CRP. These results are sure to fill current knowledge gaps within experimental gingivitis research as well as provide new insight for future studies as well as provide clinical insight for patient surveillance and treatment planning.

Contralateral effects within the human body have been identified within the eyes, ears, lungs, and even within skin; however, results from the present study provided a robust and temporal characterization of an oral contralateral effect within the human oral cavity in which localized inflammation in three teeth can results in both host mediator and microbiome community changes within subgingival pockets within distal healthy sites. Although there is a link between the severity of this oral contralateral effect and the inflammatory response associated with the different Clinical Responder Phenotypes, it remains unclear to what extent. Future studies are

needed to provide additional resolution of these contralateral changes occurring within healthy tissues as well as to identify key signatures, whether microbiome or host-based, that may be responsible for these observations. Interestingly, the microbiome triggers inflammation at the experimental site, yet the host response seems to be regulating the changes in microbiome diversity in distal subgingival pockets elsewhere in the mouth and affecting normal healthy homeostasis within the subgingival pocket. The use of the experimental gingivitis model may also provide a well-controlled way in which it is possible to study reversible inflammation in association with natural dental plaque accumulation and the systemic inflammatory effects distant and/or contralateral tissues within humans.

Variation in gingival inflammation in humans represents variations in the levels of severity of the inflammatory response to bacterial plaque accumulation and community maturation. For example, some individuals show signs of clinical inflammation as early as 4 days without oral hygiene (High-CRP), some have a delayed plaque growth rate that subsequently results in a delay in clinical inflammation (Slow-CRP), while others can have lots of plaque accumulation, but are able to modulate their inflammatory response (Low-CRP). Thus, the development of a predictive model that is able to identify an individual's severity of inflammatory response due to dental plaque accumulation within the oral cavity, represented by the Clinical Responder Phenotype, may prove to be a useful tool in identifying an individual's risk of gingival inflammation as well as risk of progressing to more devastating forms of gingival disease, such as periodontitis. Additional high-resolution temporal experimental gingivitis studies are needed to validate these predictive models prior to their broad application in dental research or as a diagnostic tool. However, the results outlined in this study represent a promising result and support the notion that the use of machine learning in dentistry may help identify individuals who are at higher risk of effects of not

maintaining good oral hygiene practices, represented by gingival inflammation, which may dictate their preventive care and treatment planning.

In conclusion, the results from these studies as part of this dissertation research project have helped identify key microbial and host mediators within the different Clinical Responder Phenotypes that can be used to predict an individual's inflammatory response to normal plaque accumulation in their natural oral health state. Additionally, we provide new evidence in which localized inflammation that results from dental plaque accumulation and community maturation within test sites has the ability to affect distant otherwise generally healthy tissues within the oral cavity. Together these results represent an exciting new avenue for future gingivitis and oral health research which aim to further improve oral health outcomes for the broader population.

References

1. Deo PN, Deshmukh R. Oral microbiome: Unveiling the fundamentals. J Oral Maxillofac Pathol. 2019 Jan 1;23(1):122.
2. JL B, B B, M A, W S, X H. Ecology of the Oral Microbiome: Beyond Bacteria. Trends Microbiol. 2017 May 1;25(5):362–74.
3. Chen T, Yu WH, Izard J, Baranova O V, Lakshmanan A, Dewhirst FE. The Human Oral Microbiome Database: a web accessible resource for investigating oral microbe taxonomic and genomic information. Database (Oxford). 2010;2010:baq013.
4. Wade WG. The oral microbiome in health and disease. Pharmacol Res. 2013;69(1):137–43.
5. Xiao J, Fiscella KA, Gill SR. Oral microbiome: possible harbinger for children's health. Int J Oral Sci 2020 121. 2020 Apr 30;12(1):1–13.
6. Takei N, Carranza K. CARRANZA'S CLINICAL PERIODONTOLOGY, 12TH EDITION. 12th ed. Saunders, Elsevier; 2015.
7. Marsh PD. Microbial ecology of dental plaque and its significance in health and disease. Adv Dent Res. 1994;8(2):263–71.
8. Trombelli L, Farina R, Minenna L, Carrieri A, Scapoli C, Tatakis DN. Experimental gingivitis: reproducibility of plaque accumulation and gingival inflammation parameters in selected populations during a repeat trial. J Clin Periodontol. 2008/09/20. 2008;35(11):955–60.
9. Hajishengallis G. Immunomicrobial pathogenesis of periodontitis: keystones, pathobionts, and host response. Trends Immunol. 2014;35(1):3–11.
10. Curtis MA, Zenobia C, Darveau RP. The relationship of the oral microbiotia to periodontal health and disease. Cell Host Microbe. 2011;10(4):302–6.
11. Dewhirst FE, Chen T, Izard J, Paster BJ, Tanner AC, Yu WH, et al. The human oral microbiome. J Bacteriol. 2010;192(19):5002–17.
12. Kistler JO, Booth V, Bradshaw DJ, Wade WG. Bacterial community development in experimental gingivitis. PLoS One. 2013;8(8):e71227.
13. Matthews CR, Joshi V, de Jager M, Aspiras M, Kumar PS. Host-bacterial interactions during induction and resolution of experimental gingivitis in current smokers. J Periodontol. 2013;84(1):32–40.
14. Eberhard J, Grote K, Luchtefeld M, Heuer W, Schuett H, Divchev D, et al. Experimental

gingivitis induces systemic inflammatory markers in young healthy individuals: a single-subject interventional study. PLoS One. 2013;8(2):e55265.

15. Bamashmous S, Kotsakis GA, Kerns KA, Leroux BG, Zenobia C, Chen D, Trivedi HM, McLean JS, Darveau RP. Human Variation in Gingival Inflammation. PNAS. 2021 Jul 6;118,27,7

16. Yan Y, Nguyen LH, Franzosa EA, Huttenhower C. Strain-level epidemiology of microbial communities and the human microbiome. Vol. 12, Genome Medicine. BioMed Central Ltd; 2020. p. 71.

17. Horst R ter, Jaeger M, Smeekens SP, Oosting M, Swertz MA, Li Y, et al. Host and Environmental Factors Influencing Individual Human Cytokine Responses. Cell. 2016 Nov 3;167(4):1111-1124.e13.

18. Belkaid Y, Harrison OJ. Homeostatic immunity and the microbiota. Immunity. 2017 Apr 18;46(4):562.

19. Srinivasan R, Karaoz U, Volegova M, MacKichan J, Kato-Maeda M, Miller S, et al. Use of 16S rRNA Gene for Identification of a Broad Range of Clinically Relevant Bacterial Pathogens. PLoS One. 2015 Feb 6;10(2):117617.

20. Chen T, Yu WH, Izard J, Baranova O V., Lakshmanan A, Dewhirst FE. The Human Oral Microbiome Database: a web accessible resource for investigating oral microbe taxonomic and genomic information. Database (Oxford). 2010;2010.

21. Callahan BJ, McMurdie PJ, Rosen MJ, Han AW, Johnson AJ, Holmes SP. DADA2: High-resolution sample inference from Illumina amplicon data. Nat Methods. 2016/05/24. 2016;13(7):581–3.

22. Callahan BJ, McMurdie PJ, Holmes SP. Exact sequence variants should replace operational taxonomic units in marker-gene data analysis. ISME J. 2017 Dec 1;11(12):2639–43.

23. M K, RJ L. Subgingival biofilm formation. Periodontol 2000. 2010 Feb;52(1):38–52.

24. Hajishengallis G, Darveau RP, Curtis MA. The keystone-pathogen hypothesis. Nat Rev Microbiol. 2012/09/04. 2012;10(10):717–25.

25. James SL, Abate D, Abate KH, Abay SM, Abbafati C, Abbasi N, et al. Global, regional, and national incidence, prevalence, and years lived with disability for 354 Diseases and Injuries for 195 countries and territories, 1990-2017: A systematic analysis for the Global Burden of Disease Study 2017. Lancet. 2018 Nov 10;392(10159):1789–858.

26. Eke PI, Dye BA, Wei L, Slade GD, Thornton-Evans GO, Borgnakke WS, et al. Update on Prevalence of Periodontitis in Adults in the United States: NHANES 2009 to 2012. J

Periodontol. 2015;86(5):611–22.

27. Haffajee AD, Socransky SS. Microbial etiological agents of destructive periodontal diseases. Periodontol 2000. 1994;5(1):78–111.

28. Socransky SS, Haffajee AD, Cugini MA, Smith C, Kent RL. Microbial complexes in subgingival plaque. J Clin Periodontol. 1998;25(2):134–44.

29. Trombelli L, Tatakis DN, Scapoli C, Bottega S, Orlandini E, Tosi M. Modulation of clinical expression of plaque-induced gingivitis. II. Identification of "high-responder" and "low-responder" subjects. J Clin Periodontol. 2004;31(4):239–52.

30. Nowicki EM, Shroff R, Singleton JA, Renaud DE, Wallace D, Drury J, et al. Microbiota and metatranscriptome changes accompanying the onset of gingivitis. MBio. 2018 Mar 1;9(2).

31. Löe H, Theilade E, Jensen SB. Experimental gingivitis in man. J Periodontol. 1965;36(3):177–87.

32. Theilade E, Wright WH, Jensen SB, Loe H. Experimental gingivitis in man. II. A longitudinal clinical and bacteriological investigation. J Periodontal Res. 1966/01/01. 1966;1(1):1–13.

33. Tatakis DN, Trombelli L. Modulation of clinical expression of plaque-induced gingivitis. J Clin Periodontol. 2004;31(4):229–38.

34. He XS, Shi WY. Oral microbiology: past, present and future. Vol. 1, International journal of oral science. Int J Oral Sci; 2009. p. 47–58.

35. Huang S, He T, Yue F, Xu V, Wang S, Zhu P, et al. Title: Longitudinal multi-omics along gingivitis development reveal a suboptimal-health gum 2 state with periodontitis-like microbiome.

36. Hajishengallis G. Periodontitis: from microbial immune subversion to systemic inflammation. Nat Rev Immunol. 2015;15(1):30–44.

37. Zhang J, Kashket S, Lingstrom P. Evidence for the early onset of gingival inflammation following short-term plaque accumulation. J Clin Periodontol. 2002/12/21. 2002;29(12):1082–5.

38. Fine N, Hassanpour S, Borenstein A, Sima C, Oveisi M, Scholey J, et al. Distinct Oral Neutrophil Subsets Define Health and Periodontal Disease States. J Dent Res. 2016/06/09. 2016;95(8):931–8.

39. Wang J, Qi J, Zhao H, He S, Zhang Y, Wei S, et al. Metagenomic sequencing reveals microbiota and its functional potential associated with periodontal disease. Sci Rep.

2013;3:1843.

40. Schincaglia GP, Hong BY, Rosania A, Barasz J, Thompson A, Sobue T, et al. Clinical, Immune, and Microbiome Traits of Gingivitis and Peri-implant Mucositis. J Dent Res. 2017;96(1):47–55.

41. Offenbacher S, Barros S, Mendoza L, Mauriello S, Preisser J, Moss K, et al. Changes in gingival crevicular fluid inflammatory mediator levels during the induction and resolution of experimental gingivitis in humans. J Clin Periodontol. 2010;37(4):324–33.

42. Patil PB, Patil B. Saliva: A diagnostic biomarker of periodontal diseases. Vol. 15, Journal of Indian Society of Periodontology. Wolters Kluwer -- Medknow Publications; 2011. p. 310–7.

43. Darveau RP. The oral microbial consortium's interaction with the periodontal innate defense system. DNA Cell Biol. 2009/05/14. 2009;28(8):389–95.

44. Barksby HE, Nile CJ, Jaedicke KM, Taylor JJ, Preshaw PM. Differential expression of immunoregulatory genes in monocytes in response to Porphyromonas gingivalis and Escherichia coli lipopolysaccharide. Clin Exp Immunol. 2009;156(3):479–87.

45. Tsukamoto Y, Usui M, Yamamoto G, Takagi Y, Tachikawa T, Yamamoto M, et al. Role of the junctional epithelium in periodontal innate defense and homeostasis. J Periodontal Res. 2012;47(6):750–7.

46. LS F, R N, SC P, SC C, R S, RM S-C. Association between interleukin-8 levels and chronic periodontal disease: A PRISMA-compliant systematic review and meta-analysis. Medicine (Baltimore). 2017 Jun 1;96(22).

47. C G. Interleukin-6 and chronic inflammation. Arthritis Res Ther. 2006 Jul;8 Suppl 2(Suppl 2).

48. MK N, M J, SH K, SR L, KH P, DH K, et al. Assessment of IL-6, IL-8 and TNF-α levels in the gingival tissue of patients with periodontitis. Exp Ther Med. 2013;6(3):847–51.

49. Cheng R, Wu Z, Li M, Shao M, Hu T. Interleukin-1β is a potential therapeutic target for periodontitis: a narrative review. Int J Oral Sci 2020 121. 2020 Jan 2;12(1):1–9.

50. M R. An Introduction to Machine Learning for Clinicians. Acad Med. 2019 Oct 1;94(10):1433–6.

51. Schwendicke F, Samek W, Krois J. Artificial Intelligence in Dentistry: Chances and Challenges: https://doi.org/101177/0022034520915714. 2020 Apr 21;99(7):769–74.

52. Li X, Kolltveit KM, Tronstad L, Olsen I. Systemic diseases caused by oral infection. Vol. 13, Clinical Microbiology Reviews. American Society for Microbiology (ASM); 2000. p.

547–58.

53. Abbayya K, Puthanakar NY, Naduwinmani S, Chidambar YS. Association between periodontitis and alzheimer's disease. N Am J Med Sci. 2015 Jun 1;7(6):241–6.

54. Cao CF, Smith QT. Crevicular fluid myeloperoxidase at healthy, gingivitis and periodontitis sites. J Clin Periodontol. 1989;16(1):17–20.

55. An JY, Kerns KA, Ouellette A, Robinson L, Morris D, Kaczorowski C, et al. Rapamycin rejuvenates oral health in aging mice. Elife. 2020 Apr 1;9.

56. Lamont EI, Gadkari A, Kerns KA, To TT, Daubert D, Kotsakis G, et al. Modified SHI medium supports growth of a disease-state subgingival polymicrobial community in vitro. Mol Oral Microbiol. 2021 Feb 1;36(1):37–49.

57. Bolyen E, Rideout JR, Dillon MR, Bokulich NA, Abnet C, Al-Ghalith GA, et al. QIIME 2: Reproducible, interactive, scalable, and extensible microbiome data science. PeerJ Preprints; 2018.

58. McMurdie PJ, Holmes S. phyloseq: an R package for reproducible interactive analysis and graphics of microbiome census data. PLoS One. 2013;8(4):e61217.

59. Genolini C, Alacoque X, Sentenac M, Arnaud C. kml and kml3d: R Packages to Cluster Longitudinal Data. J Stat Softw. 2015;65(4):1–34.

60. Kassambara A. ggpubr: "ggplot2" Based Publication Ready Plots. 2020.

61. Kassambara A. rstatix: Pipe-Friendly Framework for Basic Statistical Tests. 2020;

62. Bates D, Mächler M, Bolker B, Walker S. Fitting linear mixed-effects models using lme4. arXiv Prepr arXiv14065823. 2014;

63. Jari Oksanen Michael Friendly, Roeland Kindt, Pierre FGB, Legendre Peter R. Minchin, R. B. O'Hara, Gavin L. Simpson, DM, Peter Solymos Eduard Szoecs and Helene Wagner MHHS. Vegan: Community Ecology Package. R package version 2.5-4. . 2019.

64. Lamster IB, Hartley LJ, Vogel RI. Development of a Biochemical Profile for Gingival Crevicular Fluid: Methodological Considerations and Evaluation of Collagen-Degrading and Ground Substance-Degrading Enzyme Activity during Experimental Gingivitis. J Periodontol. 1985 Nov;56(11s):13–21.

65. Vaiserman A, Romanenko M, Piven L, Moseiko V, Lushchak O, Kryzhanovska N, et al. Differences in the gut Firmicutes to Bacteroidetes ratio across age groups in healthy Ukrainian population. BMC Microbiol 2020 201. 2020 Jul 22;20(1):1–8.

66. F M, M G, L G, A Z, S P, P N, et al. The Firmicutes/Bacteroidetes Ratio: A Relevant Marker of Gut Dysbiosis in Obese Patients? Nutrients. 2020 May 1;12(5).

67. Ley RE, Backhed F, Turnbaugh P, Lozupone CA, Knight RD, Gordon JI. Obesity alters gut microbial ecology. Proc Natl Acad Sci U S A. 2005;102(31):11070–5.

68. Sela U, Euler CW, Rosa JC da, Fischetti VA. Strains of bacterial species induce a greatly varied acute adaptive immune response: The contribution of the accessory genome. PLOS Pathog. 2018 Jan 1;14(1):e1006726.

69. Kaper JB, Nataro JP, Mobley HLT. Pathogenic Escherichia coli. Nat Rev Microbiol 2004 22. 2004 Feb;2(2):123–40.

70. Pathak M, Lal G. The Regulatory Function of CCR9+ Dendritic Cells in Inflammation and Autoimmunity. Front Immunol. 2020 Oct 2;0:2219.

71. Rubinstein WS, Acheson LS, O'Neill SM, Ruffin MT, IV, Wang C, et al. Clinical utility of family history for cancer screening and referral in primary care: A report from the Family Healthware Impact Trial. Genet Med. 2011 Nov;13(11):956.

72. Hawkes N. Cancer survival data emphasise importance of early diagnosis. BMJ. 2019 Jan 25;364:l408.

73. Grivennikov SI, Karin M. Inflammatory cytokines in cancer: tumour necrosis factor and interleukin 6 take the stage. Ann Rheum Dis. 2011 Mar 1;70(Suppl 1):i104–8.

74. Prasad G, McCullough M. Chemokines and cytokines as salivary biomarkers for the early diagnosis of oral Cancer. Int J Dent. 2013;2013.

75. Raghupathi W, Raghupathi V. Big data analytics in healthcare: promise and potential. Heal Inf Sci Syst. 2014 Dec;2(1).

76. Aljameel SS, Khan IU, Aslam N, Aljabri M, Alsulmi ES. Machine Learning-Based Model to Predict the Disease Severity and Outcome in COVID-19 Patients. Sci Program. 2021;2021.

77. Sardar R, Sharma A, Gupta D. Machine Learning Assisted Prediction of Prognostic Biomarkers Associated With COVID-19, Using Clinical and Proteomics Data. Front Genet. 2021 May 20;12:522.

78. Siettos CI, Russo L. Mathematical modeling of infectious disease dynamics. Virulence. 2013;4(4):295.

79. Christaki E. New technologies in predicting, preventing and controlling emerging infectious diseases. Virulence. 2015;6(6):558.

80. Alahmadi A, Belet S, Black A, Cromer D, Flegg JA, House T, et al. Influencing public health policy with data-informed mathematical models of infectious diseases: Recent developments and new challenges. Epidemics. 2020 Sep 1;32:100393.

81. Rodriguez-Galiano V, Sanchez-Castillo M, Chica-Olmo M, Chica-Rivas M. Machine learning predictive models for mineral prospectivity: An evaluation of neural networks, random forest, regression trees and support vector machines. Ore Geol Rev. 2015 Dec 1;71:804–18.

82. Livingston F. Implementation of Breiman's Random Forest Machine Learning Algorithm. ECE591Q Mach Learn J Pap Fall. 2005;

83. Safari S, Baratloo A, Elfil M, Negida A. Evidence Based Emergency Medicine; Part 5 Receiver Operating Curve and Area under the Curve. Emergency. 2016;4(2):111.

84. Silness J, Löe H. Periodontal disease in pregnancy II. Correlation between oral hygiene and periodontal condition. Acta Odontol Scand. 1964;22(1):121–35.

85. Team RC. R: A Language and Environment for Statistical Computing. 3.5.1. Vienna, Austria: R Foundation for Statistical Computing; 2018.